University of Southampton

Faculty of Engineering and the Environment

Mechanical Engineering

Improvement of the Soluble Lead Flow Battery Using a Novel Recovered Electrolyte

DOI

by

Keletso Orapeleng

ORCID ID 0000-0002-6920-3741

Thesis for the degree of Doctor of Philosophy

October 2018

University of Southampton

Abstract

Faculty of Engineering and the Environment

Mechanical Engineering – Energy Technology Research Group

Thesis for the degree of Doctor of Philosophy

Improvement of the Soluble Lead Flow Battery Using a Novel Recovered Electrolyte

by

Keletso Orapeleng

The soluble lead battery is one of the redox flow batteries that are suggested for MWh energy storage to assist with the integration of sustainable energy sources as well as to bring electricity to areas with no grid connection. The soluble lead battery has several advantages including the fact that it uses the same electrolyte both sides, which should reduce the need for expensive membrane separators and reduce the number of tanks and circulating pump sets to one each, reducing complexity. However, research has shown that the positive electrode redox couple has limited reversibility and as such, results in build-up of material on the positive electrode, which consequently affects stripping at the negative electrode, and results in short circuits and short cycle life. This thesis enhances the advantages of the soluble lead battery by introducing a novel method to produce electrolyte for the soluble lead battery directly out of spent lead acid batteries. By so doing the thesis introduces an inexpensive method to make electrolyte for the battery, improving the battery's competitiveness. The thesis also proves that the reagent grade electrolyte that is traditionally used in prior studies has nickel impurities in it and is as such harmful to the operation of the battery. Furthermore, the recovered electrolyte made out of spent lead acid batteries is cycled extensively in both static and flow cells to compare performance, and the recovered electrolyte is found to perform better than the reagent grade electrolyte in both cells. Hence based on the results, it is recommended that the soluble lead battery should use recovered electrolyte to avoid the detrimental effects of nickel in reagent grade electrolyte, as well as to take advantage of the relatively easy method of making recovered electrolyte, which takes advantage of the refined lead in lead acid batteries as well as the additives traditionally added to enhance operation in traditional lead acid batteries. To further improve the performance of the soluble lead battery, cycling regimes are carried out using recovered electrolyte, where it is found that current density, the inter-electrode gap, as well as the end-of-discharge voltage, have a significant effect on the performance of the soluble lead cell, and need to be controlled to optimise cycle life as well as charge, energy and voltage efficiency. Finally, further work is recommended to address questions that arose and that could not be addressed within the scope of this work.

Table of Contents

Table of Tables

Table of Tables

Table of Figures

Table of Figures

Table of Figures

Table of Figures

Research Thesis: Declaration of Authorship

Print name:

Title of thesis:

I declare that this thesis and the work presented in it are my own and has been generated by me as the result of my own original research.

I confirm that:

1. This work was done wholly or mainly while in candidature for a research degree at this University;
2. Where any part of this thesis has previously been submitted for a degree or any other qualification at this University or any other institution, this has been clearly stated;
3. Where I have consulted the published work of others, this is always clearly attributed;
4. Where I have quoted from the work of others, the source is always given. With the exception of such quotations, this thesis is entirely my own work;
5. I have acknowledged all main sources of help;
6. Where the thesis is based on work done by myself jointly with others, I have made clear exactly what was done by others and what I have contributed myself;
7. Parts of this work have been published as:

Orapeleng, K., Wills, R.G.A., and Cruden, A., Performance of recovered and reagent grade electrolyte in a soluble lead redox cell. Journal of Energy Storage, 2018. 20: p. 49-56.DOI: https://doi.org/10.1016/j.est.2018.08.017.

Orapeleng, K., Wills, R., and Cruden, A., Developing Electrolyte for a Soluble Lead Redox Flow Battery by Reprocessing Spent Lead Acid Battery Electrodes. Batteries, 2017. 3(2): 15. DOI: https://doi.org/10.3390/batteries3020015.

Signature: Date:

Acknowledgements

I would like to thank my parents for their unwavering belief in me, even when I seriously doubted myself. I would also like to thank the government of Botswana and the Botswana University of Science and Technology, for funding this research and supporting me through my studies. A special mention of Dr. Motlhabane, who showed a lot of care and concern for my mental health, especially when I was struggling.

I wish to acknowledge my supervisors, Prof. Andy Cruden and Dr. Richard Wills, both of who have provided unwavering support and have seen me through all the difficult parts of this research. Without them this work would have never been possible. I am forever grateful.

I also wish to thank Dr. Muthu Krishna, Dr. Luis F. Arenas, Dr Maria Kourasi, Dr. Rachel McKerracher, Dr A. Badr, Prof. Carlos Ponce de Leon, and others in the Energy technology research lab whose friendship and presence made my stay in Southampton pleasant.

Definitions and Abbreviations

AGM – absorbed glass mat

DoE – US Department of Energy

EC – European Commission

EoCV – End of Charge Voltage

EoDV – End of Discharge Voltage

EDTA – Ethylenediaminetetraacetic acid

EU – European Union

HDTMA – hexadecyltrimethylammonium

IPCC – International Panel on Climate Change

MSA – Methanesulfonic acid

PAM – Positive electrode material

ppba – Parts per billion atoms

ppma – Parts per million atoms

PV – Photovoltaic

RFB – Redox flow battery

RFC – Redox flow cell

SCE – Saturated calomel electrode

SLI – Starting, lighting and ignition

SLFB – Soluble lead redox flow battery

SoC – State of charge

SoH – State of health

UNFCC – United Nations Forum on Climate Change

UPS – Uninterruptible Power Supply

VRB – Vanadium redox flow battery

VRLA – Valve regulated lead acid

Chapter 1 Introduction and Research Objectives

Climate change is 'unequivocally' one of the biggest challenges of the 21st century [1], exacerbated by the use of fossil fuels that have contributed significantly to the increase in carbon dioxide emissions in the atmosphere and the subsequent global warming [2]. Recently, the IPCC confirmed that recent extreme weather conditions experienced in different parts of the world are more than likely the effects of 1.0°C global warming above pre-industrial levels and that "global warming is more than likely to reach 1.5° C between 2030 and 2052 if it continues to increase at the current rate", which would cause catastrophic climate change [3]. This confirms the urgency to expedite mitigation efforts, and renewable energy sources are recommended as one of the ways to mitigate and reduce the use of fossil fuels [4].

In Europe and other western countries, several governments have introduced and/or strengthened policies that increase the share of renewable energy in their national energy mix, gradually reducing the use of fossil fuels [5, 6]. The EU has set targets to produce as much as 20% energy from renewable sources by 2020, and some of the countries have increased their targets as the set targets were accomplished or became attainable. For example, Scotland reached its target to produce 50% electricity from renewable energy by 2015, and subsequently updated the target to 100% of Scotland's electricity demand from renewables by 2020 [7]. Germany set their target at 30% electricity from renewables by 2020, and managed to surpass it in 2018 and has since upgraded the national target to 100% electricity supply from renewables by 2050 [8].

Renewable energy has also been suggested for developing countries, not only as a sustainable energy source for ever increasing energy demands, but also as an option better suited to areas with no grid connection [9-11]. In India, recommendations were implemented through the Electricity Act of 2003, Section 14, [12] targeting rural electrification, which stipulated that small-scale producers did not need to obtain licenses but needed to conform to safety and supply regulations, and that benefits borne from government subsidy would be passed to the consumer [13]. The Global Network on Energy for Sustainable Development reported that 10,000 households in West Bengal and 35,000 in 1,400 small villages received stable electricity from micro-grids implemented by government agencies under the said policy [13]. In 2017, 147 million households in India used off-grid solar electricity [14]. In the same year Costa Rica provided over 98% of the national electricity demand from renewable sources [14].

Across the developing world, micro-grids provide access to low power electricity (1 – 20 Wp). For example, between 2016 and 2017, 9 million people each in Kenya, Tanzania, and Uganda, and 17 million in Ethiopia, gained access to electricity through off-grid solar systems [14]. A 100,000 Solar

Home Systems were installed in Bangladesh in 2006 [15]. In fact, 6% of new access to electricity across the world was due to off-grid solar systems [14]. It is clear that for the developing world, as well as rural electrification in developed countries, micro-grids and off-grid electricity generation are the most practical and accessible ways in which to improve electricity access. Therefore renewable energy will remain a critical source, especially if the seventh sustainable development goal [16] of ensuring access to affordable and clean energy is to be met by 2050.

1.1 The Need for Energy Storage

Energy storage presents an opportunity for effective utilisation of renewable energy, by storing excess energy when it is available and discharging it when it is required [17, 18].

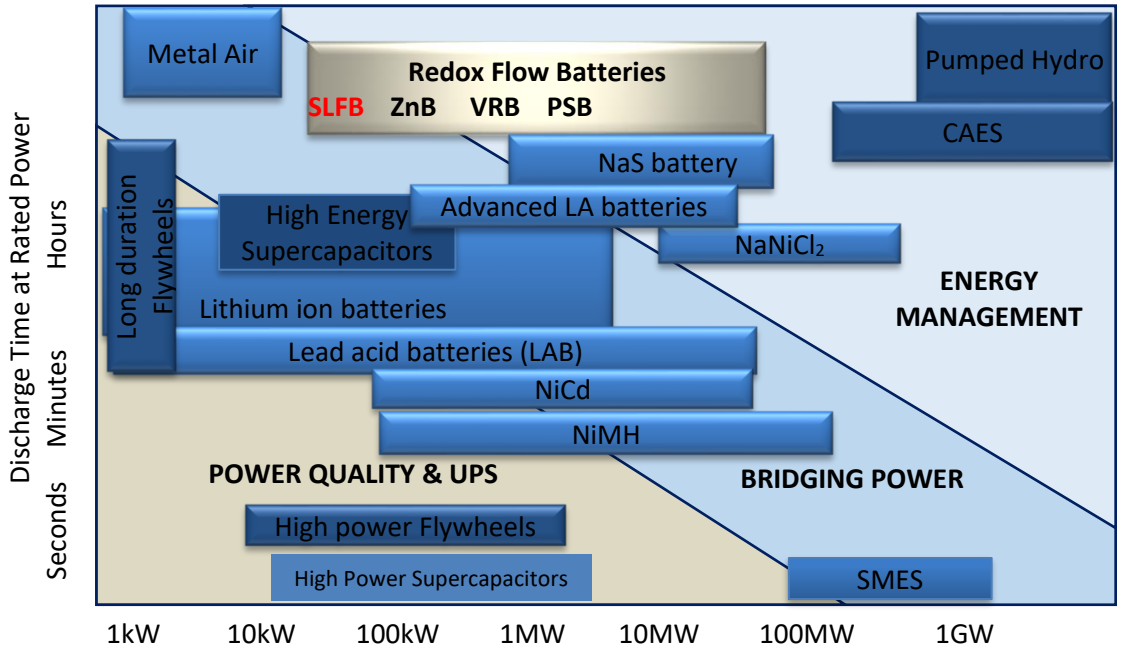

Figure 1-1: Functions that different energy storage technologies can supply to the grid[1]

[1] Adapted from: 17. San Martín, J.I., I. Zamora, J.J. San Martín, V. Aperribay, and P. Eguia. *Energy storage technologies for electric applications*. in *International Conference on Renewable Energies and Power Quality*. 2011., 19. Ibrahim, H., A. Ilinca, and J. Perron, *Energy storage systems—Characteristics and comparisons.* Renewable and Sustainable Energy Reviews, 2008. **12**(5): p. 1221-1250.DOI: http://dx.doi.org/10.1016/j.rser.2007.01.023, 20. Dunn, B., H. Kamath, and J.-M. Tarascon, *Electrical Energy Storage for the Grid: A Battery of Choices.* Science, 2011. **334**(6058): p. 928-935.DOI: 10.1126/science.1212741., 21. Yang, Z., J. Zhang, M.C.W. Kintner-Meyer, X. Lu, D. Choi, J.P. Lemmon, and J. Liu, *Electrochemical Energy Storage for Green Grid.* Chemical Reviews, 2011. **111**(5): p. 3577-3613.DOI: 10.1021/cr100290v.

However, the utility of energy storage goes beyond resource firming and load shifting; voltage and power quality regulation, energy management, price arbitration, and peak shaving, are just some of the many services that energy storage offers [22]. An overview of the range of applications provided by energy storage technologies is illustrated in Figure 1-1, and redox flow batteries are among the energy storage technologies providing these services. Demonstration projects around the world have proved that redox flow batteries are a viable option for both stationary and grid-connected energy storage applications [23, 24]. Table 1-1 gives examples of redox flow batteries providing a range of these services.

Table 1-1: Examples of functions served by redox flow batteries in renewable energy integration and micro-grids [17, 25-27].

Function	**Description [27]**	**Response Time / Sustained Energy Supply Period**	**Technology / Project Examples [26]**
Resource firming	Energy from renewable sources is intermittent and may not be available when required. Storage acts as the bridge between supply and demand, storing the energy when it is available and discharging it as electricity when it is in demand. The electricity is then supplied consistently, despite irregular generation. Energy storage can also prevent sudden shut down of renewable generating equipment, such as wind turbines, if generation exceeds demand, by storing the surplus electricity.	Milliseconds-seconds / 1 – 9 Hours	15 kW/120 kWh Vanadium redox flow battery at Risø Syslab, at Lyngby-Taarbæk, Denmark (response 20 kW/s) [28]. 15 MW/60 MWh Vanadium redox flow battery at Minami Hayakika Substation, Hokkaido, Japan [29].

Function	**Description**	**Response Time / Sustained Energy Supply Period**	**Technology / Project Examples [24, 26]**
Resource integration	Similar to resource firming, energy storage provides a buffering role between intermittent supply from renewable generators and the micro-grid, and hence enables the grid to receive electricity from different types of renewable sources.	Seconds to minutes / hours	100 kW/500 kWh Zinc bromine Redox flow batteries was used to store electricity from both solar and wind energy, at New South wales, Australia. 25 kW/ 50 kWh $ZnBr_2$ redox flow battery in Scottish community in Strathclyde [30] 15 MW / 60 MWh Vanadium Redox Flow battery at Hokkaido, Japan, used to store electricity from adjacent solar and wind farms [29].
Load matching – load levelling	Electricity produced during low demand is stored immediately, and then dispatched when demand is high. This way the need to produce peak electricity is shifted to times of low demand, when generation might be cheaper. For independent producers, this could decrease the need to buy electricity at high prices, or enable selling of cheaply produced electricity at higher prices, in what is known as **price arbitration**.	Minutes to hours / hours	80 kW/160 kWh Zinc Iron Redox flow battery by Flathead ViZn at Montana. [31]

Function	Description	Response Time / Sustained Energy Supply Period	Technology / Project Examples [24, 26]
Load matching – Peak shaving	Where it is possible to predict occasional excessive peak demand, energy storage can provide peak shaving by supplying the excess demand, on top of the usual generated capacity. In this case, energy stored during low demand can be used instead of running spinning reserve equipment, such as diesel generators.	Milliseconds to seconds / Minutes to hours	Two 500 kW zinc bromine flow battery packs for peak shaving, one for a 605 kW solar array in Everett, MA, and another for a 600 MW wind farm in Worcester, MA. [32]
Uninterruptible supply (UPS) / "Ride Through" capability	For some small networks, quick-responding energy storage can be used to supply the required full capacity almost instantaneously, instead of using emergency generating plant, ensuring there is no interruption of supply for customers.	Milliseconds to seconds / Minutes to hours	105 625 kW Imergy® vanadium redox flow batteries for uninterruptible supply for telecoms applications in South Africa and India [33].

Function	**Description**	**Response Time / Sustained Energy Supply Period**	**Technology / Project Examples [24, 26]**
Frequency regulation.	Electricity supplied to consumers needs to be within 50 to 60 Hz in order to comply to supply regulations and to prevent damaging equipment and/or disrupting production for commercial and industrial customers. However different renewable sources generate at different frequencies. To ensure the electricity fed into the micro-grid is at the right frequency, energy storage can be used as a buffer where power electronics regulate the electricity before storage and between storage and the grid, independent of the generator's fluctuations.	Seconds	1 MW Avista UET Vanadium Redox Flow Battery at Pullman, Washington, US, provides black start, energy time shift, frequency regulation, resource firming, load following, spinning reserve, and ramping energy services [34].
Power quality and voltage regulation	Energy storage also enables micro-grids to provide a consistent flow of electricity despite the fluctuations inherent in renewable energy sources.	Milliseconds to seconds / 8 hours	250 kW/1000 kWh Castle Valley Vanadium Redox Battery, US, also provided power quality and voltage regulation [24].

It is clear from Table 1-1 that redox flow batteries can provide many services to the grid, for example, a 15 MW / 60MWh vanadium redox flow battery installed at the HEPCO substation in Minami-Hayakita was used to store and discharge energy from a wind and solar farm onsite. The battery was able to supply the required energy for four hours, successfully indicating dispatchability. It also responded to sudden increases in demand within 60 milliseconds, therefore proving capability for peak shaving, ride through and voltage regulation [29]. This indicates that redox flow batteries are capable of providing the services required to enable use of renewable energy sources, including: capacity firming or time-shifting, load management, frequency regulation, voltage quality management, price arbitration, black start, among many others [25], as seen in several of the examples quoted above. It was also possible to discharge the battery to 98% SoD with no negative effect to capacity, signalling tolerance to deep discharge.

In their 'Energy for All' model scenario, the International Energy Agency predicts that the cheapest way to provide 485 million people with electricity by 2030 will be through decentralised systems [14]. Since 88% of the world population without electricity live in Sub-Africa, and 78% are in rural areas which have no grid connection, it is reasonable to assume that off-grid and mini-grid systems will continue to be essential for this task. The capacity of redox flow batteries to pair with a range of off-grid systems is essential. As shown in Table 1-1, redox flow batteries can store kWh – MWh energy e.g. the 15 MW/60 MWh Vanadium redox flow battery at Minami Hayakika Substation, Hokkaido, Japan [29] and the 100 kW/ 600 kWh vanadium redox flow battery provided for load shifting at Gyengnam, South Korea [26]. When coupled with micro-grids, redox flow batteries can provide stable and quality electricity for isolated communities.

1.2 Motivation: Energy Storage for Rural Communities and the Urban Poor

The drive to provide energy for the developing world and for rural electrification historically relied on renewable sources and on decentralised systems. In the period spanning the 1960s to early 2000s, several solar PV systems were piloted throughout Africa [35-38], and in India [39, 40], in rural electrification projects. The systems were sized between several tens of watts to kilowatts, delivering electricity for community projects such as health clinics, schools, community centres, and government office buildings [41]. Historically lead acid batteries were the most common storage technology for the projects.

However, most of the projects in both Africa [42] and India [40] failed, due to a myriad of reasons including: high initial investment costs, a lack of technical support for maintenance, inaccessibility of spares, inability to pay for the electricity despite willingness to buy [43], prohibitive

replacement costs for the battery pack, a lack of ownership by the users resulting in neglect, competing policies that made PV electricity the more expensive option compared to fossil fuel electricity, poor quality installations, which undermined confidence in technology, etc. [44, 45]. Even when projects had received financial aid from donor agencies and only required users to pay for the electricity used and for maintenance, inability to pay rendered PV electricity inaccessible and projects became obsolete sooner than the predicted end-of-life, when parts could not be sourced, or the batteries could not be replaced. Batteries, mostly lead acid at the time, were one of the most quoted reasons for failure.

The emergence of solar home systems that are much smaller and therefore cheaper changed the trajectory of electricity access for Africa. Solar Home Systems (SHSs), 0.1 – 25 W, are small systems that include a PV panel, a charge regulator, and a lead acid battery that are sold as a unit [46]. The surge in rural electrification that saw over 20 million people gain access to lighting electricity every year in Africa in the past ten years was largely driven by solar home systems [14]. The systems enjoyed better success, benefitting from the lessons learned from previous installations, as well as lower prices for PV panels as the technology had matured, lower capital cost that came with smaller PV panels, and an emergence of flexible payment options supported by mobile-phones [46, 47]. The systems have been deployed in many rural areas and have contributed to an increase in access to electricity in Africa, from 34% of the population in 2000 to 43% in 2017 [9].

Similar success has been quoted elsewhere in the world; in Central and South America, electricity access rose from 87% in 2000 to 97% in 2017, and in Asia access rose from 67% in 2000 to 89% in 2017 [48]. In India, apart from the solar home systems, subsidies were introduced to encourage installation of domestic PV systems (0.1 – 10 kW), through the regulatory framework introduced in 2003 [12]. Close to half a billion people gained access to electricity in India this way. Affordability and technical support were important in promoting access to electricity.

Unlike in India, the majority of the systems used in Africa are pico-sized (0.1 – 10 Wp) [48], and while they have improved access to lighting electricity, they are still too small to provide the energy required to power other basic household needs such as refrigerators, kettles etc, and contribute meaningfully to improving quality of life [41]. The International Energy Agency explains that people who use pico-sized solar systems are considered to be below the minimum threshold for electricity access [49]. Their use, therefore, does not preclude the need for other fuels for cooking and heating.

Solar cookers were introduced in India and China as an alternative to using scarce biomass and improving indoor air quality [50, 51]. However, uptake was low because of the prohibitive initial

cost, and in some cases the stoves fell into disuse, in some cases because of the cultural shift that was required to use the stoves. For example a meal that would normally take 20 minutes on firewood would take up to three hours on the solar cooker, sometimes men's involvement was needed to carry the solar cooker to a sunlit area, e.g. on the roof [52]. This forced users to spend too much time cooking, and to adjust their meal times, which interfered with their daily activities. Because of this reason, better methods are still required for providing energy for domestic activities without introducing too much disruption to daily life. Currently, fossil fuels remain the most widely used for cooking in developing countries [14, 37], and the number of people who lack access to clean cooking has not changed from 2000's 2.8 billion [48]. Hence the call for clean, affordable and sustainable energy needs to also include reliability and convenience. Since electricity remains one of the most convenient forms of energy in today's world, rural electrification is still imperative, but it needs to move past provision of electricity for lighting and small electronics.

The International Energy Agency projects an increase in energy demand of 119 TWh by 2030, 88% of which is in rural areas, and two thirds of which is demand for renewable energy sources [48]. This means energy storage will remain vital in order to use the renewable energy. The World Energy Outlook report estimates an additional $52 billion annual investment is required in order to ensure energy for all by 2030, 95% of which is required for Sub-Saharan Africa [48]. Energy storage constitutes 80% of an off-grid installation [53], therefore, a large portion of the investment will go to energy storage, even with the price of most battery types (lead acid, lithium ion, advanced lead, redox flow) projected to fall by 50 – 60% by 2030 [54]. Except for redox flow batteries, the cost of battery storage rises sharply with increase in size, as such, solid batteries are often too expensive for household applications [55, 56].

Of the 991 installations using electrochemical energy storage listed on the DOE energy storage database, 100 use redox flow batteries (as many as those that use lithium type batteries), confirming that redox flow batteries have firmly entered the energy storage market, and their applications ranges in size from 5 kW to 15 MW, with a 20 MW project under construction [26]. It is reasonable to conclude that they will continue to be significant, especially since they offer other advantages in comparison to solid batteries (section 2.2.6).

Redox flow batteries are not only capable of storing large quantities of energy (MW), they have milliseconds response times to changes in demand and supply, as shown in the examples in Table 1-1 [29]. Redox flow batteries are designed to operate with 100% discharge and are tolerant to storage at full or partial charge [23], unlike lead acid batteries which require float charging to counter self-discharge and prevent partial charge storage, [57] and lithium ion batteries, whose

life is extended by limiting discharge to 80% depth of discharge and storing at 40% depth of discharge [58]. Unlike lithium ion batteries, redox flow batteries can safely tolerate temperatures up to 40°C, which are common during tropical summers experienced in most African, South Asian, South and Central American countries. For example, a vanadium redox flow cell showed improvement in voltage efficiency from 87.6% to 90.5% when operated at 25° C and 55° C, respectively. The same cell displayed a negligible decrease in charge efficiency from 95.6% at 25° C to 93.7%, at 55°C [59]. Zinc bromine redox flow batteries also display a similar tolerance for temperature [60]. They have also been shown to perform steadily at current rates of 15 A, 30 A and 60 A [61]. The charge efficiency remained constant between 70% - 74% at 60 A. Operation temperature around 40°C for lead acid batteries would result in premature battery failure [62]. Another critical advantage redox flow batteries have significantly higher life cycles than the lead acid battery, for example, the vanadium redox battery with 10,000 – 200, 000 cycles [54] while a valve regulated lead acid battery will last at best 5,000 cycles if used within the constraints of standard operating conditions [63].

Due to the clear advantages that redox flow batteries present, a lot of research is focused on their development and improvement [64]. The soluble lead flow battery (SLFB) is one such redox flow battery which, during charge, deposits lead and lead dioxide on the positive and negative electrode respectively, from the same electrolyte [65]. This feature of the battery means that the battery does not require strict control of electrolyte cross-over, and hence does not require expensive membranes [66, 67]. The vanadium redox and the zinc bromine flow batteries both require control against cross over [65] and both these batteries have been demonstrated and are now commercial [26]. Since the SLFB doesn't require expensive membrane separators and allows use of the same electrolyte tank for both redox couples, and potentially reduces complexity of the system design, it could compete well with the two commercial chemistries, and it is worth pursuing as an option of energy storage for rural electrification and off-grid stationary applications.

The soluble lead flow battery uses an electrolyte of lead (II) ions dissolved in methanesulfonic acid and electrodes on which lead and dioxide are deposited during charging. Conventionally, researchers have used reagent grade lead (RGE) methanesulfonate and methanesulfonic acid to make the electrolyte, and graphite electrodes. Graphite is an earth abundant material compared to other common electrodes materials, such as platinum, gold, and titanium compounds. Therefore an opportunity to use other material sources for the lead (II) ions other than reagent grade chemicals for the electrolyte was sought. A way to extract expended lead acid battery electrode material to use as lead (II) ion source for the SLFB electrolyte was investigated for this reason.

Lead acid batteries, which were widely used with the PV projects piloted between 1960 and late 2000s are now less popular for stationary applications, and made 100 of the 991 listed electrochemical energy storage projects on the DOE global energy database [26]. Despite this they still remain widely used for starting lighting and ignition (SLI) and remain competitive with newer technologies [68]. As a well understood technology that has existed for over a century [69], with a well stablished manufacturing and recycling infrastructure [70] lead acid batteries are expected to continue to stay competitive in supporting the growing demand for vehicles.

Lead acid batteries represent the most recycled product in the world, with a recycle rate of over 95% in Europe [71, 72]. Nonetheless recycle rates vary country by country and are even more varied between developed and developing countries. While in Europe and the US recycle rates are as high as 99% [73], South Africa had lower rates at 90% in 2014 [74], and China had 38% official recycle rate [75]. A recent study estimates a 30-40% informal sector recycle rate [76]. In the latter case processes used were so inefficient that only about 60% of the lead was recovered, the rest lost during processing. Similar practices have been reported in sub-Saharan Africa, where infrastructure and policy enforcement aren't as robust, and informal recycling is rife. This results in toxic lead being released into the soil, the atmosphere, and waterways, endangering human health and contaminating the environment [77].

Growth in populations and in the consequent number of vehicles in developing countries [78] and motor bikes in Asia [75] continue to add to the use of lead acid batteries and the demand for recycling. This presents an opportunity to introduce an alternative and safer lead acid battery recycling route for developing nations, as well as another stream of use for the expended lead acid batteries that are likely to come into the recycle market.

1.3 Aims and Objectives

The vision for this project was to advance the use of renewable energy sources by providing and/or improving energy storage, to improve energy access for grid-isolated communities. The aim of the project was to create an electrolyte for the soluble lead redox flow battery using sustainable means, which also provided an additional avenue of safely recycling lead acid battery.

To achieve the above aim, the following objectives were defined.

I. Find sustainable options for the active material used in the soluble battery
    a. Reclaim/reprocess lead to use as electrolyte for the battery
II. Test viability of the solution produced as an electrolyte option and
III. Compare produced electrolyte to conventional SLFB electrolyte

IV. Investigate cycle control as a method to improve cycle life

1.4 Structure of Thesis

This thesis is divided into six chapters, the first two being the thesis introduction and the subject literature review, while the next three present results from the work carried out. The final chapter presents conclusions and further work recommendations.

The first chapter introduces the motivation for the research, where the need for energy storage to enable use of renewable energy sources, in response to climate change is presented. The chapter introduces the research work and places it in the context of world challenges of climate change and the need for sustainable solutions to energy requirements, that do not add the current problems of environmental pollution. The chapter also looks at the advancement of redox flow batteries in stationery energy storage, especially renewable energy storage and recognises their suitability for domestic energy storage.

The second chapter provides a literature review of the state of redox flow batteries, which are a practical option for enabling use of renewable energy sources in the abatement of and mitigation against climate change. The chapter also takes a brief look at lead acid batteries, which were historically used with pilot photovoltaic systems in developing countries. Since the batteries are still being used as storage for low power renewable energy storage in developing countries, the chapter looks at how the batteries are being recycled in the said areas. It identifies rampant unsafe recycling practices as a problem requiring a solution.

Chapter three presents a novel method for extracting lead from expended lead acid batteries to make electrolyte directly for the soluble lead battery. The method offers an opportunity to extend recycling of lead acid batteries in areas where existing recycling practices are not sufficient to prevent environmental contamination and human poisoning. The method also presents a low-cost way to source electrolyte for the soluble lead redox battery, enhancing its advantages as a potentially low-cost redox flow system for storage of electricity from renewable energy sources. The chapter concludes with results that show that lead (II) ions were successfully extracted from the spent lead acid batteries.

Chapter four compares the electrolyte made in chapter three to conventional electrolyte made from reagent grade chemicals when cycled in both static and flow cells. The chapter evidences the superior performance of the novel electrolyte in static cells and equivalent performance in flow cells, indicating that the novel electrolyte is suitable as an electrolyte for the soluble lead battery.

In the same chapter the reason for this is established through elemental analysis, where the additives and impurities in the electrolyte result in the performance of the recovered electrolyte. The chapter further explores the electrochemical activity of the novel electrolyte through cyclic voltammetry, confirming its suitability as an electrolyte for the soluble lead battery.

Chapter five presents cycling methods trialled to improve the cycle life of the soluble lead battery when the novel electrolyte is used, and demonstrates that relaxation times during cycling are a viable method for enhancing lead (II) ion speciation and therefore increasing cell cycle life. Finally, chapter six presents the thesis conclusions and evidence of novel findings, makes recommendations from the work done and the discoveries made, as well as recommendations for future work.

1.5 Author's Contribution to Novelty

The author claims novel contribution in the following areas, relevant to the area of study:

Table 1-2: Author's claim of novel contribution of new knowledge in soluble lead flow batteries research and supporting publications and chapters.

Ref.	Claim of novelty and supporting section in thesis	Supporting publications	Status of publication
1.	I have created an innovative method using methanesulfonic acid (MSA) and hydrogen peroxide to recover lead from spent lead acid batteries for making electrolyte for a soluble lead redox flow battery, discussed in chapter 3.	Orapeleng, K., Wills, R., and Cruden, A., Developing Electrolyte for a Soluble Lead Redox Flow Battery by Reprocessing Spent Lead Acid Battery Electrodes. Batteries, 2017. 3(2): p. 15. DOI: https://doi.org/10.3390/batteries3020015	Published
2.	I have compared the recovered electrolyte to reagent grade electrolyte, and found the recovered electrolyte's performance to be better than that of reagent grade electrolyte, both in static cells and flow cells. Discussed in chapter 4. I have also carried never before done elemental analysis of the reagent grade electrolyte and discovered that it contains nickel, which is detrimental to battery performance. Also discussed in chapter 4.	Orapeleng, K., Wills, R.G.A., and Cruden, A., Performance of recovered and reagent grade electrolyte in a soluble lead redox cell. Journal of Energy Storage, 2018. 20: p. 49-56.DOI: https://doi.org/10.1016/j.est.2018.08.017	Published
3.	I have studied different cycling regimes for the soluble lead cell and optimised open circuit relaxation time between charge and discharge to maximise cycle life and charge efficiency. Discussed in chapter 5.	Orapeleng, K., Wills, R.G.A., and Cruden, A., Impact of open circuit relaxation period on soluble lead redox cell cycle life and efficiency. In preparation for submission to: Journal of Energy Storage, 2019.	Draft intended for Journal of Energy Storage

Chapter 2 Literature Review

2.1 Electrochemical Energy Storage

There are two types of electrochemical energy storage cells; galvanic cells spontaneously convert chemical energy stored in their active material into electrical energy through oxidation/reduction reactions, when their electrodes are connected to a load. Primary batteries are galvanic cells. The second type, electrolytic cells, require external energy applied to the electrodes to force redox reactions to occur. Secondary batteries are electrolytic during charging and galvanic during discharge. During discharge, oxidation occurs at the negative electrode, called the anode, when electrons are released and they flow via an electric circuit to the positive electrode, called the cathode, which is reduced by accepting the electrons. The ions formed at the negative electrodes are released into the electrolyte, the solution that acts as a conductor for the ions to move from one electrode to another within the cell [79]. Overall electrical neutrality is maintained by movement of ions in the electrolyte. Figure 2-1 is an example of a galvanic cell that has electrolyte in separate containers, with a salt bridge that is the conduit for the charged ions.

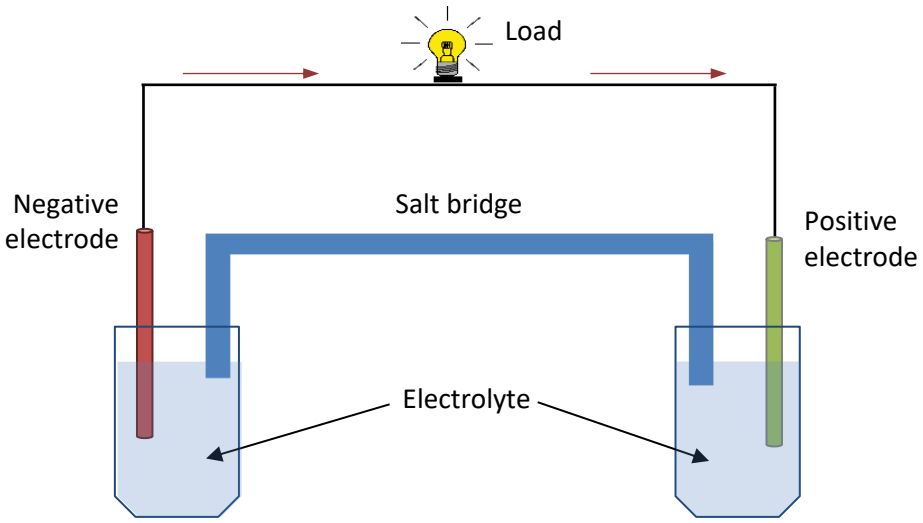

Figure 2-1: A galvanic cell spontaneously discharging to a load connected to the electrodes. The salt bridge allows ion exchange and maintains overall system neutrality.

Electrolytic cells convert electrical energy to chemical energy when an external electricity source is applied to the electrodes of the cell, forcing electrons to flow in the opposite direction and create non-spontaneous redox reactions at the electrodes. Rechargeable batteries, also known as

secondary batteries, are examples both galvanic and electrolytic cells. The process is irreversible for primary batteries, which are galvanic cells but not electrolytic.

The earliest known electrochemical energy storage device was invented by Alessandro Volta in 1793 , and was the simplest cell that converted electrical energy to stored chemical energy and discharged by converting stored chemical energy to electrical energy [80]. A battery is a collection of such units that can be arranged in series to increase voltage produced or in parallel to increase current drawn [81]. Currently there are many types of batteries available on the market, both primary and secondary type. Because they are unsuitable for renewable energy storage, this report will not discuss primary batteries.

Rechargeable batteries are used in many applications including electronic devices, where lithium ion type batteries are preferred for their high power density, sodium sulphur batteries, used in energy storage applications where operating temperatures are in the range 160 – 500 °C. For low cost, low energy requirements where charge and discharge can be controlled, and a float charge is easy to provide such as in starting, lighting and ignition in the automotive industry, and in uninterruptible power supply, lead acid batteries are commonly used [82]. Redox flow batteries are suitable for integration with renewable energy sources and for grid applications because of their quick response and economies of scale.

Rechargeable batteries commonly used for stationery applications are lead acid batteries, lithium ion battery types, redox flow batteries, and the sodium sulphur battery. Of the 1, 557 energy storage project listed on the US Department of Energy global energy storage database, 61% are electrochemical [26]. 100 are redox flow, 100 lithium ion, 86 sodium sulphur, 30 sodium-nickel-chloride (ZEBRA), 26 advanced lead and 43 are a combination of lead acid battery and electrochemical capacitor. The remaining projects are unspecified.

Redox flow batteries are in different stages of development and the next section gives a brief overview of the various chemistries. Each has their own unique advantages, apart from the generic advantages that redox flow batteries share, as well as challenges that make them the subject of current research.

2.2 Redox Flow Batteries

Redox flow batteries (RFB), shown in Figure 2-2 are a type of electrochemical energy storage technology which convert energy to chemical energy to store it and covert it back to electricity during discharge. In a divided redox flow cell such as the one shown, the electrolyte for each half-cell is stored in a separate tank and dedicated circulating pumps cycle the electrolyte between the

half-cell and the dedicated tank. Half-cell redox reactions occur at each electrode, one side releasing electrons and ions that are used on the other side to complete the redox reactions. The electrons flow via an external circuit while the ions move through an ion exchange membrane which separates the two half cells. Since unlike conventional batteries, the electrolyte is stored outside the cell in reservoirs, power, which is determined by the electrolyte concentration and the electrode area, is decoupled from the capacity, which is determined by the size of the tanks. The power capacity can be increased by increasing the electrode area or stacking the cells while energy capacity is increased by increasing electrolyte volume [83].

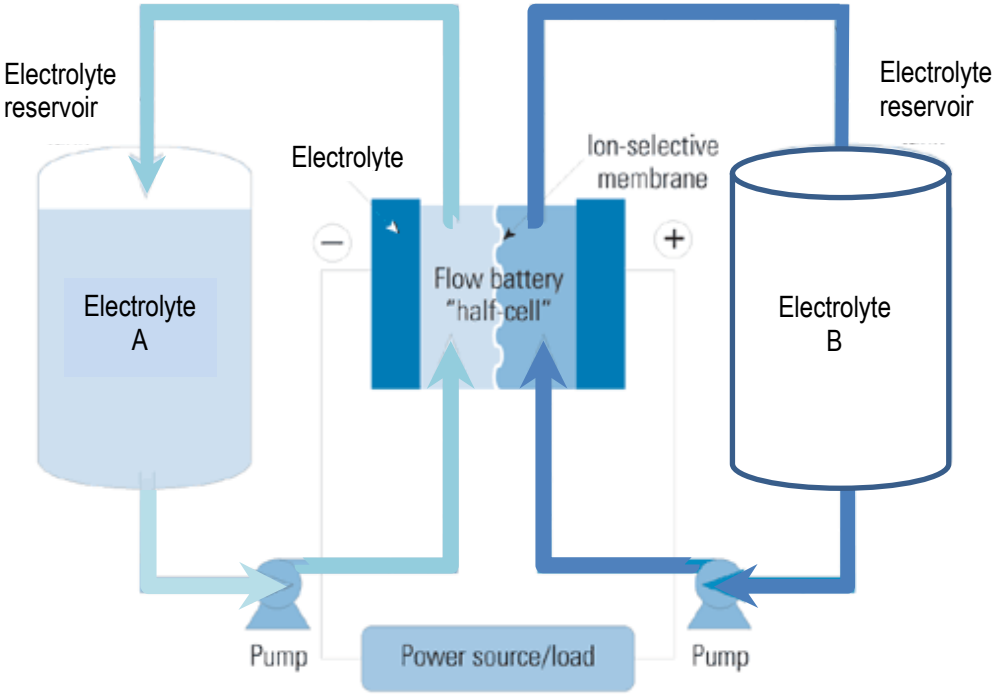

Figure 2-2: Membrane-divided redox flow battery showing electrolyte, electrolyte reservoir, electrodes, membrane separators, electrochemical half-cells, pumps and pipes and the load/power source.

Physically, redox flow batteries consist of the electrochemical cell, which includes the electrolyte reservoir, electrodes, membrane separators, current collectors and the cell chamber; the hydraulic system which includes the pumps, pipes and controls needed to move the electrolyte between the electrochemical cell and the tanks, Figure 2-2. The third component that completes a redox flow battery is the power electronics used to control charge and discharge, monitor States of Charge and State of Health, and interface with the power source and the load. Despite the different components, the scale up of redox flow batteries is simple and does not require extra

electronics for voltage stabilisation as is required in other batteries [84]. Even though the different components contribute to a large footprint and bulkiness, causing a low specific energy density, redox flow battery benefit from economies of scale; energy storage gets cheaper per Wh as storage capacity increases. In the past, RFBs tended to be too expensive at small scale, making them preferable for large-scale projects, where economies of scale increase profitability. Recently the price of the vanadium redox flow battery (discussed later) reduced and became comparable to that of lithium ion batteries [54].

Redox flow batteries offer several advantages over conventional solid batteries:

1. They can be discharged to 0% state of discharge with no damage to capacity, they have higher cycle-life, ranging between 10s of thousands to 100s of thousands, they display round-trip efficiencies up to 85% and become cheaper with increasing storage capacity [29, 85].

2. It is possible to keep the redox flow batteries for long term at low states of charge without affecting capacity or state of health, since the electrolyte is kept separate from the electrodes, which prevents self-discharge [83].

3. Redox flow batteries are tolerant to high temperatures, and even perform better between 303 K – 313 K, temperature ranges at which the lead acid battery loses capacity rapidly and the lithium ion battery runs the risk of thermal run-away and explosion.

4. Temperature and state of charge (SoC) monitoring can be achieved while the battery is online by circulating electrolyte through a monitoring cell [84].

5. This provides information required to respond quickly to energy fluctuations, and rapid charge, accomplished through replenishing the electrolyte [86] and their ability to discharge to 90% depth of discharge within millisecond with no adverse effect on capacity [29], allow this.

6. Power and energy are decoupled in most redox flow batteries, with the power determined by the size of the electrodes, while energy capacity is determined by the size of the tanks [87]. Therefore, unlike solid batteries, an increase in energy does not result in a direct reduction in power due to losses introduced by stacking more cells. Conversely, increasing power by stacking the cells in redox flow batteries does not necessarily result in bulkier batteries as it does in solid batteries [88].

7. Because of point 7 above, scale up does not result in an increase in complexity for redox flow batteries, while it does for solid batteries, which require additional control electronics to balance charge in stacked systems [84].

All these make redox flow batteries more suitable for isolated stationary applications and renewable energy storage and where rates of charge, depths of discharge and temperature fluctuations may be difficult to control while deep discharge may be necessary to meet energy demand. Because of their economies of scale, redox flow batteries are suited for community energy storage where a collection of households are connected to a mini-grid and can share the cost of the electricity. Redox flow batteries cab be supplied as plug and play modular units that have capacity for remote monitoring, which may be advantageous for communities without local technical support.

2.2.1 Standard Redox Flow Battery Properties

Similar to other electrochemical systems, RFB developers and researchers look for cell chemistries that offer the widest standard electrode potential that give the highest cell potential possible, stable reagents that are soluble in common electrolytes, low cost and non-toxic reactant materials, minimum complexity, short transverse distance between electrodes, increased electrode area and moisture control depending on the system. Several types of redox flow batteries exist, each addresses the issues in a different manner.

Like any other electrochemical storage device, redox flow battery development seeks to optimise the different qualities that are desirable in a battery. Often it is not possible to get all the qualities in one battery, therefore a trade-off is made based on the application [83]. These properties include:

Reversible redox couples so that the cell can be rechargeable. The reactive species should be stable and soluble in acid, and the redox couples' potentials as wide as possible to offer a high cell voltage. The cell voltage contributes to the battery power.

The cost of the electrolyte, electrodes, membrane separators, and materials used to make the battery should be affordable and reasonably easy to obtain. Maintenance requirements should be as low as possible, and where there are any replacement parts they should be low cost and easy to obtain.

System complexity: Ideally the battery should not require any more operations that add to the complexity. For instance, temperature or pressure control should not be a critical feature of the system as to render the battery unsafe to use without them. Instead a lessening of inherent complexity should be sought after.

Toxicity and recyclability: Ideally the electrolyte should not be toxic, and as many of the component parts as possible should be recyclable. The chemicals in use should be noncorrosive,

to keep the cost of the component materials as low as possible. The electrolyte should be as easy to handle as possible.

Developments in redox flow batteries have highlighted several design considerations which may add to the cost and complexity of a redox flow system:

I. Loss of moisture from one half cell to another, which may occur as ions carry water molecules across, or by osmosis due to concentration gradient across the membrane. In some cases compensation for water loss and water gain in the two half cells may be necessary.
II. Species migration, which can result in contamination across half cells and needs to be controlled. In such situations, a suitable membrane needs to be in place that can stop movement of species in one direction but not in another. Or that can selectively allow some species and not others.
III. IR losses due to resistance or low conductivity of the electrolyte contribute significantly to loss in energy efficiency. Ideally the inter-electrode distance should be as short as possible to shorten the distance that ions travel within the cell. Another route for IR losses in a redox flow battery could be due resistance across an ion exchange membrane, or at the current collection system. While the ideal design allows all the current to travel from the electrode directly to the current collector and out via the manifold, it is never possible to obtain a perfect system that can adequately insulate parts of the system that are not intended for conduction. This means that some of the current is lost, lowering the total power output from the stack [85]. The cell discharge voltage is then lower than the theoretical cell voltage .

Careful design of the flow distribution in the cell can improve efficiency, ensuring that electrolyte flow is laminar and constant across the face of the electrode, therefore optimally utilising the available active area.

Ponce de Leon [83] also highlights several features common to batteries that may be used to compare performance of different chemistries:

Voltage efficiency, $\eta_V = \frac{V_{cc}(Discharge)}{V_{cc}(Charge)}$ 2-1

Charge efficiency, $\eta_C = \frac{Q(Discharge)}{Q(Charge)}$ 2-2

Energy efficiency, $\eta_e = \frac{E(Discharge)}{E(Charge)}$ 2-3

Power efficiency, $\eta_P = \frac{IV_{cc}(Discharge)}{IV_{cc}(Charge)}$ 2-4

These compare charge and discharge to give an indication of how much of the input is extracted as output.

Redox flow batteries can be divided into several types depending on the phases of reactant and products of charge/discharge processes. The four types are:

I. Classical, membrane divided redox flow batteries where the redox couples remain solvated during both charge and discharge. For example, the all-vanadium [87].

II. Half flow battery and half metal battery with a membrane, such as the zinc/cerium battery, where a phase change occurs at one of the electrodes [89]. The capacity of the flow battery is stored in both the electrolyte and the electrodes.

III. Half unitized fuel cell; the positive electrode is air breathing and similar to a PEM fuel cell, where a catalyst system is required for oxygen evolution and reduction during charge and discharge respectively, for example, the zinc-air battery [90].

IV. Metal, metal oxide redox flow battery where both electrode reactions involve depositing solid phases during charge, for example, the soluble lead flow battery [66].

2.2.2 The Common Redox-Active Species Redox Flow Battery

The classical membrane divided redox flow battery as represented in Figure 2-2 uses a common active species on both half-cells. The reactants and products stay solvated during all states of charge and discharge. Each half-cell has a separate electrolyte with dedicated pumps and reservoir. A membrane separator prevents the two electrolytes from mixing. The all vanadium redox flow battery, invented by NASA in the 1930s and developed by Maria Skyllas-Kazacos and colleagues in New South Wales, Australia during the 1990s/2000s, is an example [87, 91]. It uses Vanadium (II) (V^{2+}) and Vanadium (III) (V^{3+}) couple at the negative electrode and Vanadium (IV) (V^{4+}) and Vanadium (V) (V^{5+}) couple on the positive electrode. A mixture of vanadium and sulphuric acid electrolyte is used, at a recommended concentration of 3-4 mol·dm^{-3} [87], held in separate reservoirs and circulated by separate pumps for each side. Commonly used electrodes are graphite. Current flows when V^{4+} reacts with water, VO^{2+} is oxidised to VO_2^+, liberating two protons (2-6). The water dissociates to a hydrogen proton, which travels across the cation-permeable membrane to maintain electrical neutrality of the system. The electron flows to the negative electrode via an external electrical circuit where it participates in the reduction of V^{3+} to V^{2+} [92];

Negative electrode: $V^{3+} + e^- \leftrightarrow V^{2+}$ 2-5

E°= -0.26 V (vs SHE)

Positive electrode: $VO^{2+} + H_2O \leftrightarrow VO_2{}^{+} + 2H^{+} + e^{-}$ 2-6

E°= 1.0 V (vs SHE)

Overall reaction: $VO^{2+} + H_2O + V^{3+} \leftrightarrow V^{2+} + VO_2{}^{+} + 2H^{+}$ 2-1

E_{cell} = 1.26

The battery uses solvated active species therefore power and energy capacity are independent of each other; the power is determined by the electrode and stack size, while the energy is determined by the concentration of the active species and the size of the tanks. Because both sides contain vanadium, albeit in different oxidation states, crossover of ions does not result in contamination, and the solution has an infinite shelf life, eliminating need for disposal. The battery offers other advantages generic to RFB, such as decoupled energy and power capacity, rapid recharge by replenishing electrolyte, rapid (millisecond) response, safer due to separation of reactive materials, longer life span, and relative low cost [83, 85, 93].

However due to crossover of the protons, the concentration of one side gets progressively lower than the other side which reduces overall efficiency and necessitates periodic balancing of the electrolyte. Vanadium also precipitates when kept in solution over time; Wen, Xu [94] recommend a concentration range of 1.5 to 1.6 mol·dm^{-3} for vanadium and that of 4 – 5 mol·dm^{-3} for sulphuric acid to increase electrolyte stability. Vanadium is a toxic substance and as such not very desirable for sustainable applications. Hydrogen evolution also poses a problem [93].

Despite these limitations, the vanadium redox flow battery is already in commercial use. Of the 100 listed redox flow batteries on the DOE global energy storage database, 71 are vanadium based [26]. A 4 MW, 6 MWh demonstration project in Hokkaido, Japan was reported to give over 200,000 cycles in 2016 [23, 29].

The redox reactions are highly reversible, and therefore, theoretically, the battery has an unlimited cycle life. Reversibility of the battery means the electrolyte, which is fully enclosed, theoretically has an infinite shelf life, eliminating need for disposal. The battery has been demonstrated to have up to 200,000 cycles before failure. Other advantages include; rapid recharge by replenishing electrolyte, rapid (millisecond) response, safer due to separation of reactive materials, longer life span, and easy temperature control through changing the

2.2.3 Half Flow Battery-Half Metal Battery Redox Flow Battery

The Zinc/Cerium is an example of a hybrid between a flow battery and a metal battery, where a phase change occurs at one of the electrodes. The electrolyte and one of the electrodes store the battery capacity. The Zinc/Cerium hybrid redox flow battery was developed by Plurion Inc. UK in the 2000s [95]. It has a high theoretical cell voltage of >2.4 V, resulting from the wide difference between zinc and cerium redox couples standard cell potentials [96, 97]. The cell employs the positive Ce^{3+}/Ce^{4+} couple and a very negative Zn^{2+}/Zn couple [89]. Redox reactions at the electrodes are as shown below [96].

Negative electrode: $Zn^{2+} + 2e^{-} \leftrightarrow Zn +$ 2-7

E°= -0.76 V (vs SHE)

Positive electrode: $Ce^{3+} \leftrightarrow Ce^{4+} + e^{-}$ 2-8

E°= 1.44 V (vs SHE)

Overall reaction: $2Ce^{3+} + Zn^{2+} \leftrightarrow Zn + 2Ce^{4+}$ 2-9

E_{cell} = 2.2 V

Methanesulfonic acid (MSA) is used as both the negative electrolyte, where it contains zinc ions, and as the positive electrolyte where it carries cerium ions. The solubilities of Ce^{3+}, Ce^{4+} and Zn^{2+} in MSA are 2.4 mol·dm^{-3}, 1.0 mol·dm^{-3}, and 2.1 mol·dm^{-3}, respectively. This is convenient as MSA can be used either side as an electrolyte and the high solubilities could support good reaction kinetics.

A divided zinc cerium flow cell using methanesulfonic acid either side was constructed and tested under different conditions [96]. Cyclic voltammograms of the two half-cells showed that the zinc half-cell peak current increased tenfold when the electrolyte temperature was increased from 22°C to 60°C, while that of the cerium half-cell doubled. Charge/discharge cycles also yielded a maximum energy efficiency of 71.4% when the electrolyte was 50°C, suggesting that the zinc-cerium flow cell operated better at higher temperatures. However, the cerium half-cell voltammograms also indicated a tendency for oxygen evolution at higher temperatures. Two-dimensional and three-dimensional positive electrodes were tested to increase cell performance without exacerbating hydrogen and oxygen evolution. Carbon felt three-dimensional electrodes gave coulombic and voltage efficiencies of 92% and 68%, respectively. But the electrode cycle life was too short due to poor carbon adhesion and low conductivity. A platinised titanium mesh electrode performed better than all the electrodes tested. An optimum electrolyte flow velocity

of 7.8 $cm \cdot s^{-1}$ was identified and the optimum electrolyte composition for the cerium half-cell was 0.8 $mol \cdot dm^{-3}$ Ce^{3+} and 4.0 $mol \cdot dm^{-3}$ MSA. Higher concentration of Ce^{3+} required for higher energy density were not possible because cerium precipitated at > 4.0 $mol \cdot dm^{-3}$ MSA. On the other hand, Ce^{4+} required the high MSA concentrations for solubility [96].

An undivided cell was also investigated, which had the advantage of eliminating the need for separate electrolyte tanks and the associated pipes, as well as the requirement of a separating membrane, which could be expensive, while also increasing resistance within the cell, contributing to cell overpotentials [89]. The undivided cell operated at room temperature, unlike the previous zinc-cerium flow cell, and had an electrolyte concentration of 0.2 $mol \cdot dm^{-3}$ cerium, 1.5 $mol \cdot dm^{-3}$ zinc, and 0.5 $mol \cdot dm^{-3}$ MSA. The acid concentration (and consequently, the cerium concentration) was kept low to prevent hydrogen evolution at the zinc electrode. The cell had a cell voltage of 2.1 V, which was lower than theoretical but higher than other redox flow cells like the vanadium redox flow cell. The cell yielded up to 76% and 90% energy and coulombic efficiencies, respectively. On the other hand, the low cerium concentration limited energy density to 11 $Wh \cdot dm^{-3}$. The cell also lost capacity after 7 hours when the zinc deposited at the negative electrode at 20 $mA \cdot cm^{-2}$ for 30 minutes dissolved into the electrolyte, confirming zinc self-discharge in a common electrolyte [89]. The low MSA concentration of 0.5 $mol \cdot dm^{-3}$ accelerated zinc corrosion [Leung, 2014]. Dendrite growth on the zinc electrode also inhibits

Recent advances include the use of an alkaline electrolyte (0.5 $mol \cdot dm^{-3}$ Na(OH)) on the negative side (zinc side), an acidic electrolyte (0.1 $mol \cdot dm^{-3}$ $Ce(SO_4)_2$ + 3.0 $mol \cdot dm^{-3}$ MSA + 0.1 H_2SO_4 $mol \cdot dm^{-3}$ + 0.25 $mol \cdot dm^{-3}$ Na_2SO_4), on the positive side (cerium side) and a solid sodium ion exchange membrane ($Na_3Zr_2Si_2PO_{12}$) [98] . The alkaline electrolyte circumvented zinc corrosion and improved the cell voltage by widening the difference in the standard electrode potential between the two half-cells. The electrolyte on the cerium side contained 0.1 $mol \cdot dm^{-3}$ sulfuric acid to provide the higher proton concentration required to dissolve Ce^{4+}, without limiting the solubility of Ce^{3+}. The same cell used a solid sodium ion exchange membrane which allowed sodium ions to shuttle between the two sides while preventing crossover of the aqueous electrolytes as well as inhibiting zinc dendrite penetration to the cerium half-cell [98].

2.2.4 Half Unitized Fuel Cell Redox Flow Batteries

The half-unitized fuel cell redox flow battery has an air breathing positive electrode similar to a PEM fuel cell, where a catalyst system is required for oxygen evolution and reduction during charge and discharge respectively, and the metal is converted between solid and aqueous ions, respectively [90]. The zinc-air battery is an example. Like other metal-air batteries, it has high

energy density because the cathode uses air, which makes the electrode lighter than in other redox batteries, and contributes to an overall light cell and high energy density [90]. The battery also uses oxygen, which is free, as well as benign earth abundant metals. This makes the battery potentially cheaper and safer than others [99, 100]. Metal-air batteries also have a long shelf-life, due to the slow kinetics of the redox reactions [100]. The alkaline zinc-air battery is made of a zinc metal anode held in a gel form, and a cathode made of porous carbon and saturated in an alkaline electrolyte. The cathode is porous to allow air to filter through it and it is thin, which leaves most of the space for the anode. An air separator separates the anode from the cathode. The air-breathing cathode has a catalyst to help with the reduction of oxygen to hydroxyl ions. At the anode zinc metal reacts with the hydroxyl to form a zinc hydroxide. The hydroxide then decays to zinc oxide. [101]

Positive electrode: $\frac{1}{2}O_2 + H_2O + 2e^- \leftrightarrow 2OH^-$ 2-10

E°= 0.401 V (vs SHE)

Negative electrode: $Zn \leftrightarrow Zn^{2+} + 2e^-$ 2-11

: $Zn^{2+} + 2OH^- \leftrightarrow Zn(OH)_2$ 2-12

E°= -1.25 V (vs SHE)

Overall reaction: $Zn + \frac{1}{2}O_2 \leftrightarrow \mathrm{ZnO}$ 2-13

$E°_{cell}$ = 1.65 V

The design of the cathode is essential for the operation of metal air batteries and the zinc air battery has a layered cathode design. The cathode has a current collector made of foam or porous material, which is saturated in electrolyte. A catalyst layer is next, which is permeable to hydroxyl ions. The reduction of oxygen to hydroxyl ions occurs on this layer, with the help of catalyst. The catalyst layer in zinc air batteries is made of carbon particles loaded with either Pt, Pd, Ag or MnO_2 catalyst. The gas diffusion layer is next, and it is made of carbon felt, it has medium porosity and is waterproof to prevent leaking. Air diffuses through this layer into the cell. The cover of the cell on the cathode side is porous to allow air to enter the cell. For the zinc-air battery, the anode is made of zinc held in a gel-like suspension

Challenges faced by metal-air batteries include slow kinetics on both the reduction and evolution of oxygen, which results in high over-potentials for both reactions [90]. Zinc also has high kinetics, which causes fast dissolution and corrosion of the zinc electrode. The fast dissolution of zinc results in dendrite growth and subsequent shorting in the cell, as well as degradation of the

electrode, which causes gradual capacity loss. Even though the zinc-air battery has a nominal cell voltage of 1.65 V, in operation discharge voltage only goes to 1.0 V. The anode and the cathode also degrade with cycling, resulting in short life cycles [90]. Other challenges faced by metal-air batteries include a tendency for the metal anode to self-discharge when it reacts with hydroxyl ions to form a metal hydroxide and hydrogen. At high currents, the battery polarisation reverses, making the battery unsuitable for high power applications. Carbon dioxide adsorbs to the carbon cathode and forms carbonate crystals, which blocks the air passage for oxygen and damages the surface of the cathode. Water transpiration can also occur on the cathode, which can cause flooding or drying of the cathode. [101]

2.2.5 Metal, Metal Oxide Hybrid Redox Flow Battery

In this type of battery both electrode reactions involve depositing solid phases during charge, for example, the soluble lead flow battery. A metal and metal oxide are deposited on the electrodes during charge and dissolved back into the electrolyte during discharge. The battery uses the same electrolyte for both redox couples and hence precludes the need for two electrolyte tanks and two sets of circulating tanks. Lead, an earth abundant and highly recycled metal is the active material, while MSA is the electrolyte used in which lead ions are dissolved. The system is relatively cheap compared to other systems that use rare metals and expensive corrosion resistant materials. The materials used are also non-volatile, which makes the system safe.

The soluble lead battery uses MSA electrolyte to deposits lead and lead dioxide solids on to the negative and positive electrodes, respectively. The system is based on the two redox couples Pb/Pb^{2+} and Pb^{2+}/PbO_2 [102]. The reactions, shown below, indicate discharge towards the right and charge to the left [66, 103].

Positive electrode: $PbO_2 + 4H^+ + 2e^- \leftrightarrow Pb^{2+} + 2H_2O$ 2-14

E°=1.46 V (vs SHE)

Negative electrode: $Pb \leftrightarrow Pb^{2+}\ 2e^-$ 2-15

E°= -0.126V (vs SHE)

Overall reaction: $Pb + PbO_2 + 4H^+ \leftrightarrow 2Pb^+ + 2H_2O$ 2-16

E_{cell} = 1.586 V

During charge lead metal is deposited on the negative electrode while lead dioxide is deposited on the positive electrode. During discharge the deposit from both electrodes is stripped back into the electrolyte as Pb^{2+} ions [104]. The soluble lead flow battery is further explored in section 2.3.

2.2.6 Comparison of Redox Flow Batteries

A summary of the redox flow batteries covered in the previous subsection is presented in Table 2-1 and in **Error! Reference source not found.**. The tables highlight the differences in kinetic and thermodynamic properties, the performance of existing batteries from literature, as well as each battery's unique design considerations. The state of development for each is indicated.

Table 2-1: Comparison of redox flow batteries to the lead acid battery

Technology	**Energy density**	**Cell Voltage /V**	**RT Energy Efficiency /%**	**Cycle Life: @DoD**	**Cost /€·(kWh)$^{-1}$**	**Optimum Operation Temp. /°C**	**Self-Discharge /% left after 12 hrs**	**Response Time**	**Material Recycle Rate /%**	**References**
Lead Acid Battery [c]	24-45 Wh·kg^{-}	2	75-85	200-2000 70% - 30%	50-150	20-25	(3-4% self-discharge per month)	Sec-min	99	[81, 82, 105]
All Vanadium	15-25 Wh/g at 50 mA·cm^{-2}	1.26	80-85	12,000 :100%	140-450 [93]	5-40	100%	millisec	~90	[91] [106] [107] [93, 108]

Technology	**Energy density**	**Cell Voltage /V**	**RT Energy Efficiency /%**	**Cycle Life: @DoD**	**Cost /€·(kWh)$^{-1}$**	**Optimum Operation Temp. /°C**	**Self-Discharge /% left after 12 hrs**	**Response Time**	**Material Recycle Rate /%**	**References**
Zinc-Air	(180-200 Wh·kg^{-1})	->2	52% @ 50 mA·cm^{-2}	200 (C/15)	360 - 400	25 - 50	92%	sec	>80%	[100, 106]
Zinc-Cerium [a]	11 – 20 Wh·m^{-3}	2.1 - 2.4	75		Est. 100		0%			[65, 89, 96]
Soluble Lead RFB[b]	50 Wh·m^{-3}	1.8	65%	2,000 @ C/10, sc [109] :100%	175-250	25-50 [ref]	100%	Sec	>90	[102, 104, 110, 111]

[a] – an undivided cell

[b] – 64 cm² bi-polar electrode cell, cycled at 120 – 140 mA·cm^{-2}

c – at 20°C and C/20

RT – Round Trip

Cycle life has a bearing on reliability of the technology and in operational cost of the system. As shown in Table 2-1, flow batteries offer higher cycles than lead acid batteries. In addition to this, the soluble lead redox flow battery offers the following sought-after advantages:

1. Use of highly recyclable (lead) abundant earth materials
2. Use of non-corrosive materials
3. Reversible redox couples in MSA
4. Use of the same electrolyte both sides, which results in
    a. Use of one electrolyte tank
    b. No cross-contamination
    c. No need for expensive ion separators

Also from Table 2-1:

- Lead acid batteries are the cheapest (€50-150/kWh) and also have the lowest self-discharge (3-4%/month). They also display the lowest cycle life at higher depths of discharge. The cycle life only becomes comparable with other batteries when the discharge is kept shallow at 30% DoD. The lead acid battery, along with the lithium ion battery, and all vanadium redox flow battery, have the highest round trip efficiency.
- The lithium ion battery is the most energy and power dense battery in the market. This has contributed to its success in mobile devises, which, though small, require high power supplies. The lithium ion also has the highest cell voltage at 3.8 V.
- The largest operational project among the compared chemistries is the lithium ion battery at 40 MW.
- Redox flow batteries have the highest cycle life with little effect on capacity, which is desirable quality for repetitive operation. They also operate at 100% DoD, which maximises energy efficiency. Though the nickel iron battery has a nominal cycle life of about 2,000 cycles, it has the highest service life at over 85 years of known batteries in operation.
- Except for the nickel iron and the lithium ion batteries, all the chemistries are known to be toxic. Lead acid batteries have the highest recycle rate of all at 99% recycle rate [110].

Table 2-1 indicates that different batteries have different strengths and weaknesses. Of particular interest is the soluble lead redox flow battery. As indicated the lead acid battery is the cheapest type of battery. This is due to the well-established infrastructure for its manufacture as well as its recycling. The very high recycle rate has contributed to a lowering in lead costs, and very little virgin material is used in making lead acid batteries. The soluble lead redox flow battery could benefit from this property of lead. Apart from that, the battery would use MSA, which is a benign acid that supports lead solubility as upto 2.4 $mol \cdot dm^{-3}$ methanesulfonate. The lack of a membrane and use of one electrolyte, which was demonstrated with a zinc/cerium cell [89] and a soluble lead redox flow cell [66], offer the benefit less bulkiness compared to other flow cells because of fewer tanks, and consequently, a lighter system. If a membrane were to be used, species migration and cross-contamination would still not be a concern, hence low cost

membranes can be used. The soluble lead redox flow battery has all these advantages and is therefore worth exploring as an energy intensive and low-cost option to energy storage.

2.3 Soluble Lead Redox Flow Battery

The soluble lead flow battery was introduced as a membrane-less cell which uses MSA as the electrolyte [102]. The battery attracted attention because not only does it use earth abundant lead, which has a 99% recycle rate in Europe and the US [73], it uses the same electrolyte on both electrodes, theoretically eliminating the need for a separating membrane, reducing the number of electrolyte tanks and circulating pump sets. It also uses carbon electrodes, which are the cheapest material for electrodes available for redox flow batteries.

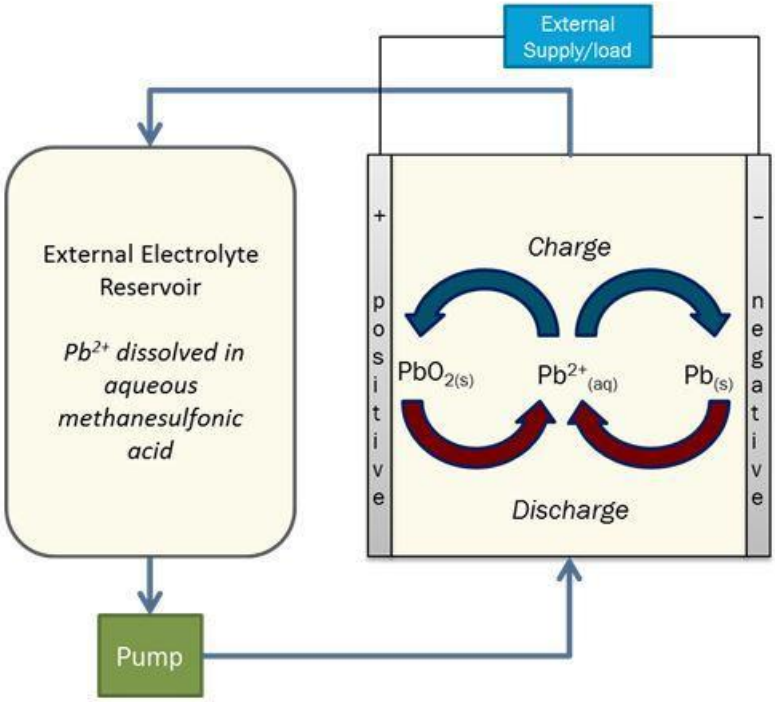

Figure 2-3: Non-divided soluble lead redox flow battery principle of operation [112].

2.3.1 Redox Couples and Operation

The system, shown in Figure 2-3, is based on the two redox couples Pb/Pb^{2+} and Pb^{2+}/PbO_2 [102]. It employs controlled deposition (charge) and dissolution (discharge) of solid lead and lead dioxide on the negative and positive electrodes respectively. The reactions, shown below, indicate charge towards the right and discharge to the left [66, 103].

Positive electrode: $Pb(CH_3SO_3)_2 + 2H_2O \leftrightarrow PbO_2 + 4H^+ + 2e^-$ 2-17

E°=1.46 V (vs SHE)

Negative electrode: $2Pb(CH_3SO_3)_2 + 2e^- \leftrightarrow Pb$ 2-18

E°= -0.126V (vs SHE)

Overall reaction: $2Pb(CH_3SO_3)_2 + 2H_2O \leftrightarrow Pb + PbO_2 + 4CH_3SO_3H$ 2-19

E_{cell} = 1.586 V

During charge lead metal is deposited on the negative electrode while lead (IV) oxide is deposited on the positive electrode. During discharge the deposits from both electrodes are electrochemically converted to Pb^{2+} ions solvated back into the electrolyte [104].

Good reversibility for the Pb^{2+}/Pb couple has been demonstrated; 0.92 ratio of charge/discharge with minimal over-potentials and hydrogen evolution [66]. The PbO_2/Pb^{2+} couple was found to have moderate kinetics and was a source of cell efficiency. While the charge/discharge behaviour was not as simple as for the other couple, the ratio was found to be 0.90; reasonable for renewable energy applications. Good electrodeposition of lead and lead oxide was also demonstrated. Low concentrations of lead (0.3 mol·dm^{-3}) in high concentrations of MSA (3.0 M) were found to result in a high conductivity of electrolyte; 0.338 $(\Omega.cm)^{-1}$, potentially reducing cell resistance. On the other hand lead solubility in MSA was found to peak at 2.5 mol·dm^{-3} of the acid [66]. A cell made of 10 mm x 20 mm electrodes and 1.5 mol·dm^{-3} lead methanesulfonate and 0.9 mol·dm^{-3} MSA yielded 1.78 V open circuit voltage and maximum coulombic and energy efficiencies of 85% and 65%, respectively [102].

2.3.2 Electrolyte and Lead Solubility

Electrolyte for the soluble lead redox flow battery was developed by Hazza et al. [66]. The electrolyte is made from lead methanesulfonate and methanesulfonic acid. Pb^{2+} ions have a solubility limit of 2.6 mol·dm^{-3} in methanesulfonate at room temperature [113], which makes this electrolyte attractive for maintaining lead in solution when required during cell operation. Methanesulfonic acid replaced flouroboric acid and other toxic and volatile acids which have been suggested for soluble lead cells, because methanesulfonic is benign and non-corrosive at low concentrations. It also provides the conductivity required to conduct ions in a storage cell.

2.3.3 Thermodynamics and Cell Capacity

The work done by any electrochemical cell is electrical, and can be deduced from the cell's change in Gibbs Free Energy, ΔG°. At standard conditions, the cell's Gibbs Free Energy is also equal to its formal potential, $E°_{cell}$. where, during discharge;

$$E°_{cell} = E_{cathode} - E_{anode} = \Delta G° \quad \text{2-20}$$

$\Delta G° = E°_{cell}$ = 1.460 V – (0.126V) = 1.586 V

For a cell with an initial $[Pb^{2+}]$ = 0.7 mol·dm^{-3} and [MSA] = 1.0 mol·dm^{-3}, the cell equilibrium potential at room temperature (25°C) can be estimated using the Nernst equation as follows:

$$E = E°_{cell} + \frac{RT}{nF} ln \frac{[Pb^{2+}]}{[H^+]^4} \qquad 2\text{-}21$$

$$E = E°_{cell} + \frac{2.3RT}{nF} log \frac{[Pb^{2+}]}{[H^+]^4}$$

E = 1.586 + 0.0296log(0.7) = 1.58 V

The energy capacity of a redox flow battery is given by:

$$Capacity = \frac{nFC}{3600} \ (Ahr \cdot dm^{-3}) \qquad 2\text{-}22$$

At standard conditions, based on equation 2-19, the Nernst equation for the soluble lead cell is:

$$\mathrm{E}_{cell} = \mathrm{E}°_{\mathrm{cell}} + \frac{2.3RT}{2F} \log \frac{[H^+]^4}{[Pb^{2+}]} \qquad 2\text{-}23$$

This equation allows us to determine the cell voltage, it also indicates that the cell voltage decreases with subsequent discharges. On the first charge, the proton concentration increases four fold, while $[Pb^{2+}]$ decreases by half. If all the lead dioxide is reduced to Pb^{2+} on the discharge cycle, then the next charge cycle would result in the same cell voltage. However, if the stripping efficiency of lead dioxide is lower, then $[Pb^{2+}]$ in the electrolyte reduces and therefore the next charge cycle has a higher cell voltage.

2.3.4 Challenges Faced by the Soluble Lead Flow Battery

The soluble lead battery faces challenges such as current inefficiencies that cause material build-up in the positive half-cells, limit its cycle life. This curtails the advantages stated before.

Tests on a 64 cm^2 and a 100 cm^2 cell revealed that cycle life was limited to less than a hundred cycles [114]. Dendrite growth on the negative electrode, lead dioxide creep (deposit growth of positive electrode material); and debris build up resulted in shorting and eventual failure of the

scale up cells [114] and a 10 cm by 10 cm flow cell [115]. In time the build-up of solids depletes Pb^{2+} ions out of the electrolyte, and causes eventual gas evolution. Hydrogen peroxide has been proposed to recover the Pb^{2+} ions lost as solid-build up [116]. But use of hydrogen peroxide dilutes the electrolyte and results in O_2 build-up in the cell, necessitating Pb^{2+} and acid replenishment as well as offline operation.

Voltammetry studies on the PbO_2/Pb^{2+} couple and those made on test cells revealed that the PbO_2/Pb^{2+} redox couple had limited current efficiency that resulted in insufficient stripping of deposit off the positive electrode, which subsequently resulted in deposit growth on both electrodes [117]. The conductivity of PbO_2 deposit was also found to be an order of a magnitude smaller than that of lead. Oury, Kirchev [111] later confirmed that at higher concentrations of acid (>1.0 M) passivation of the positive electrode occurred. The phase structure of lead oxide was also found to affect energy efficiency, where deposition of α-PbO_2 on the positive electrode resulted in better performance than β-PbO_2 [117].

On the negative side, at current densities of 10mA·cm² and 20 mA·cm², the deposit grain was uniform and compact, but at higher current densities (50 mA·cm² and 375mA·cm²) the deposit grew as dendrites and as the distance between the electrodes reduced, current density would surge at the sites with the shortest distances between the electrodes, causing more rapid dendrite growth [118]. Overtime the dendrites caused short-circuiting between the cells and resulted in cell failure. Studies also revealed that smoother deposit resulted in better adhesion and less dendrite growth [119]. Additives were introduced to prevent dendrite growth on the negative electrode and improve deposit conductivity and morphology on the positive electrode. A membrane was introduced to prevent the additives intended for one side from affecting the other side of the cell.

2.3.5 Electrodes

Carbon-based electrodes have been used historically in lead electroplating because carbon is inexpensive, highly conductive and electrically stable. Different electrode materials and configurations have been tested for cells that use lead methanesulfonate and methanesulfonic acid as electrolyte [114]. Electrodes materials tested for both the Pb/Pb^{2+} and the PbO_2/Pb^{2+} redox couples cell include reticulated vitreous carbon (RVC), carbon felt, and nickel foam (ibid). Different combinations and configurations included making composites of the two or more of the materials as well as using them as coatings on a PTFE substrate. Ibid found that different electrode materials had little to no effect on the cell voltage and performance [114].

Pletcher and Wills [102] tested a 2D custom-made electrode by bonding nickel foam and reticulated carbon onto a carbon and high density polyethylene (C-HDPE) composite substrate. The nickel foam layer was scrapped off to increase electrode surface area, and the electrode was used for lead dioxide deposit. Even though the electrode was found to be stable in highly oxidising potentials, lead dioxide adhesion was poor, and the deposit layer would get dislodged from the electrode during cycling [120]. The nickel foam also dissolved into the electrolyte, poisoning the electrolyte and causing a fall in charge efficiency [120].

2D Sigracell graphite electrodes, manufactured by the SGL Group, are stable in acidic and corrosive media, and are good conductors of electricity. The electrodes are made of a graphite flouro-polymer. The polymers have a low electrical resistivity at 270 Ω·mm. The surface of the electrode is smooth and can be made smoother or rougher by polishing with Buehler micro-cloths of different smoothness.

2.3.6 Membrane Separators

Even though it was introduced as an undivided cell [66], it was found that the soluble lead flow battery performance was limited by low kinetics at the positive electrode and deposit roughness at the negative electrode [119]. Subsequently additives were introduced to each side to improve performance, which necessitated separation of the two half-cells and dedicated electrolytes [119] [67]. The membrane also kept the two sides physically separate, ensuring that even if deposit and debris grew in the cell, short-circuiting was prevented [67]. Because prevention of crossover was not essential for the SLFB operation, selectivity of the membrane was not critical. The ability of the membrane to maintain ionic balance and to have low resistance so as not to introduce significant ohmic losses into the cell was essential and therefore prioritised [67].

Four membrane separators were compared for the SLFB; AmerSil FF60 microporous separator, Fumatech FAP-450 anion exchange membrane, Fumatech VPX-20 anion exchange membrane, Fumatech F-930 Cation exchange membrane, and the DuPont Nafion 115 Proton exchange membrane [67]. The anion exchange membranes revealed the least sensitivity to changes in electrolyte Pb^{2+} content, from 0% to 100% Pb^{2+} utilisation. The membrane resistance remained low at different Pb^{2+} and MSA concentrations. The Fumatech VPX-20 anion exchange membrane had the lowest ohmic losses at all concentrations, and was therefore the best performing.

2.3.7 Electrolyte Additives

To prevent and/or reduce the growth of deposit in the soluble lead cell, both organic and inorganic additives were tested to improve deposit morphology and size. Inorganic additives including Ni^{2+}, Fe^{3+}, and Bi^{3+}, were introduced to the PbO_2/Pb^{2+}side to improve deposit morphology as well as improve deposit conductivity. Sodium ligninsulfonate and HDTMA, among others, were tested [119] to counter dendrite growth on the negative electrode.

2.3.7.1 Sodium Ligninsulfonate Additive

Sodium ligninsulfonate was used to improve the smoothness of lead deposit on a nickel rotating disk electrode [119]. The levelling effect was noticeable even at current densities as high as 375 $mA \cdot cm^{-2}$. In a cyclic voltammetry cell, the additive caused an increase in lead nucleation over-potential from 35 mV vs SCE (Saturated Calomel Electrode) to 60 mV vs SCE. However an increase in additive concentration did not result on further increase on the over-potential. The limiting current remained unchanged and the charge efficiency remained close to 100%. The beneficial effect was most apparent at both 50 $mA \cdot cm^{-2}$ and 375 $mA \cdot cm^{-2}$, where the deposit was more compact and uniform compared to deposit without the additive. The additive was deemed successful in improving compactness and uniformity of the lead deposit [119].

The same research found that on the positive electrode, at concentration above 1.0 $g \cdot dm^{-3}$, increase in additive content resulted in a lowering of both current density and charge efficiency, while the nucleation overpotential increased from 120 mV to 157 mV at 5 $mA \cdot cm^{-2}$. Above 1.0 $g \cdot dm^{-}$ the sodium ligninsulfonate had a detrimental effect on the positive redox couple reactions. However, below 1.0 $g \cdot dm^{-3}$ the effects were insignificant. The lead dioxide deposit layer on a vitreous carbon electrode was unaffected by addition of the additive, remaining compact and uniform with or without the additive [119].

In a flow cell, increasing the concentration of the additive resulted in compact deposit grains on a 2D negative electrode. The spaces between the grains reduced for a cell containing 0.2 $g \cdot dm^{-3}$ sodium ligninsulfonate compared to one without, and were completely eliminated for a cell with 5 $g \cdot dm^{-3}$ sodium ligninsulfonate. On a 2D positive electrode, the deposit was smooth and compact without the additive, and became more so when 1.0 $g \cdot dm^{-3}$ was added to the electrolyte. At 5.0 $g \cdot dm^{-3}$ additive, gas evolution was observed on the electrode surface. On a 3D negative electrode, lead was deposited on the surface of the electrode but did not reach the electrode pores, both with and without additives. On a 3D positive electrode, the deposit of PbO_2 penetrated the foam and was well connected, ensuring good conduction throughout the electrode. Hence for the 3D positive electrode, the additive achieved the intended purpose of

improving conduction. The results for both the positive and negative electrodes were similar at higher cycle rates [119].

While the additive sodium lignosulfonate inhibited the formation of dendrites on the negative electrode and created an unbroken deposit layer of lead dioxide on a 3D electrode, thereby ensuring continuous conduction, the additive decomposes over extended battery use.

2.3.7.2 Bismuth Additive

A bismuth additive was used on a divided static cell, and resulted in a 20 fold improvement in cell cycle life [121]. The study added 10 mmol·dm^{-3} Bi^{3+} to electrolyte at the positive electrode and observed an improvement on the stripping peak of lead dioxide, which tended to flatten and broaden with cycling beforehand. They also observed a shift in the equilibrium potential for the PbO_2/Pb^{2+} couple from 1.440 V vs SCE at 0% content to 1.651 V vs SCE at 20 mmol·dm^{-3} Bi^{3+}. Since the stripping peak of PbO_2 tends towards more negative values with cycling, adding Bi^{3+} improved the coulombic efficiency of the couple. Bismuth is also credited with improving contact and therefore conductivity between PbO_2 particles in a lead acid battery positive electrode material (PAM) [121].

2.3.7.3 Hexadecyltrimethylammonium Additive

From literature, the Hexadecyltrimethylammonium (HDTMA) additive caused a shift of lead deposition towards negative potentials by 110 mV on a Pb/Pb^{2+} cyclic voltammogram, implying the additive adsorbed to the electrode surface and prevented lead deposition [104]. The same study showed that at current densities of 10-30 mA·dm^{-3}, the lead deposit layer was compact and uniform with or without the HDTMA additives, but at higher current densities; 40-50 mA·dm^{-2}, without the additive large randomly orientated angular crystals formed on top of the layer of the deposit. Presence of the additive resulted in a uniform compact layer even at 40-50 mA·dm^{-2} Pletcher, Zhou [104].

At 1.5 mol·dm^{-3} Pb^{2+} concentration the formation of dendrites was pronounced, even at 25 mA·dm^{-2}. However addition of 5 mmol·dm^{-3} of HDTMA resulted in smoother deposit. At 2.4 mol·dm^{-3} MSA the deposit was rough, the grains had what appeared to be smaller crystals forming on top of the large boulder like crystals. The effect of the additive was diminished compared to cells with 1.0 mol·dm^{-3} MSA, which had well adhered and compact deposit at all current densities, 25, 50 & 70 mA·dm^{-2}. At 0 mol·dm^{-3} MSA the deposit remained uniform and

compact, growing smaller at low current densities (25 $mA \cdot dm^{-2}$). For all cases without acid, secondary crystals formed on top of the larger deposit grains [104].

This additive resulted in compact and uniform lead deposit on the negative electrode. The additive improved the uniformity and smoothness and prevented dendrite growth and had negligible effect on the cell voltage, at a concentration of approximately 5 $mmol \cdot dm^{-3}$. It also had no adverse effect on the positive electrode. The effect was maintained over a large range of concentrations for MSA and Pb^{2+}; but was more prominent at low concentrations of both the acid and Pb^{2+}.The effect of high acid concentrations was most significant on the size and shape of the lead deposit and the authors cautioned against using MSA concentration above 2.0 $mol \cdot dm^{-3}$. An initial concertation of 1.2 $mol \cdot dm^{-3}$ Pb^{2+} and 0 $mol \cdot dm^{-3}$ MSA was recommended, with a current density of 100 $mA \cdot dm^{-2}$.

2.3.8 The Future of the Soluble Lead Flow Battery

The soluble lead flow battery has the potential to offer a cheaper option to kWh – MWh-sized energy storage, thereby enabling more penetration of sustainable energy sources into the grid as well as providing energy storage for grid-isolated areas. With an undivided configuration, it requires fewer components in terms of pumps and tanks. It also operates well with carbon electrodes, which are low priced compared to electrodes used by some redox flow batteries. Even though the battery still faces many challenges that prevent it from progressing to demonstration stage, the advantages it presents are still significant, and as such researchers continue to invest time and effort in its improvement. This research contributes to this effort in advancement of the battery as another option for renewable energy storage.

2.4 The Conventional Lead Acid Battery

The most commonly used secondary battery is the lead acid battery, which has been in use since 1860, after invention by Plante in 1859 [69, 122]. Its long life of development has made it a well-understood technology, and a well-established infrastructure for supply, distribution, collection of expended batteries and recycling infrastructure, are in place world-wide [123]. Because of this, the battery has remained popular, especially for SLI applications. Even with the entrance of newer battery technologies into the market, between 1990 and 2016 the lead acid battery had maintained a yearly lead in battery markets, and in 2016 it and was at 90% GWh market-share [68]. It is predicted that the lead acid battery will remain relevant for Starting Lighting and Ignition (SLI) applications for the next 10 to 20 years even as the developed world slowly transitions to electric vehicles [110]. In Africa, where the number of cars grew by an average 5.1% annually

between 2007 and 2013, lead acid batteries are expected to grow in proportion or more steeply because of other uses apart from SLI [78].

2.4.1 Operation of Lead Acid Batteries

Lead acid batteries are made of a lead negative electrode and a lead oxide positive electrode, a porous membrane and a 33.3% (at full charge) dilute sulphuric acid as the electrolyte [123]. The electrodes are made of a lead oxide (PbO) paste, called leady oxide because it contains lead, dilute sulphuric acid, lead alloy grids covered with the paste and electricity connections made of lead. During discharge the lead electrode releases two electrons and combines with sulphate ions from the electrolyte to form Pb^{2+} sulfate, while the lead (IV) electrode accepts the two electrons and combines with sulfate ions to form solid lead sulfate. During charge the opposite happens, the lead sulfate on the positive electrode loses two electrons and is converted back to lead (IV) oxide, while that on the negative electrode gains two electrons and is converted back to solid lead [124]. As the electrolyte loses and regains sulfate ions between charge and discharge concentration of the electrolyte changes between charge and discharge. At high States of Charge the concentration of the electrolyte is highest and at low States of Charge the concentration of the acid is lowest. The specific gravity of the electrolyte is used to estimate the battery state of charge. The forward reactions in equations 1, 2 and 3 below indicate discharging [123]:

Negative electrode: $Pb + {SO_4}^{2-} \leftrightarrow PbSO_4 + 2e^-$ 2-24

E° = -0.36 V (vs SHE)

Positive electrode: $PbO_2 + 4H^+ + {SO_4}^{2-} + 2e^- \leftrightarrow PbSO_4 + 2H_2O$ 2-25

E° = 1.69 V (vs SHE)

Overall reaction: $Pb + PbO_2 + 2H_2SO_4 \leftrightarrow 2PbSO_4 + 2H_2O$ 2-26

E_{cell} = 2.05 V

This redox reaction results in a spongy lead at each discharge, which increases the electrochemical surface area [125].

The lead acid battery is employed in a wide variety of applications, the most common being starting, lighting and ignition (SLI) in vehicles. In this role the lead acid battery provides short bursts of high current and should ideally be discharged to a maximum of 20% depth of discharge and operate at ~20°C, to ensure a good cycle life, about 1500 cycles or three to five years of operation [126]. Another role is in providing power for forklifts and similar cartage vehicles in which the cell has thicker electrodes, and therefore has more energy but provides low power

levels. In this configuration the battery is more rugged. Application in renewable energy storage has been rising for the past 40-50 years, in which the battery needs to store more energy over a longer period and hence, like in the forklift batteries, the electrodes are larger and the battery is more rugged [125].

Lead acid batteries are widely used and easy to assemble, making them readily available in many localities. Their widespread use has resulted in comparatively low prices [124] and an infrastructure so widespread that they are available in almost all countries. Recycling infrastructure and practices are also well established. The United States boast a recycle rate of 99% [127] while the International Lead Association estimates a global recycle rate of 80% for all lead products. Progress in their manufacture has ensured that they are available in many different sizes and shapes. Their availability, low cost at $1.50 - $2.00 per watt [128], reputation as a tried and trusted technology and well established recycle infrastructure make them a dominant battery technology worldwide.

Lead acid batteries have a relatively low cycle life of circa 500 cycles, low energy density (50 Wh/kg), suffer from stratification and sulfation borne of intolerance to storage at partial charge, are intolerant to over-discharge beyond 10.5V for a 12 V battery, and to operating temperatures above 25°C [56, 126, 129]. For this reason, lead acid batteries are unsuitable for uncontrolled applications, such as isolated renewable energy storage, where it may be impossible to provide a continuous trickle charge. Where they have been applied, their early failure due to abuse resulted in escalating costs for the energy supply systems [39, 130].

2.4.2 Failure Modes of Lead Acid Batteries:

For lead acid batteries, charge regulators have been employed to control charge and discharge, to maintain float charge, prevent heat runaway and cell drying, and to equalise charge in stacked cells [62, 126, 131, 132]. These controls improve cycle life and ensure safe operation of lead acid batteries. The softening and loss of Positive Electrode Material (PAM) in a lead acid battery is a natural failure mode that progresses with battery use [126]. With continued cycling coherence between the materials of the positive electrode lessens and eventually the material disintegrates and no longer participates in electrochemical activity [133]. Use and abuse of the battery can accelerate this failure mode, when the battery is over-charged [126]. Charge regulators impose an End of Charge Voltage (EoCV) to prevent overcharge and premature PAM loss. Float charge at high current also improves cycle life by increasing the cell internal temperature, which promotes coherence in PAM and promotes $PbSO_4$ dissolution to PbO_2 [126]. However cell temperatures need to stay under 60°C to prevent sulfation, therefore temperature monitoring and control is

also necessary in battery management. Sulfation also occurs when VRLA are subjected to high rates of charge (~ 18C) and discharge under partial charge conditions. High rates of discharge lead to rapid formation of lead sulfate on the surface of the negative electrode plate, which does not penetrate the plate, but instead accumulates on the surface. This reduces the effective area for electrochemical activity and blocks diffusion of H^+ into the electrode plate. This reduces the capacity of the battery. Partial charge results incomplete conversion of lead sulfate to lead, therefore the lead sulfate becomes a site for hydrogen evolution, which is exacerbated at high charge currents [132]. Charge regulators ensure that the charge and discharge rates for lead acid batteries is kept low enough to enhance battery life and protect battery capacity.

Using charge controllers to force a full charge for VRLA used in conjunction with PV energy restored the batteries' full capacity, which was otherwise lost when the batteries were operated under constant partial charge [134].

The lead acid battery requires charge control to prevent battery state-of-charge falling below a set value due to self-discharge, which if allowed could result in sulfation. Sulfation occurs when the sulfate ions of a discharged battery form large crystals which are difficult to convert back to lead and lead dioxide during charge. Discharging at high current rates cause sulfation, as does operation at temperatures above 60°C, for VRLAs. By supplying a float charge, charge controllers prevent self-discharge of stored batteries and prevent permanent damage to battery capacity.

2.5 Recycling of Lead Acid Batteries

Lead acid batteries are the most recycled product in the world and have the widest and best-established infrastructure for recycling. The International Lead Association [72] reported lead acid battery recycle rates higher than 95% for Europe and the US while the Battery Council International (BCI) reported over 99% recycle rates in the US [73]. Nonetheless recycle rates vary country by country and are even more varied between developed and developing countries. A BCI study for the US gives a lead acid battery national recycle rate of 99.3% in 2017, up from 99% in 2014 [71]; in Australia, 98% of the material used to make lead acid batteries is recycled [135]; South Africa's biggest battery manufacturer, First National Battery, reported a national recycle rate of 90% in 2014, [74]; and in 2013, 60% of China's lead acid battery recycle plants were privately owned and used informal recycle methods [75]. In the latter case processes used were so inefficient that only about 60% of the lead was recovered, the rest lost during processing.

From the 1920s, when lead acid batteries were introduced as feed into smelting plants, the informal sector was the dominant battery recycling market in the US [136]. The US informal sector consisted of hundreds of small operators who collected and sold expended lead acid batteries in a network of many different operations; the batteries were sold to service stations, garages, scrap dealers, battery breakers, private smelters and finally to industrial-size secondary and primary lead smelters [136]. The informal sector operators and the smelting plants were located in cities, close to the source of the expended lead acid batteries, and just like the informal sector of today, resulted in environmental pollution and human (and animal) poisoning [137]. In Europe, the EU Commission introduced the Batteries and Accumulators Directive in 1991, making it the responsibility of battery producers to finance the collection, treatment and recycling of batteries placed in the EU market [138]. At the time the UK had a recycle rate estimated above 90% because of an existing lucrative scrap battery collection system, however collection was fragmented and remained led by the informal sector up to 2001 [139]. Today the informal lead acid battery recycling sector resembles that of the US before the 1950s, but this time it thrives in cities and highly populated areas of non-industrialised countries [140].

The informal sector found in many developing countries includes foraging for scrap batteries in dumping sites, reconditioning batteries for reselling, manually breaking batteries, retrieving lead pastes and grids, storing, sometimes at home, and smelting in open furnaces, often out in the open in highly populated residential areas [77, 140]. No pollution controls are in place [141]. Exposure to toxins can occur during scavenging of battery material, during repurposing, where usable parts are salvaged from other spent batteries to repair another for selling; during breaking, when lead particles and lead oxide dust are released into the atmosphere on impact, during the handling of the lead battery electrodes and grids, and as fumes from the smelting. The contamination can be extensive since sulphuric acid would be spilled into the ground, polluting the soil and underground water, the dust and particulate lead can carry in the air and in ground water, and the fumes from the smelting are also carried in the air [77, 140, 141]. While the operator and sometimes their family, who may be in close proximity because operations may be located within the family home, are at high risk for contamination, the community within which the businesses operate are also at risk [141]. The risks cannot be overestimated as severe health consequences and even deaths have resulted from informal lead acid battery recycling [77, 142, 143]. Safer alternatives to spent lead acid battery handling could provide some relief for the operators and their communities.

In industrialised countries, the dominance of the informal sector in secondary lead processing ended in the 1950s, when expended lead acid batteries became the main source of lead for industrial lead smelters [136]. The industrial-size lead processing plants, which are licensed by

host countries, as well as the expended battery collection network, make up the formal lead recycling sector. Three methods are commonly used in formal lead battery recycling; pyro-metallurgy, electrolysis, and hydro-metallurgy . Pyrometallurgy uses high temperatures to melt the lead into a liquid before it is refined and alloyed, then formed into bullions that are then sold to manufactures [139]. Electrolysis uses electrochemistry to deposit high purity lead on an anode, while impurities remain in the electrolyte [144]. Hydrometallurgy involves the use of chemicals to extract lead and lead compounds out of lead-rich slags and pastes [145]. The last two methods leave mineral rich solutions which require further processing while the former leaves lead-rich slag and emits noxious gases that need to be captured to prevent environmental contamination.

2.5.1 Pyrometallurgical Recycling Method

The pyrometallurgical recycling process was developed a century ago and has not changed by much, except to improve flue gas scrubbing as well as refinery of the lead to a higher purity using less energy. Commercially, pyrometallurgy is the most widely used lead recycling method [139]. The method evolved from primary lead mining and as such has benefitted from the mining industry's historical knowledge [139]. Furnace designs in use today are adapted for secondary lead feed stock, and include sorting, crushing and separation of materials to cater for the battery feedstock [146]. The plants are fitted with modern equipment to capture sulfur oxides, nitrogen oxides, and metal hazardous air pollutants, before they are released into the atmosphere. The technology has developed into a $52 billion industry worldwide [110], where over 90% of the feedstock is expended lead acid batteries while the rest is scrap lead from other lead applications [72].

The method is supported by robust collection infrastructure that differs slightly from region to region. Across the world, even in developing areas where recycling rates are lower, the formal recycling industry follows a similar established route; collection and/or drop off points where motorists and auto dealers can drop off expended lead acid batteries; the batteries are then packaged for transportation and transferred to the relevant recycle centres; there the batteries are sorted into types to prevent mixing of dissimilar chemistries and ensure safe handling; crushing and separation follows, where the acid, battery cover, and the grids/electrode pastes are separated; melting and smelting follows at high temperature in a furnace, the lead is then refined to remove impurities, finally the lead is alloyed to suit clients' requirements, often for battery manufacture [72, 147, 148]. A visit to the H.J. Enthoven & Sons Ltd. Recycling plant in Darley Dale, UK, resulted in the schematic in Figure 2-4 showing the process flow for the formal lead acid battery recycling. The process is similar to others across the world, including South Africa's First National Batteries' process in Benoni, Johannesburg [147, 149].

Espinosa, 2004, gives examples of different technologies/processes for recycling different battery chemistries.

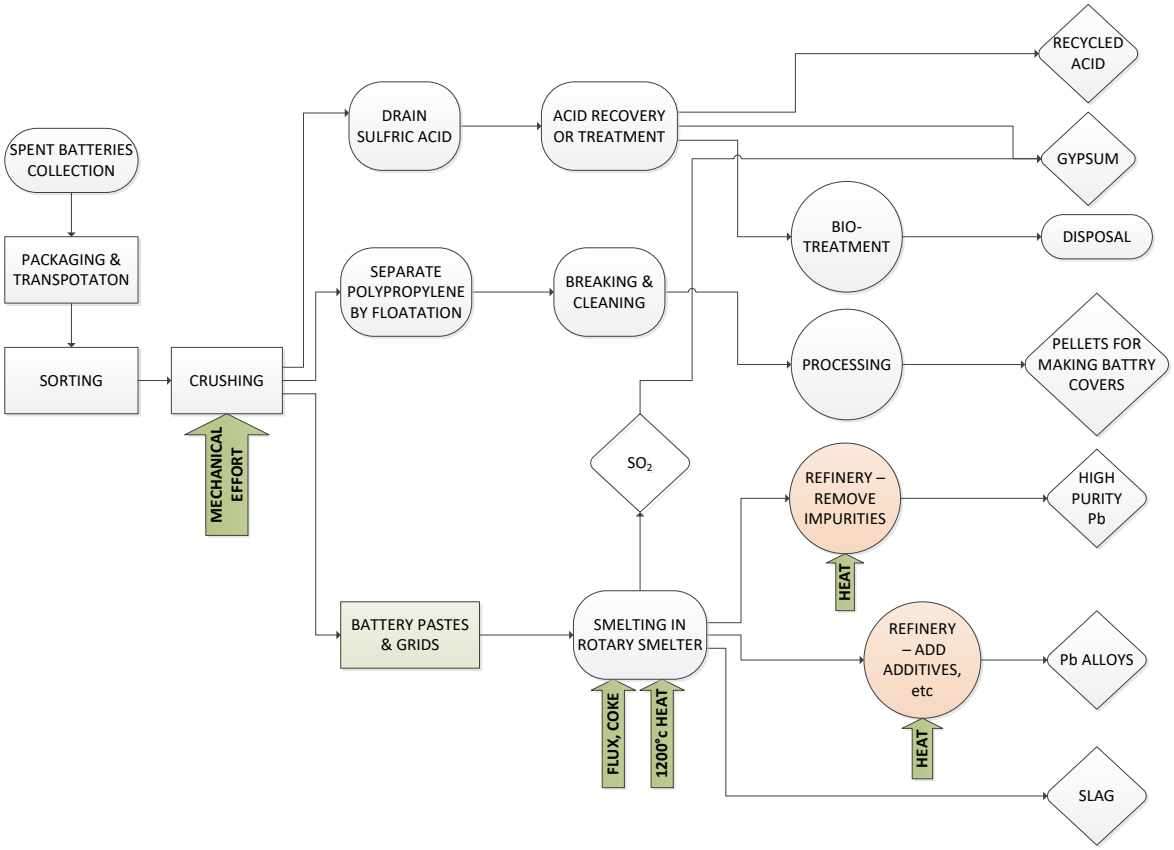

Figure 2-4: Example of pyrometallurgical lead acid battery recycling process flow fashioned after the H. J. Enthoven & Sons Ltd. Recycling plant in South Darley, United Kingdom.

The steps in conventional lead acid battery recycling are shown in Figure 2-4 and are outlined below:

1. Collection: The commercial lead acid battery recycling process has established battery collection networks throughout the world. Used batteries may be collected at motor vehicles dealerships during battery replacement or at designated collection points. [139, 147] In South Africa, First National Battery established an expended battery collection network similar to that in developed countries, with 120 drop-off points for used lead acid batteries. Nationally, a battery collection scheme is in place where a levy is imposed on anyone who buys a replacement lead acid battery without handing over the spent one. Sellers of replacement batteries are charged with imposing the levy on consumers [150].

2. Packaging and transportation: The batteries are packaged and labelled according to specific standards: UN 2794 in the UK and EU, and Code of Federal Regulations, 49 CFR Section

173.159 in the US [151], depending on whether the batteries will be sent overseas or will travel by road, before being sent to the recycle centre.

3. Sorting then crushing: Once the batteries get to the recycle facility, they are further sorted to ensure there are no unwanted and/or dangerous chemistries such as lithium ion, among the batch. The sorted batteries are then introduced into the recycle plant, where mechanical crushers break the batteries into small pieces. This process results in production of dust within the plant and workers in the area are required to wear personal protective clothing.

4. Sulfuric acid is collected and either neutralised before disposal, or used to make other chemicals such as gypsum, which is used to make products like formaldehyde for fertiliser, detergent powder, construction wallboard etc. At the H. J. Enthoven Ltd Darley site, sulfuric acid is used, along with the sulfur dioxide produced during lead smelter, to make gypsum for the fertiliser industry and/or construction plaster and wallboards. A similar process is used at the First national battery recycling facility in Johannesburg, South Africa [147].

5. Solids separation: The solids are tipped into a flotation conveyor belt, where the light polypropylene floats to the top and is collected, cleaned and processed into pellets in a different crusher. The polypropylene produced is of such high purity that it is used to make new battery covers without further refining. The pellets may also be sold to other industries that make products from polypropylene.

The heavier lead, lead sulfate and lead oxide settle at the bottom, and are sent via conveyor belt to become feedstock to the smelting process.

6. Reduction of pastes to obtain lead: The process involves smelting the lead and lead pastes in a furnace, reducing it using coke to obtain antimony rich lead, then secondary refining in specific kettles to customise the soft lead produced, either by further removing impurities, or adding specific impurities to make alloys. The lead compounds are smelted with metallurgical coke or other reducing agents to make crude lead with high antimony content. Bullion produced contains all the alloying materials found in the lead acid battery including antimony, calcium, tin, copper and barium. The smelting process produces gaseous emissions containing carbon dioxide, nitrogen oxides, and sulphur oxides. Metal-rich slag collects at the bottom of the furnace and is collected, neutralised, and discarded or sold to electrolytic or hydrometallurgy recyclers [139].

   In rotary furnaces, the smelting can be modified to a two-step process that produce a soft lead with lower antimony content [139]. Other impurities such as tin and copper can also be removed in a similar way. The H.J. Enthoven & Sons smelter uses a reverberatory rotary

furnace. In the Isasmelt, pre-treatment of the feed involves removal of sulfates, and the furnace accepts feed in any form, including slurry, powder and wet or dry agglomerates [146]. Oxygen supply and agitation facilitate rapid reaction in the furnace. The slag produced is then reduced to yield antimonial lead [139].

7. Refining is further achieved by smelting in smaller refineries where zinc is removed by vaporisation, copper and tin are removed by smelting at higher temperatures and removing by floatation. In some cases, some additives are added in controlled quantities to satisfy clients' requirements for alloying.

Modern plants are equipped to filter pollutant gases to within the recommended minimum, of 5 $mg \cdot cm^{-3}$ Pb in EU [139] and 0.15 $mg \cdot m^{-3}$ in South Africa [152]. The furnaces are made to conform to the EU's Best Available Technique (BAT) recommendations for low emissions [153, 154].Even then some plants still do not meet the minimum requirements, and have contributed to contamination of nearby populations [155]. The pyrometallurgical method is also energy intensive, since it uses smelting temperatures of 1200°C or more, and it produces slag that may contain up to 5% lead and not suitable for further processing, and which ends up in landfill [156]. Apart from this, across the developing world, this type of recycling is only a portion of the whole recycling industry. The informal sector is a significant part [157], and it contributes to environmental pollution and is a hazard to human health and life [143].

2.5.2 Electrolytic Lead Recycling Method

The electrolytic method is often suggested as a less polluting method in comparison to pyrometallurgy. It is another method used in lead recovery from lead acid batteries, which is applied to lead-rich residue from secondary lead processing [158]. Use of electrolysis for primary lead recovery began as early as 1904 using the Betts electrolytic lead refining process [159]. It was also suggested for processing lead sulfate to make lead, using either anglesite ($PbSO_4$) deposits or lead sulfate from primary lead mining or sulphuric acid production, as feedstock [144].

Electrolysis was first successfully used for the recovery of lead from lead acid battery sludge in 1983 when the Betts process was modified to prevent deposit of solid lead dioxide on the cathode during electrolysis in flourisilic acid [160]. In the Betts electrolysis process, a large anode electrode is made out of bullion lead which does not contain copper, a cathode is made of thin high purity lead and a sulfamate electrolyte is used to set up an electrolytic cell [160]. During electrolysis lead dissolves from the bullion and is deposited on the cathode. The impurities go into the electrolyte solution. The process results in high levels of lead purity and electrolyte solutions

rich in metals, no gaseous fumes are emitted, and material handling during processing is easier [161].

Nevertheless, electrolysis is energy intensive at 2–12 $kW \cdot h \cdot kg^{-1}$ [153]. The investment in energy is justified only by the demand for high purity lead and where there is significant copper to recover, the revenue from the copper sales. The method also produces toxic flourisilic acid rich in lead, which requires extensive treatment before safe disposal [153]. The method is applied to slag from pyrometallurgical processing of lead acid batteries, and rarely to the unprocessed lead acid batteries. Because of cost and intensive use of energy, it had not grown as well commercially.

2.5.3 Hydrometallurgical methods of lead recycling from spent lead acid batteries

Hydrometallurgical methods are often suggested as more environmentally friendly and less energy intensive methods compared to pyrometallurgical and electrolytic methods [158, 162, 163]. Habashi suggested hydrometallurgy as a more affordable and attainable mining method for mineral-rich developing countries to process their minerals, rather than selling the minerals as concentrates or trying to set up large pyrometallurgical mining plants that may be too expensive [161]. A similar argument can be used for the recycling of spent lead acid batteries, especially where existing methods are unsafe and a hazard to human life. A method that recovers lead for the SLFB electrolyte was developed to meet this demand, and it is described in chapter 3.

Most hydrometallurgical methods involve first leaching the minerals of interest (lead) out of sludge using chemical treatment, then desulphurisation of $PbSO_4$, and finally the solutions thus obtained are treated further with chemicals to precipitate the lead [161]. Some examples of methods that have been suggested in literature are given below. In all cases, the two steps of leaching then precipitation are evident, with some examples including desulphurisation or some more steps to arrive at the purified lead result.

One of the earliest examples of hydrometallurgy for lead pastes was a patent assigned to Gaumann [164] in 1978. The method proposed to recover lead from spent lead acid battery pastes by dissolving the lead oxide and lead sulphate out of the spent lead acid batteries in an alkaline solution and electrolysing the dissolved product to retrieve pure lead powder. The suggested alkaline solutions were metal hydroxide, ammonia, alkali metal carbonate, or ammonium carbonate solution with a concentration of at least 3 $mol \cdot dm^{-3}$. A recommended concentration of the alkaline solution was $5 > n > 12$. To improve solubility of the lead compounds in the alkaline solutions, organic compounds such as molasses, sugar, mannitol, glycerol, glycol,

neopentyl-glycol, tartaric acid, citric acid, alkali tartrates, and triethanol amine were recommended, with a preference for organic compounds with 5 to 8 hydroxyl groups. These were recommended for achieving optimum solubility of lead compounds in alkaline solutions and to achieve optimum conditions for the precipitation of lead powder during electrolysis.

Ferracin, Chácon-Sanhueza [158] tested tetrafluoroboric acid; glycerol and sodium hydroxide; and sodium potassium tartrate and sodium hydroxide for leaching and electrolysis of lead from lead battery sludge. Tetrafluoroboric acid gave the best yield of leachate and sodium hydroxide was used for desulphirisation. Compact adherent and high purity lead was obtained in electrolysis. However the process efficacy was low and most of the lead obtained was from lead dioxide only, therefore leaching lead out of the other constituent materials in the lead acid batteries was not successful.

Smaniotto, Antunes [127] used the chelating effect of EDTA on slag (6% Pb & 60% Fe content) to extract Pb by complexing it with EDTA. To prevent EDTA complexing with Fe, which has a higher complexing constant with EDTA than Pb, they used fluoride ions to block Fe complexation. To identify the Pb ions in the EDTA-Pb complex obtained, iodide solution was used to knock the lead off the EDTA complex into PbI_2. The yellow colour of the PbI_2 confirmed the presence of Pb ions in the solution.

Sonmez, 2009, [165] introduced leaching of lead acid battery pastes using citric acid, and crystallisation of the precursor obtained using sodium citrate solution. Reagent grade chemicals were used to model the PbO and PbO_2 in lead acid battery pastes. A citric acid solution was used to leach PbO and PbO_2 into crystalline lead citrate. For the PbO, an analyte to acid concentration ratio of 0.25 gave 98.75% Pb^{2+}, the highest yield and increasing the ratio to 1 yielded 50% Pb^{2+}, and 2 gave ~0% yield, indicating that increasing the analyte to acid ration reduced the yield. Increase in leaching time (10 – 60 minutes) and temperature (from 20°C to 40°C) improved the leaching yield to 99.5% and 82%, respectively.

For the PbO_2, hydrogen peroxide was used along with citric acid to leach lead. A mole ratio of 4 mols H_2O_2 to 1 mols PbO_2 yielded 100% results. A solids to liquids ratio of 1/5 was sufficient to give 98.5% yield. Increasing temperature to 40°C reduced yield to 95.2%, from 96% at 30°C and 97% at 20°C. A minimum of 60 minutes was required to convert 1 mol of PbO_2 to 4 mol Pb^{2+}, when analyte : acid = 1/5, $[H_2O_2]$: $[PbO_2]$ = 2, and temperature = 20°C, and yield was 99%.

For $PbSO_4$, Sonmez [166], achieved desulphurisation and crystallisation in one step by using sodium citrate. An analyte : acid ratio of 0.5 resulted in a maximum of 98% yield. Increasing temperature reduced yield. The paper successfully demonstrated the application of the

crystallisation method to leaching lead out of a combination of PbO, PbO_2 and $PbSO_4$, theoretically indicating that the method could be applied to lead acid battery pastes.

Reducing the number of steps required to get to the product is desirable, however, Sonmez [165, 166] used citric acid, which is expensive. To get around the cost, Zhu, He [167] presented another method that eliminated desulphurisation and they used acetic acid instead of citric acid to leach Pb out of PbO_2, Pb. They also used hydrogen peroxide to aid the reduction of PbO_2 to PbO. The method included crystallisation of the leachate by reacting it with sodium citrate ($Na_3(C_6H_5O_7)_2{\cdot}3H_2O$) to form pure lead acetate ($Pb_3(C_6H_5O_7)_2{\cdot}3H_2O$). $PbSO_4$ was also directly crystallised with the addition of sodium citrate without the leaching step nor a separate desulphurisation step. For the dissolution of PbO acetic acid was added to leach lead into $Pb(CH_3COO)_2$ first, and a ratio of 1:2 for the analyte to acid was required to complete the dissolution of PbO. Increasing the ratio of PbO:acid to 2:4 aids dissolution rate without violating the solubility limit of lead acetate. Lead was then crystallised and precipitated out of acetic acid by adding crystalline sodium citrate.

A similar method was developed by Sun, Yang [168] where they used acetate trihydrate precursor to make ultrafine lead dioxide from spent lead acid battery pastes. In this approach lead pastes from lead acid batteries were desulphirised using ammonium carbonate and then converted to lead acetate by leaching with an acetic acid solution and hydrogen peroxide. The lead acetate trihydrate precursor was crystallised and glacial acetic acid was used to remove the excess acetic acid solution. Calcination of the precursor in N_2 or air at 320°C – 400°C yielded ultrafine lead dioxide. The lead dioxide exhibited reversibility and good stability to 20 cyclic voltammetry cycles and batteries using cathodes made from the lead dioxide exhibited good cycle stability for 80 charge/discharge cycles at 100% depth of discharge.

Other methods proposed production of leady oxide from lead acid batteries using hydrometallurgy. Sun, Yang [168] proposed a four-step method where, first, lead pastes from a recycling plant were desulphirised using ammonium carbonate $(NH_4)_2CO_3$, then acetic acid was used to leach lead into lead acetate $(PbCH_3COO)_2$, next, the lead acetate precursor was crystallised by adding glacial acetic acid, which produced lead acetate trihydrate $(PbCH_3COO)_2{\cdot}3H_2O$. Finally, that precursor was calcinated in N_2 or air at 320 – 400 °C. The result was an ultrafine (200-400 nm particle size) lead oxide of the phases, α-PbO and β-PbO, as well as metallic lead.

Research in hydrometallurgical methods is ongoing and many approaches are suggested. The interest is motivated by the fact that hydrometallurgical methods result in high levels of lead purity, no gaseous fumes are emitted, use of energy is lower and material handling during

processing is easier. However hydrometallurgy still leaves undissolved lead compounds that require further processing or may require safe disposal. Approaches that use hydrometallurgy on its own are also rare and therefor the method is used in conjunction with other methods, which are even more polluting and energy intensive.

2.6 Summary

Redox flow batteries of different chemistries are being developed for energy storage, and are expected to aid in renewable energy uptake. The soluble lead flow battery could be one of the batteries that serve this purpose and, as a chemistry that uses highly recycled lead and has fewer structural components, could become competitive. The method developed in the next chapter presents an opportunity to improve the battery's competitive advantage by producing an electrolyte for the battery from discarded lead acid batteries, eliminating the need for reagent grade lead ions, and potentially advancing the chances of the soluble lead redox batteries to become competitive in storage of electricity from renewable energy sources.

Before the novel method is introduced, conventional recycle methods were reviewed. The pyrometallurgical recycle method described in section 2.5.1 is the most widely used recycle method across the world and has resulted in a 95% recycle rate of lead acid batteries across the world. However the method is energy intensive, requiring high temperatures (1,200°C) for smelting and refining of the lead and lead products. It also produces toxic flue gases as well as greenhouse gases from the thermal processes. A robust infrastructure is required not only for the smelting and refining, but also for collection and sorting of the batteries to ensure the right battery chemistry goes into the smelters. The South African recycle industry is comparable to that of industrialised countries, with established collection networks and smelting plants that use Best Available Technology [150].

However in other parts of Africa, infrastructure and policy enforcement are not as robust, and informal recycling is rife, which results in toxic lead being released into the soil and waterways, endangering human health and the environment. Reports of lead poisoning in children in Kenya and Nigeria persist, and more is needed to recycle lead safely [169]. Similar reports have been made for China [75], where bad disposal and recycle practices resulted in a reported 24% of surveyed children having blood lead content levels above 100 μg/dL, well above the reported average 4% of children worldwide [140] and much higher than the 5 μg/dL limit recommended by the Center for Disease Control and Prevention [170].

The hydrometallurgical methods which are suggested as green alternatives also produce toxic sludge which requires significant processing before disposal. Electrolysis is required to extract the

lead and other precious metals remaining in the solution. Because of the high current required for electrolysis, most of the suggested electrolysis processes are also not financially viable, and hence have not become commercial yet.

This thesis presents a novel method for extracting lead from expended lead acid batteries to directly make electrolyte for the soluble lead battery. The method, covered in chapter 3, presents an opportunity to extend recycling of lead acid batteries in areas where pyrometallurgical recycling practices may not be sufficient.

In the next chapter I outline a novel method for making electrolyte for the soluble lead battery directly from expended lead acid batteries. Unlike some of the methods outlined above, this method makes electrolyte directly out of the battery electrodes without need for desulphurisation nor crystallisation of the analyte. Unlike pyrometallurgy or electrolysis, the method does not require intensive energy use. The method achieves leaching of lead from PbO, PbO_2 and $PbSO_4$ without a separate step for desulphurisation and there is no need for crystallisation to extract lead since the lead is used in ionic form. In this way, the method has fewer steps and retains simplicity.

Chapter 3 Recovery of Lead from Expended Lead Acid Batteries

3.1 Introduction

The soluble lead redox flow system uses electrolyte made from reagent grade chemicals; Pb^{2+} ions and methanesulfonic acid [66, 102]. The electrolyte supports redox couples at both the negative and the positive electrodes, and therefore is used in both half-cells [102]. However because of inefficiencies in the cell caused by insufficient stripping of the lead dioxide during discharge, additives had to be introduced that improve conditions at either half-cell, necessitating the division of the cell so that dedicated additives can be added to the relevant side [118, 119]. Because of this, the soluble lead battery could no longer be considered undivided nor membrane-less [67] and addition of different additives to the two sides makes the reagent grade electrolyte (RGE) somewhat different either side.

The lead acid battery, which is made out of mostly recycled batteries, contains lead in the form PbO_2, PbO and $PbSO_4$. Ways to retrieve the lead from the battery pastes have been explored [165-168], apart from the traditional pyrometallurgical methods in use today [76, 171]. The traditional recycle of lead involves making bullions that are alloyed per clients' requirements, and these predominantly include lead acid battery makers. The trace elements added to the battery during manufacture are meant to enhance the properties of the lead acid battery during operation [172, 173].

Even though it appears that the lead acid battery life cycle is a closed loop, inefficiencies exist around the world in the recycle loop, causing toxic lead contaminants to spread into the environments with dire consequences for human health and life [174]. In this chapter, a method that safely recycles lead acid battery pastes while also producing electrolyte for the soluble lead flow battery out of the expended battery pastes is presented.

3.2 Methods of Retrieving Lead From Spent Lead Acid Batteries

This section presents procedures used to retrieve lead out of expended lead acid batteries. A combination of electrochemical, chemical and mechanical methods were used, where low energy and low complexity were preferred. The following subsections explain the choice of treatment methods further.

3.2.1 Discharging the Lead Acid Battery

A used lead acid battery contains compounds of lead in the form of lead oxides, lead sulfate and metallic lead as battery pastes and grids. The battery also contains sulphuric acid. Since the soluble lead redox couples release solvated Pb^{2+} ions into solution during discharge, equation 3-1, the lead acid battery could potentially be discharged in methanesulfonic acid to yield Pb^{2+} ions from the Pb and PbO_2 electrodes. Investigations to check feasibility of this were undertaken. In the proposed method, sulfuric acid was drained out of the battery, before the battery was rinsed with de-ionised water. 2.5 mol·dm^{-3} methanesulfonic acid was added to the battery, and the battery was connected to an electronic load to force discharge at C/10 (0.7 A over 10 hours).

With PbO_2, $PbSO_4$, PbO and Pb as the battery's main constituents, the discharge redox couples for each would be:

For PbO_2: $PbO_2 + 4H^+ + 2e^- \rightarrow Pb^{2+} + 2H_2O$ (3-2)

For Pb: $Pb \rightarrow Pb^{2+} + 2e^-$ (3-3)

For PbO: $PbO + H_2O + 2e^+ \rightarrow Pb + \ 2OH^-$ (3-4)

For $PbSO_4$: $PbSO_4 + 2e^- \rightarrow Pb + \ {SO_4}^{2-}$ (3-5)

The PbO and $PbSO_4$ are reduced to Pb metal and PbO_2 to Pb^{2+} ions, while Pb is oxidised to Pb^{2+} ions. Based on these reactions it was expected that all lead compounds will be converted to Pb^{2+} ions, which could be directly used as electrolyte.

With an initial acid concentration of 2.5 mol·dm^{-3}, and according to the second law of thermodynamics, the Gibbs free energy required for each reaction to occur is:

$$\Delta G = -nFE_{cell} \quad (3\text{-}6)$$

where,

$$E_{cell} = E° + \frac{2.30RT}{nF} logQ \quad (3\text{-}7)$$

$$E°_{cell} = E_c - E_a \quad (3\text{-}8)$$

and $Q = \frac{[products]}{[reactants]}$ (3-9)

The Gibbs Free Energies are:

$\Delta G_{2-18} = \ 29{,}975$ J·mol^{-1}, $\Delta G_{3-1} = -143{,}055$ J·mol^{-1}, $\Delta G_{2-17} = \ 283{,}425$ J·mol^{-1}, $\Delta G_{3-2} = \ -63{,}577$ J·mol^{-1}

The Gibbs free energies imply that the conversion of PbO and $PbSO_4$ to Pb^{2+} will occur spontaneously, while conversion of PbO_2 and Pb will require an overpotential. However this does not indicate how fast the reactions will be. The concentration of the electrolyte was measured before and after discharge at 0.7 A over 10 hours.

3.2.2 Chemically Dissolving Lead in Acid

A good electrolyte should be able to dissolve the redox couple at both charged and discharged states [175]. The RGE is made of dilute lead methanesulfonate in methanesulfonic acid. Lead methanesulfonate has a solubility of 2.6 $mol \cdot dm^{-3}$, and a conductivity of (275 $S.cm^{-2} \cdot mol^{-1}$ [113] . Therefore, methanesulfonic acid was used as the solvent for the lead and lead compounds found in the electrode material.

Compared to acids normally used as electrolytes, Table 3-1, lead is more soluble in methanesulfonic acid [113], and it is non-volatile, non-corrosive, and less toxic in solution than other electrolytes previously used for lead dissolution, such as perchloric or fluoroboric acid [176, 177]. Where nitric acid reacts with metals to evolve hydrogen, MSA does not. MSA does not attack organic compounds nor does it require pre-disposal treatment like H_2SO_4 [113]. MSA is also relatively cheaper than other common acids. A comparison of lead solubility in common acids is shown in Table 3-1.

Table 3-1: Comparison of acid on lead solvation, corrosiveness and cost.

Acid	**$[Pb^{2+}]$ / $mol \cdot dm^{-3}$**	**Ionic Conductivity in 1N Acid /$S \cdot cm^2 \cdot mol^{-1}$**	**Stable at T/ °C**	**Cost (Chemicals UK, 2020)**	**At purity**
MSA	2.600	299.95	17 – 167	(£34.40/L)[2]	(70%)
Sulfuric acid*	0.0001	444.88	10 – 300	£10.30/L	(98%)
Hydrochloric acid*	0.034	346.11	-30 – 61	£8.42/L	(36%)
Nitric acid*°	1.803	370.00 [178]	-42 – 83	£25.10/L	(69%)
Flouroboric acid	0.301	(0.61 $\Omega^{-1} \cdot cm^{-1}$)		(£60.5/L)[2]	(48%wt of 500g)

*Highly corrosive °Explosive with oxides [2]Sigma Aldrich prices at Jan 2020

Methanesulfonic acid reacts chemically with lead oxide, lead sulfate, and lead metal in the following ways to produce lead methanesulfonate:

$$PbO_2 + 2CH_3SO_3H + 2H^+ \rightarrow Pb(CH_3SO_3)_2 + 2H_2O \quad (3\text{-}10)$$

$$\mathrm{PbO} + 2CH_3SO_3H \rightarrow Pb(CH_3SO_3)_2 + H_2O \quad (3\text{-}11$$

$$Pb + 2CH_3SO_3H \rightarrow Pb(CH_3SO_3)_2 + 2H^+ \quad (3\text{-}12)$$

$$PbSO_4 + 2CH_3SO_3H \rightarrow Pb(CH_3SO_3)_2 + H_2SO_4 \quad (3\text{-}13)$$

Stoichiometrically, the solubility limit of lead methanesulfonate in MSA is indicated at 1.25 mol·dm^{-3} Pb^{2+} in 2.5 mol·dm^{-3} MSA at 25 °C [103, 113], and the solubility of Pb^{2+} is inversely proportional to the concentration of methanesulfonic acid [103]. The conductivity of electrolyte made from Pb^{2+} ions in methanesulfonic acid increases with increasing acid concentrations and reducing lead concentration [66, 179]. Conversely, more lead is required to yield more energy from the cell. The electrolyte acidity also reduces during discharge, as the concentration of Pb^{2+} ions in the electrolyte increases [equation 3-14]. It is therefore important to balance the concentrations to avoid precipitation of lead methanesulfonate into the cell when it is fully discharged. It has been recommended that the concentration of acid in the electrolyte should be limited to 2.4 mol·dm^{-3} MSA to prevent formation of flaky deposits [120]. Therefore, the initial concentration of MSA required to make electrolyte was limited to 2.5 mol·dm^{-3}, in order to yield a minimum of 1.0 mol·dm^{-3} Pb^{+2} ions.

The procedures for obtaining a targeted concentration of the electrolyte, as well as diluting concentrated recovered electrolyte to make the required concentrations are outlined in section 3.3.

3.2.3 Heating

PbO_2 reacts with warm acids to form more stable Pb^{2+} ions and release oxygen [180]. Heat was used to speed up the reaction between MSA and PbO_2. As a preliminary measure, the heating temperature was limited to 50° C to minimise energy use.

3.2.4 Use of Hydrogen Peroxide

Hydrogen peroxide (H_2O_2) is capable of reducing Pb^{4+} to Pb^{2+} ions as well as oxidising Pb metal to Pb^{2+} ions [181-183]. This unique quality of hydrogen peroxide can be used to form PbO shown in equations 3-7 and 3-8 below. When reacted with MSA, Pb^{2+} ions are formed as lead methanesulfonate, shown in equation 3-8.

$$PbO_2 + H_2O_2 \rightarrow PbO + H_2O + O_2 \quad (3\text{-}15)$$

$$Pb + H_2O_2 \rightarrow PbO + H_2O \quad (3\text{-}16)$$

$$PbSO_4 + H_2O_2 \rightarrow Pb + H_2SO_4 + O_2 \quad (3\text{-}17)$$

$$PbO + 2CH_3SO_3H \rightarrow Pb(CH_3SO_3)_2 + H_2O \quad (3\text{-}18)$$

The combination of acid, heat and hydrogen peroxide results in reactions below, which occur within minutes to seconds because of heat and depending on H_2O_2 quantity.

$$PbO_2 + 2CH_3SO_3H + H_2O_2 \rightarrow Pb(CH_3SO_3)_2 + H_2O + O_2 \quad (3\text{-}19)$$

$$Pb + 2CH_3SO_3H + H_2O_2 \rightarrow Pb(CH_3SO_3)_2 + 2H_2O \quad (3\text{-}20)$$

$$PbSO_4 + 2CH_3SO_3H + H_2O_2 \rightarrow Pb(CH_3SO_3)_2 + {SO_4}^{2-} + 2H_2O \quad (3\text{-}21)$$

Desulphurisation of lead pastes has been suggested for hydrometallurgical recycling of lead acid batteries, where the PbSO4 paste is converted to lead citrate in the presence of ascetic acid [167] and citric acid [166]. A similar mechanism is assumed in equation 3-17.

To arrive at the Pb^{2+} ions, the procedure as outlined in section 3.3 was followed.

3.3 Experimental

3.3.1 Equipment

An LD300 DC Electronic Load was used to fully discharge the 12 V 7Ah VRLA battery and a multimeter was used to check the battery open circuit voltage. A hacksaw was then used to remove the cover of the sealed VRLA.

For heating purposes a water bath and Yellow Line MST basic C stirrer with a coated chemical-resistant heating base was used and a TC 3 electronic contact thermometer was used to monitor mixture temperature. A Sigma 2-6E centrifuge machine was used to settle solids.

3.3.2 Samples and Materials

A 7 Ah 12V Valve Regulated Lead Acid (VRLA) battery, Yuasa NP7-12L was disassembled to extract lead from a spent lead acid battery [184]. The battery had 6 cells of 2 V each. Each cell had five negative electrodes and four positive electrodes in an overlap arrangement, and an Absorbed Glass Mat (AGM) separator between the electrodes. The separators were soaked in sulphuric acid electrolyte with 33.3% concentration (6 mol·dm^{-3} at 100% SoC). The electrodes were made of lead calcium alloy grids for extra strength and a leady oxide paste. Apart from the covered vents at each cell the battery was completely sealed. Physical dimensions of the battery were 151 mm x 65 mm x 94 mm and a mass of 2.8 kg. [184]

Methanesulfonic acid, MSA (CH_3SO_3H, Sigma Aldrich, #471356, 99.5%), lead methanesulfonate ($Pb(CH_3SO_3)_2$, Sigma Aldrich, #462667, 50% w/w), Hydrogen peroxide (H_2O_2, Sigma-Aldrich, #H1009, 30% w/w) were used as received. MSA was diluted to 2.5 mol·dm^{-3}. All chemicals were used as received. All aqueous solutions were prepared with de-ionised water from the Purite water purifier in the lab.

3.3.3 Lead Extraction From Spent Lead Acid Battery

To check State of Health (SoH) of the 12 V VRLA battery before lead recovery, the battery was connected to the Solartron equipment 1470E CellTest, and the following test were performed: (As recommended by IEEE:SA)

i. Open circuit voltage was measured. Batteries with an open circuit voltage above 11.8 V were not used as they could potentially be recharged and reused.

ii. Charging at 0.7 A constant current over 10 hours to an end of charge voltage of 12.6 V. 12.6 V would represent 100% SoC for a new battery.

iii. The 12 V VRLA battery was also cycled between 12.6 V (100%) end of charge voltage and 9.5 V (0% SoC) end of discharge voltage at 0.7 A, over 10 cycles, using the same equipment. Galvanostatic cycling at 0.7 A constant current over 3 hours per cycle to end of charge and end of discharge voltages of 12.6 (100% SoC) and 9.5 V (0% SoC)

respectively. This test was done to check the battery's capacity to hold charge and supply energy.

The sealed 12 V VRLA battery was then disassembled by:

1. Discharging the lead acid battery completely at 0.7 A for 12 hours on the LD300 DC Electronic Load at room temperature. The open circuit voltage of the battery was subsequently measured using a multimeter.
2. Emptying electrolyte via the exhaust nozzles.
3. Flushing with distilled water and emptying the water to remove excess electrolyte. Rinsing was repeated three times. The battery was flushed with distilled water and left to stand for a week, then emptied and rinsed with distilled water again.
4. Removing the top cover, and separating electrodes from the membrane, as shown in Figure 3-1a.

(a) (b)

Figure 3-1: (a) 12 V VRLA battery with sawn-off lid. (b) Retrieving contents of cell 1.

Each of the electrodes set was placed in a separate container to be treated individually. In the first container 500 mL 2.5 mol·dm^{-3} MSA was added and heated to 30° C with continuous stirring. A sample of known volume was collected from the container every hour for analysis.

Electrodes in the second container were treated similarly except the acid was heated to ~40° C. Samples were collected from this container as well, and the same measurements made to monitor change in density over time as well as to confirm the concentration of lead in the supernatant solution.

For the third and fourth experiments, 450 mL MSA was used and 50 mL of 0.09 mol·dm^{-3} hydrogen peroxide was added to the electrodes and the container contents were heated to 30° C and 40° C respectively. In the fifth and sixth experiments the concentration of hydrogen peroxide

was increased to 0.9 mol·dm^{-3} and the mixture was heated to 30° C and 40°C respectively. The results are shown in section 0.

For simplicity each of the electrode pairs were named cells and numbered sequentially, as shown in Figure 3-2.

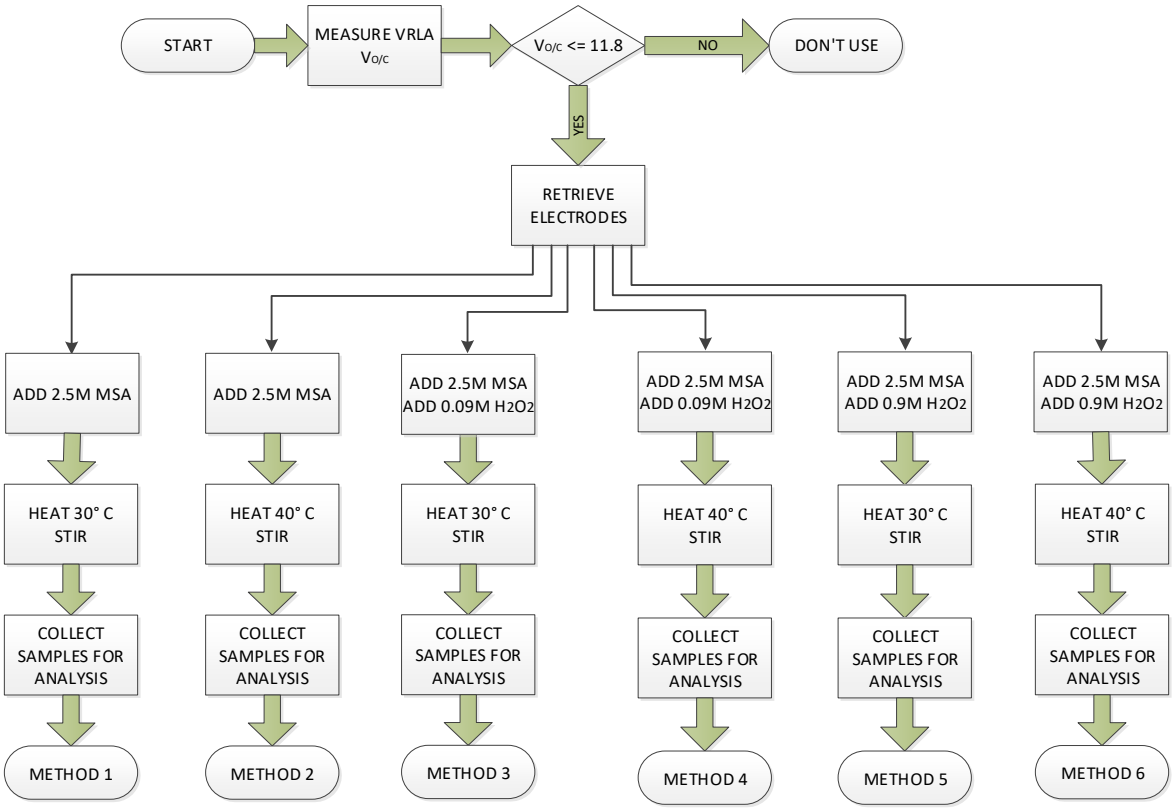

Figure 3-2 Lead recovery plan for electrolyte preparation. The electrodes retrieved from a spent VRLA battery with open circuit voltage less than 11.8 V were each placed in a beaker. 2.5 mol dm^{-3} MSA was added to the electrodes. The contents were heated at either 30°C or 40°C. In the first two cases no H_2O_2 was added, in the next two cases 0.09 mol dm^{-3} H_2O_2 was added to the beaker while the last two had 0.90 mol dm^{-3} H_2O_2.

3.3.4 Quantifying Recovered Lead (II) Ions

The quantity of Pb^{2+} ions recovered was monitored by monitoring the change in solution density, as well as by titration.

3.3.4.1 Density Measurements

For density measurements, a sample was collected from each mixture every hour and centrifuged at 3,600 rpm for 20 minutes to separate the liquid from the solids. A 10 mL sample of the supernatant liquid was collected and its mass was measured and recorded. This was used to monitor the change in density of the solution[185]. Assuming that the increase in mass of the clear solution was due to Pb and PbO2 solids being converted to Pb^{2+} ions, the concentration of Pb^{2+} ions was estimated from the change in mass, using the equation 48 below.

$$[Pb^{2+}] = \frac{\Delta m}{V_S MM_{Pb}}, \qquad 22 \text{ (3-23)}$$

where $[Pb^{2+}]$ is the concentration of Pb^{2+} ions, in $mol \cdot dm^{-3}$

Δm is change in mass of recovered solution over specific period, in grams

V_s is the volume of the sample weighed, in dm^3

MM_{Pb} is the molar mass of lead, in $g \cdot mol^{-1}$

3.3.4.2 Titration

Titration was also used to monitor the concentration of the recovered Pb^{2+} ions. This method, also described by Orapeleng, Wills [185], involved the complexometric titration of samples with EDTA acid and Eriochrome Black T dye, as described by Fitch [186].

The formation constant for the Pb^{2+}-EDTA complex is high, at 1.1x1018 [187]. In a basic buffer solution with pH10, the formation constant remains high at 3.3 x 10^{17}, therefore the complex formation is expected to proceed to completion, according to reaction 49.

$$H_2Y^{2-} + Pb^{2+} \rightarrow PbY^{2-} + 2H^+ \qquad 24$$

where H_2Y^{2-} is the EDTA acid and PbY^{2-} is the Pb^{2+}-EDTA complex.

The titration of Pb^{2+} with EDTA followed these steps:

1. An aliquot of the Pb^{2+} solution collected after centrifuging was diluted a 100 times. The solution was made to 25 cm^3.
2. To make the solution basic, 5 mL of pH 10 ammonium hydroxide was added to the solution. This resulted in formation of solid $Pb(OH)_2$.

$$Pb^{2+} + 2(OH)^- \rightarrow Pb(OH)_2 \qquad 25$$

3. To keep the Pb^{2+} ions in solution, a spatula tip of powder tartaric acid was added. Tartaric acid complexes weakly with Pb^{2+} ions, keeping the Pb^{2+} ions aqueous.

$$Pb^{2+} + {C_4H_4O_6}^{2-} \rightarrow Pb(C_4H_4O_6) \quad 26$$

4. Before titration a colour indicator was added to the solution. The indicator was prepared by grinding 100 mg of Erio Black T with 5 g of KCl. The indicator attaches to Pb^{2+} ions to form a reddish violet coloured complex, as indicated by equation 13:

$$Pb^{2+} + In \rightarrow PbIn \quad 27$$

where *In* is the indicator.

5. A standard solution of 0.01 mol dm^{-3} EDTA was titrated out of a burette into the solution under investigation.

6. The EDTA replaced the indicator from the $PbIn$ complex to form the strongly bonding PbY^{2-} until the indicator existed as a free protonated dye with a blue colour. Replacement of the indicator by EDTA is shown in equation 53.

$$H_2Y^{2-} + PbIn \rightarrow PbY^{2-} + H_2In \quad 28$$

At the end-point the colour of the solution changed from violet to blue.

7. The concentration of lead in the solution was related to the concentration of EDTA by the equation:

$$C_{EDTA}\ V_{EDTA} = [Pb^{2+}]V_{Pb^{2+}} \quad 29$$

The concentration obtained from the titration experiments was recorded and compared to the concentration estimates made from density measurements. The comparison is presented in Table 3-2 compares sample values of Pb^{2+} ions concentration calculated using the change in mass of the solution as well as using titration.

Table 3-2. Comparison of the concentration of Pb^{2+} ions obtained by mass measurements and by titration. The variance between the two values is lower than 10% in all cases.

The concentration of Pb^{2+} ions calculated from the change in mass of the solution differs from that obtained by titration measurements by less than 10%. The mass measurements could therefore be considered a reliable method. The close agreement of the results also confirms that

the assumption that the change in mass of the solution was due to Pb and PbO_2 solids being converted to Pb^{2+} ions was reasonable.

It is worth noting that the difference between the values from the two methods lessened the longer the sample was allowed to settle. In those cases, it was not necessary to centrifuge the sample before aliquots were collected.

There were concerns about interference from calcium (II) ions complexing with EDTA, since calcium (II) ions complex with EDTA at the same pH as do lead (II) ions. However because of the much higher formation constant of Pb-EDTA (1.1x1018) as compared to Ca-EDTA ($5.0x10^{10}$), the Pb-EDTA complex is expected to reach equivalence before the Ca-EDTA complex is formed, hence the titration results are considered reliable.

3.4 Results and Discussion

3.4.1 State of Health of Lead Acid Battery

The VRLA battery manual states that at 25°C, a battery voltage of 12.6 V corresponds to 100% SoC while an open circuit voltage under 11.8 V indicates 0% state of charge [188]. Upon testing the maximum battery open circuit voltage measured was 11.6 V, well below the 0% SoC mark. Therefore these batteries were considered to have reached the end of their lives.

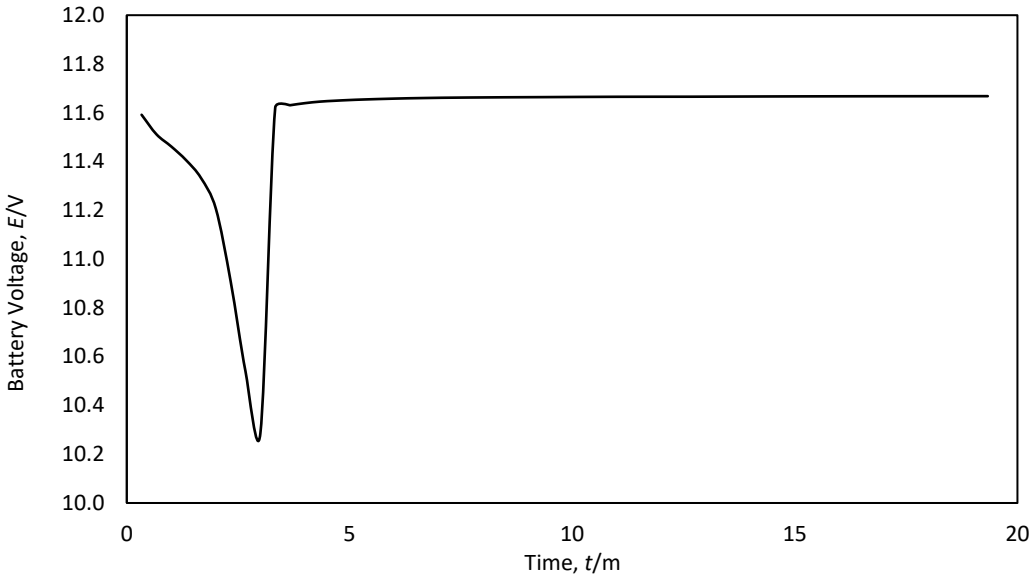

Figure 3-3: Voltage profile of charging Yausa NP7-12L, 12 V VRLA battery to 12.6 V, at 0.7A constant current

The battery was subjected to galvanostatic cycles, cycling it ten times at 0.7 A constant current for 3 hours on charge and discharge. End-of-charge voltage of 12.6 V and end-of-discharge voltage of 9.5 V were maintained. The lead acid battery appeared to get charged, albeit to a voltage lower than 100% SoC, but no energy could be extracted out of the battery. The battery also reached its end of charge and end of discharge voltages much sooner than the set three hours. This indicated the battery's lack of capacity to hold charge and supply energy. Clause 8 of the recommended practices for maintenance, testing and replacement of VRLA recommends that a battery should be replaced if its capacity falls below 80% of rated capacity as it is deemed to be at the end of its life [189]. The battery's behaviour is shown in Figure 3-4, which is a plot of the ten cycles of the battery.

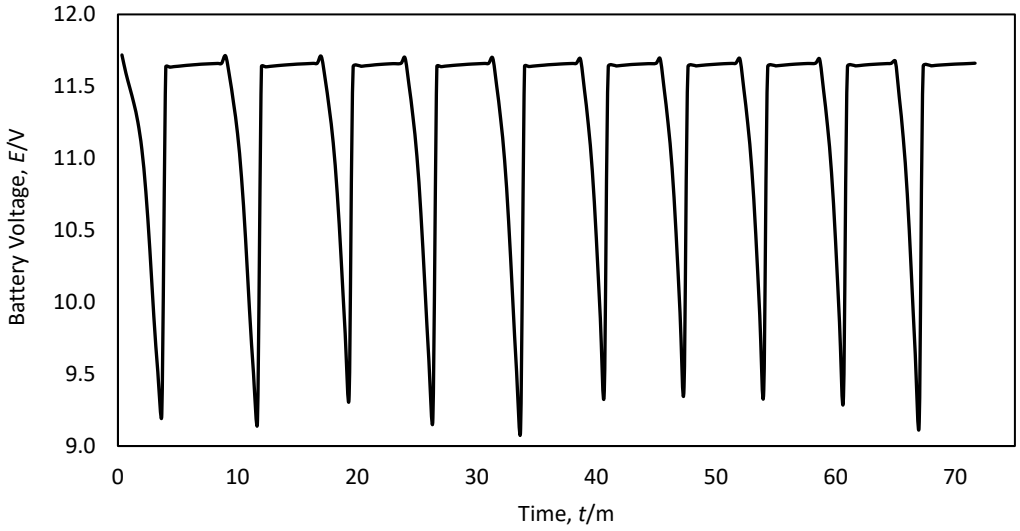

Figure 3-4: Charge/discharge of Yuasa lead acid battery at 0.7 A constant current for 3 hours each, 10 cycles. End-of-charge voltage 12.6 V and end-of-discharge voltage 9.5 V

The Ah charge capacity of the batteries was less than 1% of the nominal capacity. This was another indicator that the batteries had reached the end-of-life, as indicated in the battery manual. Using these indicators, the batteries were chosen for lead recovery.

3.4.2 Lead Recovered

3.4.2.1 Yield From Lead Recovery Methods

The methods described in section 3.3.3 and by Figure 3-2 yielded different concentrations of lead Pb^{2+} ions. Table 3-3 shows the results for each method.

Table 3-3. Amount of Pb^{2+} ions in the solution made by dissolving solid VRLA battery electrodes.

The temperatures shown are averaged over six hours.

Method	Electrode Material (g)	Average Temperature (° C)	$[H_2O_2]$ ($mol \cdot dm^{-3}$)	$[Pb^{2+}]$ ($mol \cdot dm^{-3}$)
1	250	30	0	0.16
2	250	40	0	0.07
3	250	30	0.10	0.51
4	250	40	0.10	0.75
5	250	30	0.98	1.00
6	250	40	0.98	0.91

The density of the collected samples tended to stabilise after six hours and it was found that without hydrogen peroxide, the amount of lead (II) ions recovered was lower than 0.2 $mol \cdot dm^{-3}$. Addition of 0.10 mol dm^{-3} H_2O_2 yielded 0.5 $mol \cdot dm^{-3}$, which was half the required amount of Pb^{2+}. Solutions with the higher concentration of H_2O_2 of 1.0 $mol \cdot dm^{-3}$ yielded the highest concentration of Pb^{2+} ions, and the required 1.0 mol dm^{-3} was obtained.

The quantity of hydrogen peroxide was kept at 10% of the total volume to control reaction volatility. The concentration of recovered electrolyte was limited at 1.0 mol dm^{-3} of Pb^{2+} ions by the initial concentration of acid.

3.4.2.2 Effect of Hydrogen Peroxide and Temperature

An example of the effect of adding hydrogen peroxide to the electrode material and methanesulfonic acid mixture is illustrated in Figure 3-5.

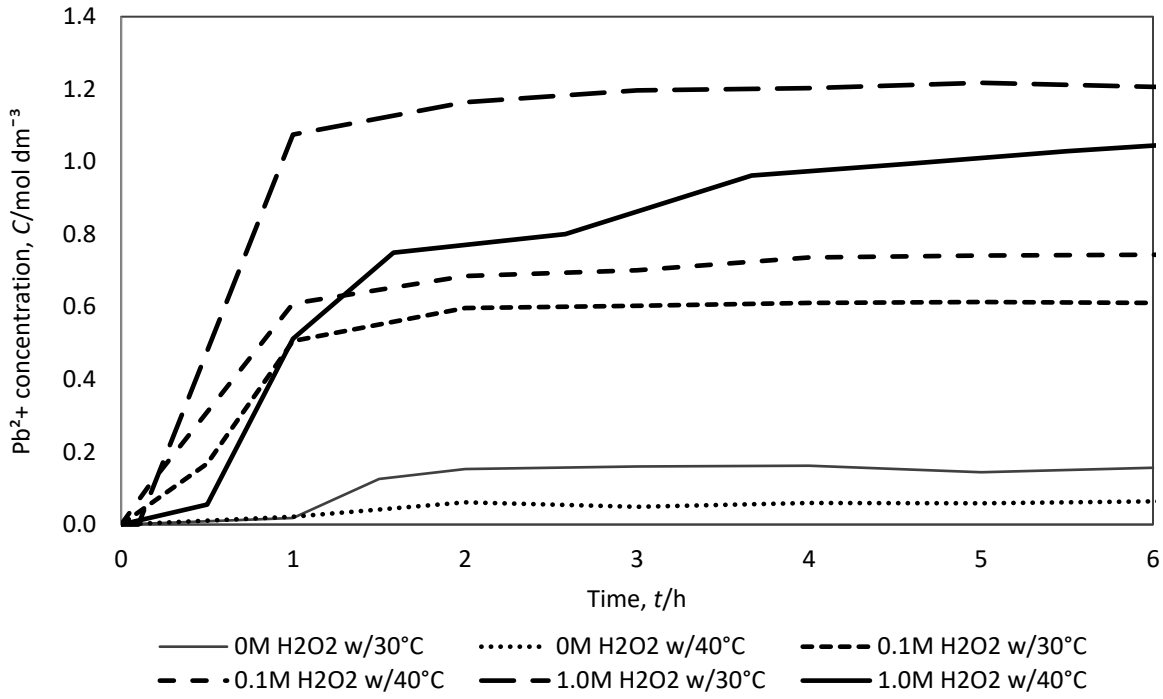

Figure 3-5: [Pb^{2+}] yield from the lead recovery when 250 g electrode solids were dissolved in 2.5 $mol \cdot dm^{-3}$ MSA and different quantities of hydrogen peroxide were added, and the temperature of the solutions were varied, as indicated.

The results indicate that, without hydrogen peroxide, the Pb^{2+} ions yield remained below 0.2 $mol \cdot dm^{-3}$, which is less than 20% of the expected yield. Once hydrogen peroxide is added, the amount of rises quickly to 0.65-0.75 $mol \cdot dm^{-3}$. This confirms the reducing effect of H_2O_2 on PbO_2, and indeed this effect has been exploited in the recycling of spent lead acid battery pastes to make crystalline lead citrate $Pb(C_6H_6O_7) \cdot H_2O$ [165] and $Pb_3(C_6H_6O_7)_2 \cdot 3H_2O$ [167]. At 0.9 $mol \cdot dm^{-3}$ H_2O_2, the concentration of Pb^{2+} ions yielded rose to at least 1.0 $mol \cdot dm^{-3}$ each time. In all the cases where hydrogen peroxide was added, even at 0.09 $mol \cdot dm^{-3}$ H_2O_2, the concentration of Pb^{2+} rises to the maximum within the first hour, and stabilises for the rest of the six hours under consideration. Similar results were obtained elsewhere [165, 167]. The concentration of the yielded Pb^{2+} ions was limited by the solubility of Pb^{2+} in methanesulfonic acid.

3.4.2.3 Comparison of methods used to quantity lead (II) ions recovered

The quantity of Pb^{2+} ions recovered was monitored by checking solution density, as well as by titration. Table 3-4 compares sample values of Pb^{2+} ions concentration calculated using the change in mass of the solution as well as titration. Calculations of [Pb^{2+}] concentrations using

mass of the solution recovered and using titration were performed using equations 48 for the mass measurements and equation 54 for titration.

Table 3-4: Chemicals detected in an aliquot from solution made by dissolving VRLA battery electrodes in 2.5 mol·dm^{-3} MSA and 9.79 mol dm^{-3} H_2O_2 at 40°C, over six hours.

[Pb^{2+}] in mol·dm^{-3} by		**% Variance**
Mass measurements	**Titration**	
0.65	0.656	0.9
0.68	0.67	1.5
0.73	0.72	1.9
0.87	0.86	1.2
0.95	0.89	6.3
0.96	0.90	6.3
1.06	0.93	9.7

The concentration of Pb^{2+} ions calculated from the change in mass of the solution differs from that obtained by titration measurements by less than 10%. The mass measurements could therefore be considered a reliable method. The close agreement of the results also confirms that the assumption that the change in mass of the solution was due to Pb, $PbSO_4$ and PbO_2 solids being converted to Pb^{2+} ions was reasonable.

It is worth noting that the difference between the values from the two methods lessened the longer the sample was allowed to settle. In those cases, it was not necessary to centrifuge the sample before aliquots were collected.

There were concerns about interference from calcium (II) ions complexing with EDTA, since calcium (II) ions complex with EDTA at the same pH as do lead (II) ions. However, because of the much higher formation constant of Pb-EDTA ($1.1x10^{18}$) as compared to Ca-EDTA ($5.0x10^{10}$), the Pb-EDTA complex was expected to reach equivalence before the Ca-EDTA complex was formed, hence the titration results were considered reliable. The next chapter includes elemental analysis of the recovered electrolyte to determine the electrolyte composition.

3.5 Chapter Conclusions

A novel method for making electrolyte for a soluble lead redox flow battery has been developed by the author using methanesulfonic acid and hydrogen peroxide [185]. The method involved

dissolving spent lead acid electrodes in warm MSA and using hydrogen peroxide to catalyse chemical oxidation PbO_2 and reduction of solid and Pb and $PbSO_4$.

The method successfully yielded the amount of lead (II) ions (0.1 to **1.1** mol.dm^{-3}) sought, over a period of at least six hours. The methods used to recover lead yielded varying amounts of lead (II) ions, indicating that some were more favourable than others. The addition of hydrogen peroxide catalysed the retrieval of lead ions from PbO_2. As shown by the cyclic voltammetry results, the recovered electrolyte displays similar electrochemical activity as does the conventional electrolyte used in soluble lead redox flow batteries developed by others. **A lead (II) concentration of 1.5 mol·dm^{-3} would give an equivalent storage capacity of 40 Ahr·dm^{-3} of electrolyte or 60 Whr·dm^{-3} (at a discharge voltage of 1.5 V).**

The novel method outlined requires minimal pre-treatment compared to other conventional methods for lead recovery, it is easy, uses low amounts of energy compared to pyrometallurgy or electrolysis and it yields results quicker. This makes the method simpler and quicker to carry out. Compared to informal recycling practices introduced in chapter 2, the method is safer and more environmentally friendly. The ability to reprocess waste conventional lead acid batteries at the end of their useful life and directly make electrolyte for the soluble lead battery offers a simple and low cost route to obtaining an electrolyte for the soluble lead flow battery in the most direct route possible.

The results of this chapter are supported by the published paper below:

Orapeleng, K., Wills, R., and Cruden, A., Developing Electrolyte for a Soluble Lead Redox Flow Battery by Reprocessing Spent Lead Acid Battery Electrodes. Batteries, 2017. 3(2): p. 15. DOI: https://doi.org/10.3390/batteries3020015

A comparison of recovered and standard (made from laboratory reagent-grade chemicals) electrolytes in operational cells will be presented in the next chapter. Further, detailed characterisation for the recovered electrolyte in a flow cell environment is presented.

Chapter 4 Comparison of Recovered Electrolyte to Reagent Grade Electrolyte and its Characterisation

4.1 Introduction

The recovered electrolyte (RE), made from the published method [185] described in chapter 3, is compared to the SLFB conventional electrolyte, which is made from reagent-grade lead methanesulfonate and methanesulfonic acid, thus called reagent grade electrolyte (RGE). In this chapter the two electrolytes are cycled in static and flow cells and their performance compared. Results from this chapter demonstrated that the RE performed better in terms of cycle life and charge, energy and voltage efficiencies in both static cells and flow cells [190]. Elemental analysis of both RE and RGE was performed to determine the elemental makeup of the two electrolytes, and determine the reason for the RE competitive advantage. Apart from cycling in galvanic cells, the density, viscosity and conductivity of the electrolyte were determined. Cyclic voltammetry for both the PbO_2/Pb^{2+} and Pb/Pb^{2+} redox couples was done for the RE.

Cycling electrolyte in small cells, where failure behaviour is exaggerated gives conservative results which overstate the failure behaviour of the electrolyte. This is the reason the cells in Figure 4-1 and Figure 4-2, described in 4.2.1 and 4.2.2 were used. Cycling the electrolytes in the galvanic cells gave a conservative indication of the cells' cycle life, as well as the charge, energy, and voltage efficiencies of the cells. The charge efficiency is the cell's coulombic efficiency, which indicates the amount of charge retrieved after charging. It is an indication of the cells' ability to return the energy deposited during charge.

The RE is made from electrode material from lead acid batteries, which contains alloys and additives normally added to enhance performance of the lead acid battery [173]. Lead alloys used to make lead acid battery grids contain antimony, calcium, tin, silver, and other trace elements introduced to manipulate the properties of the lead [191]. Calcium and tin are normally added to improve the mechanical properties of the battery grids. The latter also prevents passivation and increases rechargeability, reduces corrosion, and increases the conductivity at the grid/active-material interface [191]. Adding silver to lead-calcium-tin alloys improves corrosion resistance and reduces creep [ibid]. Apart from the alloying metals in the grid, lead acid battery electrode pastes contain trace elements which are added during production of refined lead, either as additives or as impurities, including arsenic, bismuth, cadmium, copper, nickel, and beryllium [173, 174, 191, 192].

It was therefore expected that the RE, made from expended battery electrodes, would contain some of these trace elements. Hence, elemental analysis was carried out to determine the qualitative and quantitative composition of the RE. The analysis of the electrolyte was performed using Inductively Coupled Plasma Mass Spectroscopy.

ICP-Mass Spectral analysis of lead was first carried out by Nier and others [193]. Lead was initially converted to tetramethyl lead and injected as a gas into a spectral analyser. Fitch 2010, p. 330. The gas was ionised into atoms in a 27 MHz RF field at a temperature range of 6,000 – 8, 000 °C, where argon was used to provide the ionising temperature. The ionised atoms were pulled into an electric field and underwent a 9 magnitude pressure drop. The low pressure ensured that no gas phase passed through, only allowing the ionised atoms through, it also allowed detection of individual ions, providing detection levels as low as parts per trillion.

The density, kinematic viscosity, and conductivity of the RE was measured and compared to that of the RGE. The latter's density has been found to be linearly proportional to the concentration of the Pb^{2+} ions [179]. The same research also revealed that in MSA, the viscosity of RGE increases linearly with both Pb^{2+} and MSA concentrations, while the ionic conductivity follows a multipart relationship; at 0.1 $mol \cdot dm^{-3}$ MSA and below, conductivity decreases with Pb^{2+} concentration, and at 0.25 $mol \cdot dm^{-3}$ MSA and above, conductivity increases with Pb^{2+} concentration. The research identified an optimum electrolyte concentration of 0.75 $mol \cdot dm^{-3}$ Pb^{2+} and 1.0 $mol \cdot dm^{-3}$ MSA at which charge efficiency was 84% and cycle life 48, the highest combination recorded for the study [179]. A difference in these properties for the RE and RGE could explain differences in the performance of the electrolytes.

Cyclic voltammetry was carried out on RE electrolyte to determine its electrochemical properties. Cyclic voltammetry is used to study the oxidation and reduction processes of electrochemical species at an electrode surface. It is a useful tool for measuring the rate of the reactions that occur at the electrode surface when a potential sweep is applied, by directly mearing the current due to the reactions. Cyclic voltammetry occurs in an electrolyte, which supplies and accepts the ions that undergo reduction and oxidation at the working electrode. In a three-electrode system, the potential is measured between the working electrode and the reference electrode, and current is measured between the working electrode and a counter electrode, ensuring there is no current to the reference electrode. A sinter or lug is used to isolate the cell from any products of electrolysis that may occur at the counter electrode [194]. Cyclic voltammetry can also be used to determine the formal potential of the PbO_2/Pb^{2+} and Pb/Pb^{2+} redox couples.

In cyclic voltammetry, a potential is applied to a working electrode at a constant rate, called the sweep rate, until oxidation or reduction occurs at the electrode surface. Once the range of

reactions have occurred, the sweep is reversed so that reduction or oxidation of the products and intermediates formed during the forward sweep can occur [195]. The voltammetry is performed in a supporting electrolyte, which maintains charge neutrality and prevents migration of charged ions [196, 197]. In the three-electrode electrochemical cell, redox reactions occur at the working electrode, current is monitored at the reference electrode and the counter electrode balances the potential of the cell [197].

4.2 Methodology

4.2.1 Static Cell

A static cell was made of two 5 cm x 5 cm x 2 mm Sigracell graphite electrodes. The electrodes were separated by a silicone insulator, which created a 5 cm x 5 cm x 8 mm cell chamber in which electrolyte was held. The silicone gaskets also provided a seal against electrolyte leaks. A 5cm x 5 cm x 0.1 mm thick nickel foil was placed flush against the back of each electrode to act as a current collector. Silicone gaskets were used to insulate the cell's conductive parts from the clamps that held the cell together. The current collectors were connected to the battery analyser leads. The cell had an active area of 25 cm^2 on each electrode. The variable cell-gap was maintained at 8 mm, unless otherwise specified. The cell is shown in Figure 4-1.

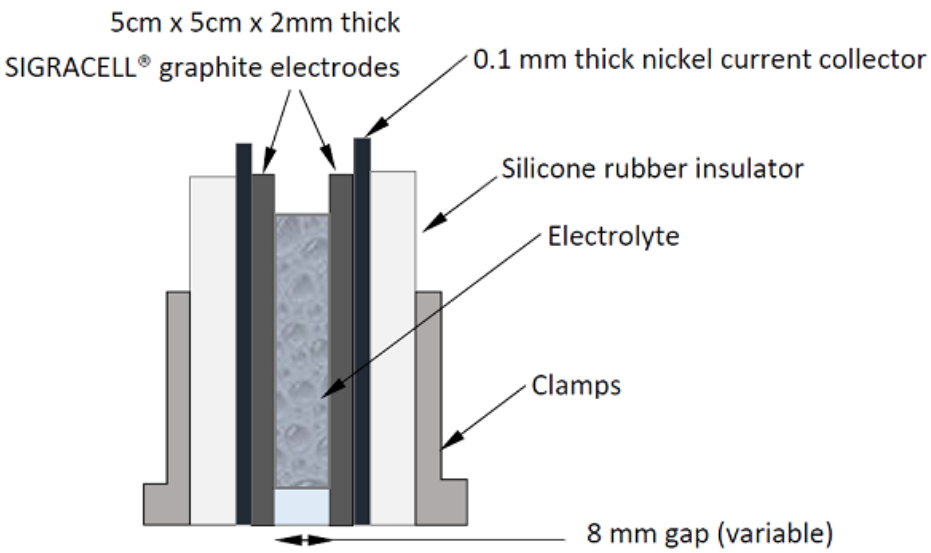

Figure 4-1: Cross section of static soluble lead cell. The static cell has a 5cm x 5cm x 8mm wide cell chamber with two 5cm x 5cm x 0.2cm graphite electrodes on either side. 0.1 mm thick nickel foils are placed against each electrode to collect current from the electrodes. The whole cell is held together by clamps and insulated with silicone rubber to minimise leakage.

The electrodes of the cell were prepared by cleaning first with soap and warm water, then rising with dilute methanesulfonic acid, then polishing with a 150 (92 µm) carbide sandpaper under running deionised water.

4.2.2 Flow Cell

The soluble lead flow cell, shown in Figure 4-2, was made of a polyvinyl chloride (PVC) backing board which gives the cell structural support. Silicone rubber sheets provide insulation of electrodes from the metal backing boards, while also preventing leakage of the electrolyte. The cell had 5.0 cm x 4.0 cm x 2.0 mm thick Sigracell graphite electrodes. A 5.0 cm x 4.0 cm x 0.1 mm thick nickel foil was used to collect current from each electrode. Two acrylic cell chambers provided a 4.0 cm x 2.5 cm by 2 cm half-cell chamber either side of a VPX-20 anion exchange membrane. Each of the acrylic chambers had an inlet and an outlet through which electrolyte entered and left the cell. The electrolyte was circulated between the reservoir and the cell using Watson Marlow 505S peristaltic pumps and Masterflex Norprene® 06402-25 tubes. An Erlenmeyer flask was used as a single electrolyte reservoir. Since the electrolyte from either side of the cell went into the same tank, the cell was classified as semi-divided [67]. The setup is shown in Figure 4-3.

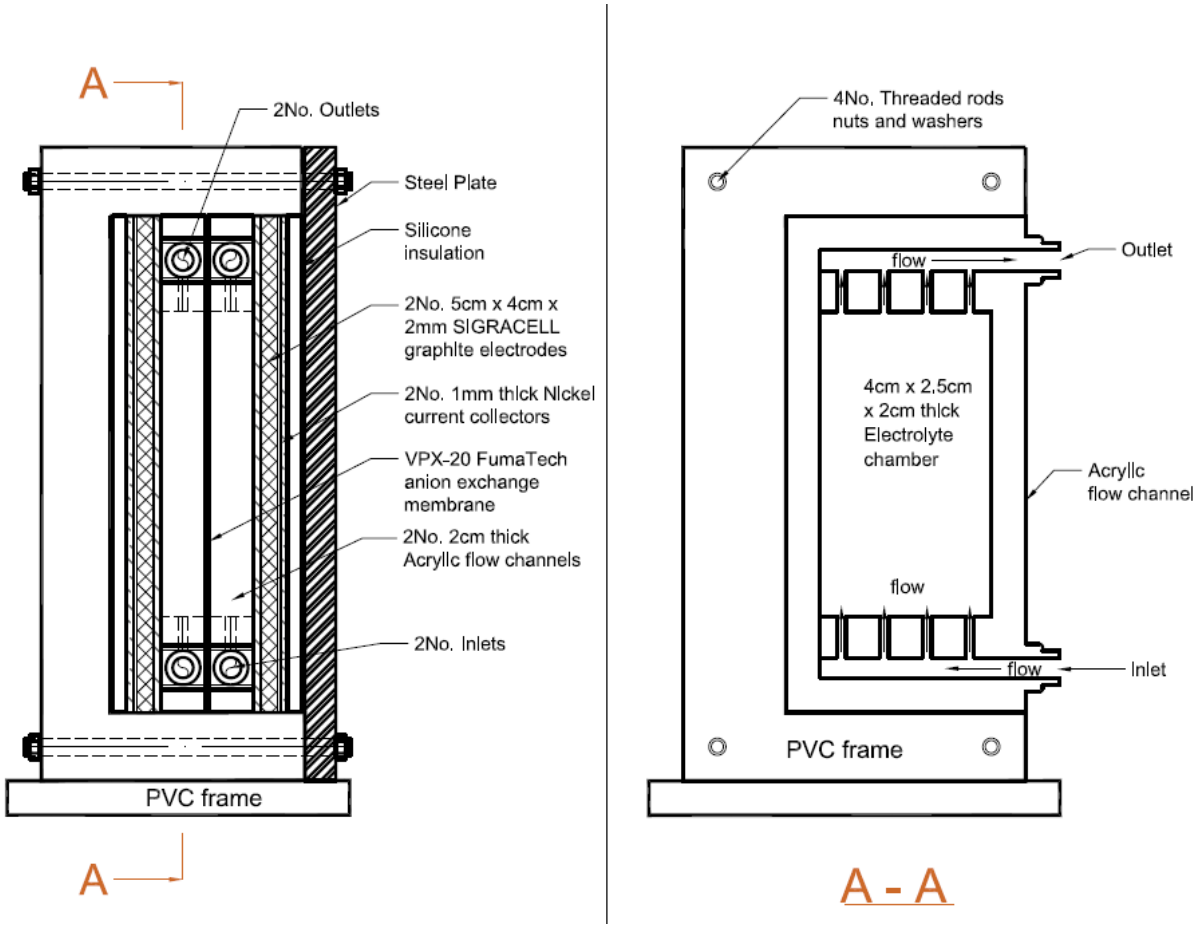

Figure 4-2: A soluble lead flow cell made of a structural PVC backing board, silicone spacers to isolate the functional parts of the cell, and 5.0 cm x 4.0 cm x 2.0 mm thick Sigracell carbon electrodes. 0.1 mm thick nickel foils were used as current collectors. 2No. acrylic cell chambers provided a 4 cm x 2.5 cm by 2.0 cm half-cell chamber either side of a VPX-20 anion exchange membrane. Each acrylic chamber had an inlet and outlet through which electrolyte entered and left the cell.

The electrodes were cleaned the same way as the static cell electrodes. The volume for each experiment was 150 mL of RE placed in a tank (Erlenmeyer flask). A Watson Marlow 505S peristaltic pump was used to circulate the electrolyte between the tank and the cell at 4.58 $cm^3 \cdot s^{-1}$ (2.29 $cm \cdot s^{-1}$). The setup is shown in Figure 4-3.

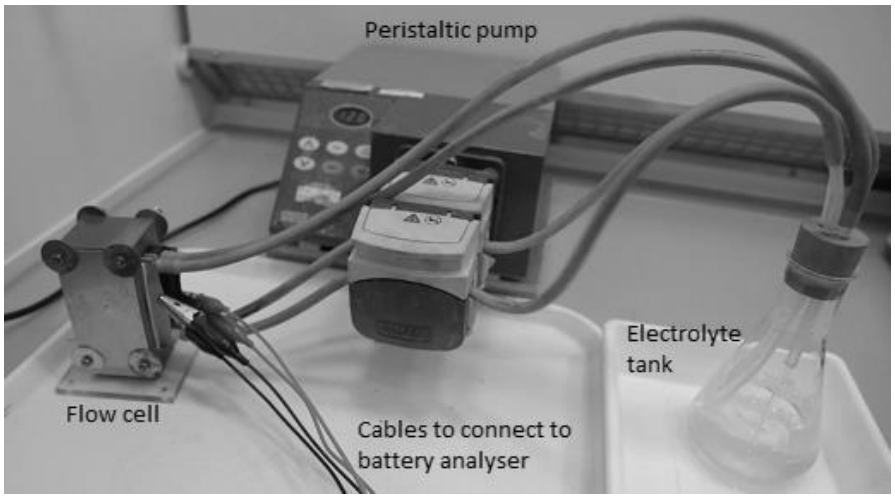

Figure 4-3: Setup of the redox flow cell, showing the redox flow cell in a vertical orientation, the Erlenmeyer flask as the electrolyte tank and peristaltic pumps. The cables connect the current collectors to the battery analyser.

4.2.3 Battery Analyser

An eight-channel battery analyser MTI 8-channel BT8-3A battery analyser (MAX 5 V, 3 A) by MTI Corporation, was used to control the cycles and record the galvanostatic cycling data. A laptop that had BTS Control battery management software, connected to the analyser, was used to control the experiments and record the experimental data. During flow cycling, a Watson Marlow 505S peristaltic pump and Masterflex Norprene tubes were used to circulate electrolyte for the soluble lead flow cell.

4.2.4 Galvanic Cycling

RE and RGE were cycled in static cells as well as flow cells to compare charge performance. The cells are described in sections 4.2.1 and 4.2.2, respectively.

The static soluble lead cell shown in Figure 4-1 was assembled and connected to the MTI 8-channel BT8-3A battery analyser (MAX 5 V, 3 A). The cell was charged at 4 $mA \cdot cm^{-2}$ for 20 minutes to an End of Charge Voltage (EoCV) of 2.6 V, allowed a two minutes open circuit period between charging and discharging, discharged at 4 $mA \cdot cm^{-2}$ to End of Discharge Voltage (EoDV) of 0.5 V for another 20 minutes, and allowed another open circuit two minutes. The EoCV was based on the SLFB cell voltage [66], while also allowing for over-potential. The EoDV was set low to ensure as complete a discharge cycle as possible. Each cell was cycled until the charge efficiency fell below 60%, at which point the cell was deemed to have failed.

The flow cell was charged at 10 $mA \cdot cm^{-2}$ to an EoCV of 2.6 V for one hour, allowed a two minutes open circuit period between charging and discharging, discharged at the same current density to EoDV of 0.5 V for an hour, allowed another two minutes of open circuit, and the cycles were repeated until the cell charge efficiency fell below 60%, which was used to describe cell failure.

RGE with the same MSA and Pb^{2+} ion concentrations as the RE was cycled in the same fashion. The concentration of acid and Pb^{2+} ions was varied to compare, as was the current density. An Erlenmeyer flask was used as a single electrolyte reservoir. The electrolyte was cycled at 4.58 $cm^3 \cdot s^{-1}$ (2.29 $cm \cdot s^{-1}$). The results are outlined in Table 4-3 in section 4.3.1.

4.2.5 Electrolyte Conductivity and Viscosity

The conductivity of electrolyte is an important factor that determines how well an electrochemical cell performs. The conductivity of electrolyte for SLFB has been measured and it was confirmed that increasing the concentration of acid increases conductivity of electrolyte [114, 179]. However [179] also found that for electrolytes with 1.0 $mol \cdot dm^{-3}$ MSA, conductivity reduced with increasing Pb^{2+} concentration, resulting in a low conductivity of 225 $mS \cdot cm^{-1}$ recorded for an electrolyte with 1.5 $mol \cdot dm^{-3}$ Pb^{2+}.

To compare the RE made through this research with that of RGE, the conductivity of RE with concentration 0.7 $mol \cdot dm^{-3}$ Pb^{2+} and 1.0 $mol \cdot dm^{-3}$ MSA was measured at room temperature (294 K). The results are shown in section 4.3.1

An Ostwald viscometer with a calibration constant, C = 0.009236C was used to measure the kinematic viscosity of the electrolyte. Density was measured by measuring the mass of 10 mL of the RE on a digital scale with ±0.001 g precision. The density and kinematic viscosity were used to calculate dynamic viscosity. Conductivity was measured using an Analytical Technology ATI Orion 162 (Pt electrode) conductivity meter, which also recorded the temperature of the electrolyte. All measurements were repeated thrice, and the average used.

4.2.6 Elemental Analysis of Recovered Electrolyte

The elemental composition of the RE was analysed using Inductively Coupled Plasma Mass Spectroscopy. A Thermo Scientific iCAP RQ ICP MS analyser, which employed Argon plasma, was used. Standards were prepared based on the list of elements in a refined lead ingot that conforms to BS EN 12659:1999 [192]. The samples were prepared in triplicate and quantified against the available standards.

The ICP-Mass Spectroscopy to identify and quantify the trace elements in the RE was performed by an independent lab at the H.J. Enthoven & Sons lead recycle facility in Darley Dale, UK, where they used the Thermo Scientific iCAP RQ ICP MS analyser. An argon plasma was used in standard operating mode, which means the plasma temperature was 6,000 °C, except for detection of Arsenic and Selenium, where the Kinetic Energy D was used, using helium instead of argon.

4.2.7 Voltammetry

To assess the electrochemical performance of the electrolyte, cyclic voltammetry of the electrolyte was carried out in a three-electrode cell, pictured in Figure 4-4, where both the Pb/Pb^{2+} and the PbO_2/Pb^{2+} redox pairs were investigated.

The three-electrode cell had a vitreous carbon rotating disc working electrode with surface area 0.126 cm^2, where solid Pb or PbO_2 was deposited, depending on the redox pair, and a 1.2 cm^2 platinum-mesh counter electrode completed the electrical circuit between the working electrode and the electrolyte. A saturated calomel reference electrode (SCE) was used to measure the voltage at the working electrode.

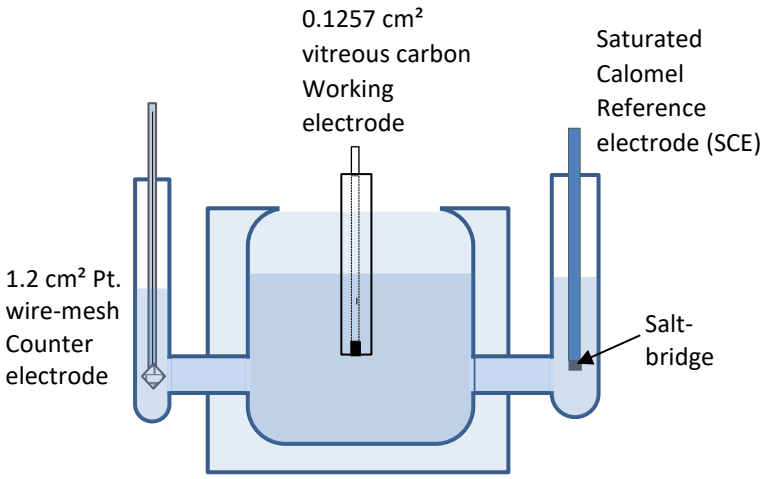

Figure 4-4: Sketch of a 3-electrode cell for cyclic voltammetry with 1.2 cm^2 Pt wire mesh counter electrode, 0.1257cm^2 vitreous carbon rotating disc working electrode and a saturated calomel reference electrode.

An AutoLab potentiostat, using NOVA software to control and record data, was used to perform all cyclic voltammetry experiments.

An aliquot of the RE was placed in 1.0 mol·dm^{-3} methanesulfonic acid electrolyte. A potential sweep of 25 mV·s^{-1} was applied. The working electrode was polished on a Buehler 736-3 8" microcloth with 0.3 μm alumina suspended in water between each experiment, unless stated otherwise. For the Pb/Pb^{2+} redox couple, a potential sweep was made between -0.7 V and -0.2 V, while the potential range was 0.2 V to 1.9 V for the PbO_2/Pb^{2+} redox couple. Where cycles were repeated, the electrode was not cleaned between cycles to prevent disturbing the setup. The results are presented in voltammograms in section 4.3.5.

4.2.8 Scanning Electron Microscopy with EDX

The Scanning Electron Microscope (SEM) allows viewing of particles at resolutions of mm to nm scales, and when combined with an Energy Dispersive X-Ray Analyser, allows identification and quantification of elements at 0.1% minimum concentrations. Lead acid batteries contain trace elements used for alloying, as additives to enhance performance of the lead acid battery as well as impurities picked from lead processing. Therefore, SEM imaging was conducted to identify the trace elements present in lead acid batteries as well as in RE and RGE.

A Philips XL30 ESEM SEM was used to analyse powder samples of positive and negative electrodes of an expended YUASA NP Series: NP7-12 valve regulated lead acid battery. Similar analysis was carried out for dried electrolyte samples of both RE and RGE under a Scanning Electron Microscope with EDX to determine the sample composition. The results are presented in section 4.3.6.

4.3 Results and Discussion

4.3.1 Comparison of Electrolytes in Static Cells

RE and RGE at 0.9 mol·dm^{-3} Pb^{2+} and 0.8 mol·dm^{-3} MSA were each cycled in the static cell shown in Figure 4-1. The cells were charged and discharged at 4 mA·cm^{-2} for twenty minutes, allowed to rest on open circuit voltage for three minutes, and discharged at the same current density for another twenty minutes. The end of charge voltage was set at 2.6 V and the end of discharge voltage was 0.5 V. The cycles were repeated until charge efficiency fell below 60%.

Figure 4-5 shows a comparison of the first two cycles of static cells running with RE and RGE electrolytes. It illustrates the difference in over-potential and in length of discharge period for the two cells. On charge, the voltage of the cell with RE is 69.2 mV lower than that with RGE, while at the same time the RE discharge cycle is 6 minutes shorter than for the RGE cell. In cycle 2, the two

cells run for the same length of time while the difference in voltage is maintained. The lower charge voltage for RE indicates a lower overpotential for charging the static cell with RE. Also clear is the two-stage charge profile on the second cycle, especially for the RGE cells, discussed in the next page.

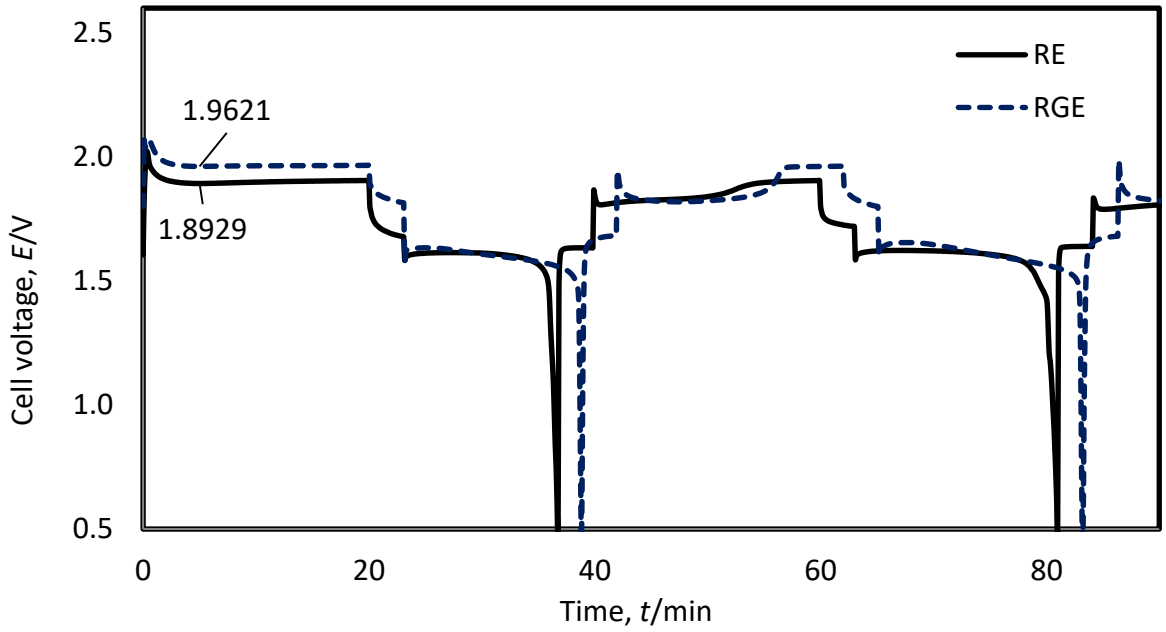

Figure 4-5: First 2 cycles of both recovered electrolyte (RE) and reagent grade electrolyte (RGE), ([Pb^{2+}]=0.9 mol·dm^{-3}) in static cell (active electrode area of 25 cm^2) charged at 4 mA·cm^{-2} for 20 minutes to 2.6 V, left on open circuit voltage for 2 minutes, discharged at 4 mA·cm^{-2} for 20 minutes to 0.5 V, another 2 minutes on OCV and cycled until charge efficiency fell below 60% (failure).

In the first cycle the charge efficiency for the RGE cell was 78%, 13% higher than that for the RE, indicated by the 6 minutes longer discharge period (Figure 4-5). In the second cycle both had risen to 90%, and the two cells displayed comparable discharge periods. But over the next cycles, shown in Figure 4-7, the charge efficiency for the RE stayed consistently above 90%, while that for the RGE cells dropped to 78% and continued on a steady decline until it fell below 60% after nine cycles, shown in Figure 4-6. The voltage efficiency for the RGE and RE cells averaged 85% and 86%, respectively, before cell failure.

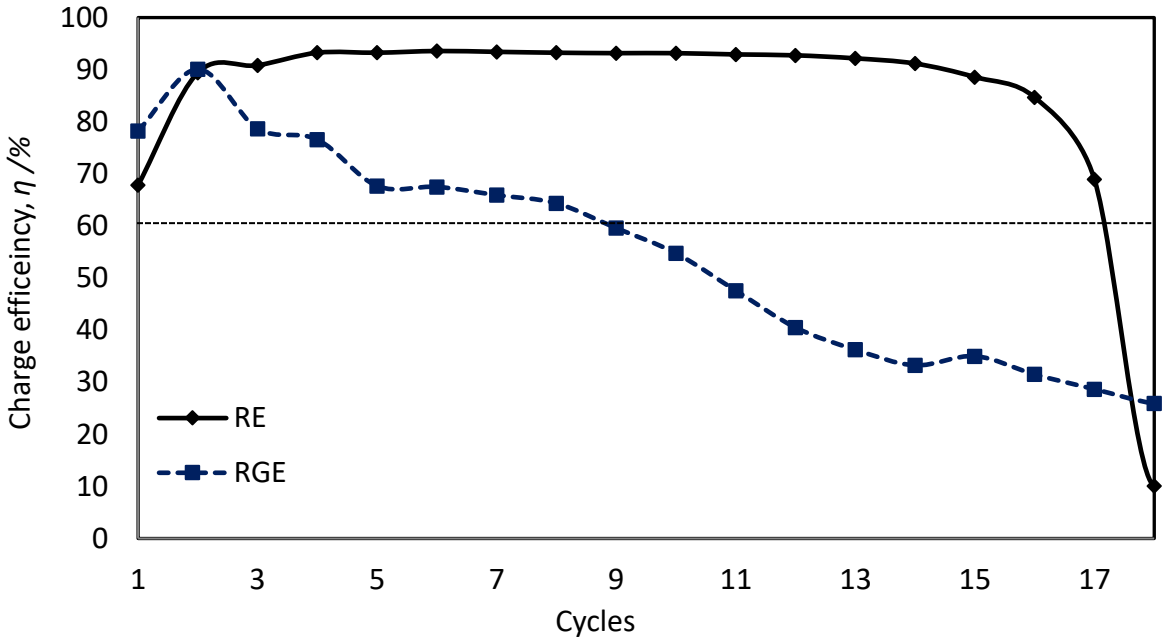

Figure 4-6: The charge efficiency of static cells (active electrode area of 25 cm^2) using RE and RGE at 0.9 $mol \cdot dm^{-3}$ Pb^{2+} and 0.8 $mol \cdot dm^{-3}$ MSA, charged and discharged at 4 $mA \cdot cm^{-2}$ for 20 minutes, with 3 min O/C rest between charge and discharge. End of charge and end of discharge voltages set at 2.6 V and 0.5 V, respectively.

Figure 4-7 includes subsequent cycles for cell with the two electrolytes. From the fourth cycle, the RE cells had consistently longer discharge cycles, by at least six minutes longer than those of the RGE cells, visible in cycles 5 and 6. This allowed for more capacity recovery during discharge and resulted in better charge efficiency, an average 90% for RE compared to 78% for RGE.

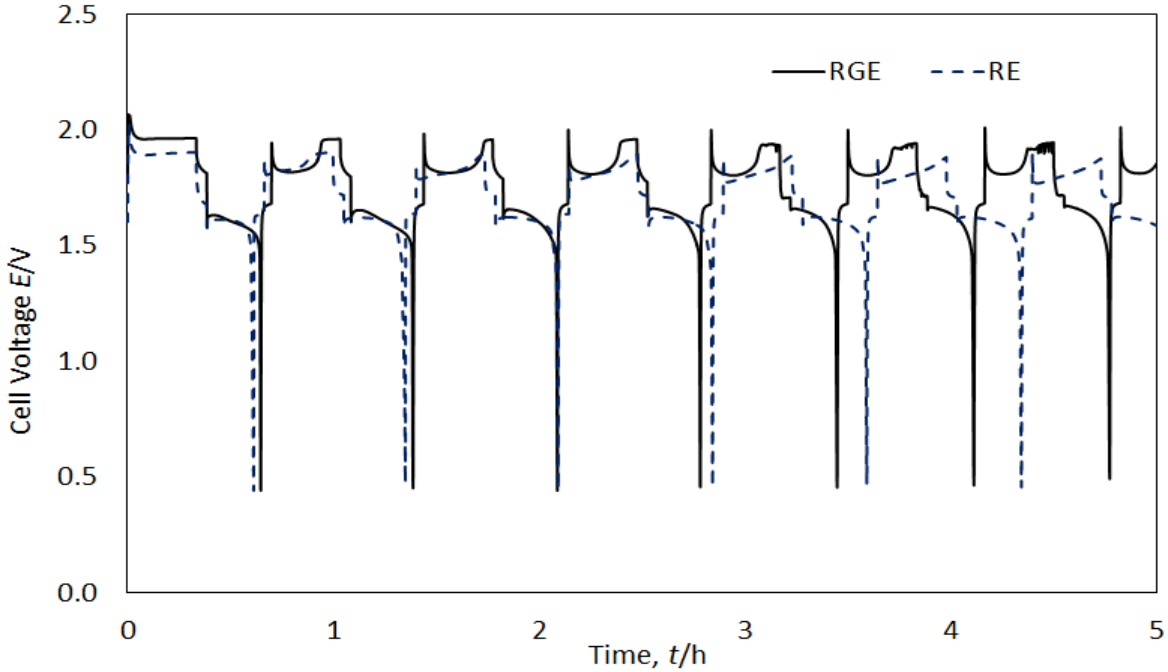

Figure 4-7: First 7 cycles of recovered electrolyte (RE) and reagent grade electrolyte (RGE) $[Pb^{2+}]$=0.9 mol·dm^{-3} in static cells (active electrode area of 25 cm^2) charged at 4 mA·cm^{-2} for 20 minutes to 2.6 V, 3 minutes on open circuit voltage (OCV), discharged at 4 mA·cm^{-2} for 20 minutes to 0.5 V, another 2 minutes on OCV. Cycled until charge efficiency fell below 60%.

Both Figure 4-5 and Figure 4-7 show that the charge/discharge curves start with over-potentials of 0.12 V for the RE cells and 0.14 V for the RGE cells. Both curves then adopt a flat charge profile in the first cycle, at 1.9 V and 1.96 V for the RE cells and RGE cells, respectively. These voltages, though slightly different are normal for converting Pb^{2+} to solid PbO_2. Subsequent cycles show two voltage levels, 1.8 V and 1.9 V for RE cells and 1.85 V and 1.96 V for RGE cells. This phenomenon has been observed and studied by others [66, 102, 115, 198, 199] and it has been demonstrated that the shape of the curve is affected by activity at the positive electrode. The two-tiered charge voltages occur when an insoluble PbO_x ($1 \geq x > 2$) species is preferentially converted to PbO_2 at 1.8 V, before the conductive solid is depleted and Pb^{2+} is converted to solid PbO_2 at a voltage closer to 2.0 V [198]. Insoluble PbO_x species form during discharge, when the boundary layer between the electrode and the electrolyte becomes saturated with Pb^{2+} ions beyond the solubility limit and the acid concentration at the electrode falls below the limit required to convert PbO_2 to Pb^{2+} [198]. Therefore, PbO_2 is converted to PbO_x instead [198]. Overtime, with more cycling, the undissolved lead dioxide becomes visible in the electrolyte, with both types of electrolytes, and on inspection after cycling, both types contain lead deposit on the negative electrode and lead dioxide on the positive electrode. This was the most prominent method of failure for the soluble lead battery. In

undivided static cells, the growth of solids on both electrodes result in shorting of the circuit and failure of the cells much sooner than in divided cells [118].

In Figure 4-7, the positive electrode of a static cell was photographed after failure. Adhered lead dioxide deposit is visible on the electrode, as well as lead dioxide sludge, some of which flowed out when the cell was dismantled. During cycling the sludge collects at the bottom of the cell and creates a conduction bridge that connects the two electrodes, causing the cell to short circuit. Shorting occurred sooner with RGE than it did with RE electrolyte, indicating that solids accumulation was slower with RE than it was with RGE.

Further cycling of static cells was carried out at different Pb^{2+} concentrations, and the average results are presented in Table 4-1.

Table 4-1: Average performance of static cells using recovered (RE) and reagent grade (RGE) electrolytes. The static cell had an active electrode area of 25 cm^2 and was cycled at 4 $A \cdot cm^{-2}$ for 20 minutes to EoCV of 2.6 V, allowed to rest and discharged at 4 $A \cdot cm^{-2}$ for 20 minutes to EoDV of 0.5V.

Electrolyte	$[Pb^{2+}]$ /$mol \cdot dm^{-3}$	Charge Efficiency /%	Energy Efficiency /%	Voltage Efficiency /%	Cycles before Failure*
1 RE	1.0	89	86	96	23
2 RGE	1.0	63	49	78	7
3 RE	0.9	89	77	87	17
4 RGE	0.9	74	63	85	8

* Failure is defined when the charge efficiency fell below 60%.

In all cases the cells with RE cycled more times before the charge efficiency fell below 60%. The charge and energy efficiencies for the cells with RE were also consistently higher than that using RGE. The charge efficiency of the cells with RE was consistently higher than 80%, while that of the lab reagent electrolyte cells peaked at 74%. Table 4-1 indicates that in the static cell, the RE overall produced an improved cell performance and cycle life than the cells using the RGE. The conclusion for static cells is that the RE performs better in terms of charge efficiency and cycle life than RGE.

There appears to be a delay in solids accumulation in the recovered electrolyte, which delays cell failure compared to RGE cells.

Since both cells with electrolytes eventually failed when cycling was continued, some tests were performed in static divided cells. The cell in Figure 4-1 was divided by adding more silicone dividers and placing a permeable membrane to keep the two sides separate. The modified cell is shown in Figure 4-8.

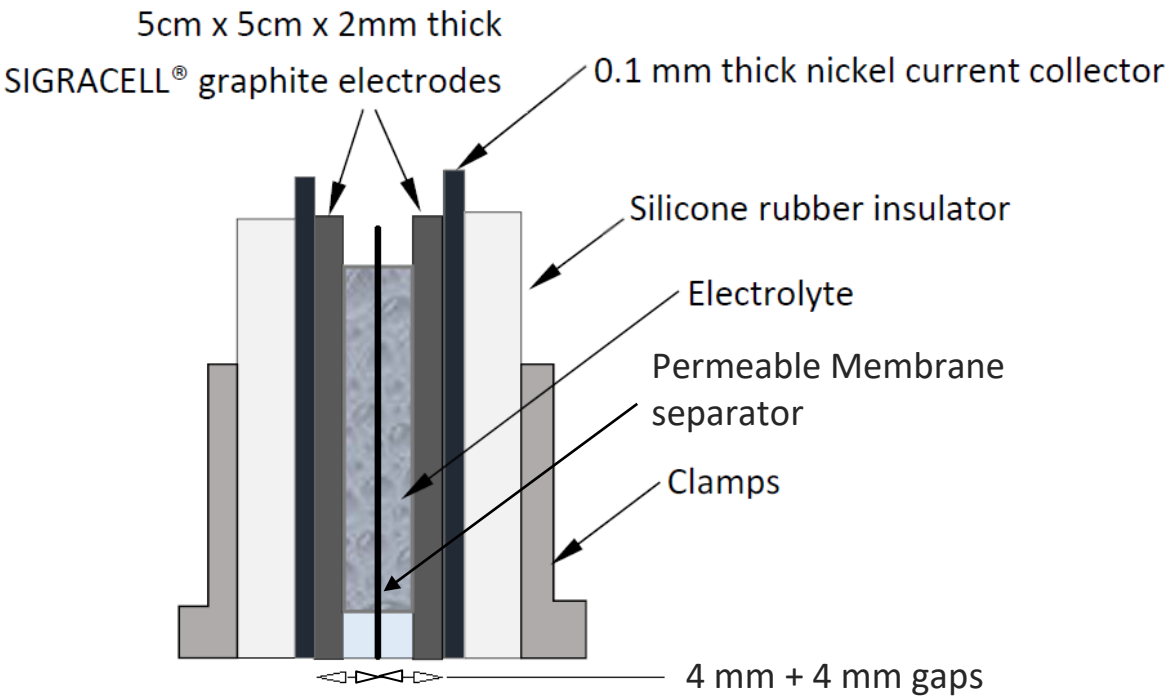

Figure 4-8: Modified static cell with a permeable membrane separator, and an inter-electrode gap of 4 mm either side of the separator.

The divided static cells were cycled at different current densities and also with different end-of-discharge voltages to compare the effect on the performance. The end of charge voltage was increased to 3.0 V to allow a wide voltage range for cell operation. The table below gives a summary of the effect of the different conditions on cycle life and efficiency.

Table 4-2: Comparison of divided and undivided static cells with different end-of-charge voltages and current densities. O/C rest period was 2 min. Electrolyte: 0.8 mol·dm^{-3} Pb^{2+}, 0.9 mol·dm^{-3} MSA.

Current density/ mA·cm^{-2}	**Config-ration**	**Inter-Electrode gap/mm**	**EoDV - EoCV /V**	**Cycles before failure**	**Average Charge efficiency**	**Average Energy efficiency**	**Average Voltage efficiency**
5	Divided	4 + 4	0.1 – 3.0	83	87	65	74
5	Divided	4 + 4	0.5 – 3.0	145	90	71	64
20	Divided	4 + 4	0.1 – 3.0	4	63	66	42
5	Undivided	8	0.1 – 3.0	22	77	62	78
5	Undivided	8	0.5 – 3.0	28	84	67	80

In Table 4-2 above, cells with the same recovered electrolyte and the same cycling regime are compared when some are divided and some are not. It is clear that divided cells cycle last longer than those without a separating membrane. A divided cell with 0.1 V end-of-discharge voltage lasted 145 cycles compared to an undivided one's 22 cycles with the same end-of-discharge voltage. Another divided cell lasted 83 cycles when its end-of-discharge voltage was raised to 0.5 V. Compounding the effect of a high current density (20 mA·cm^{-2}) and a high end-of-discharge voltage (0.5 V) severely limited cycle life to 4. In this instance the division of the cell did not help. The cell in question also had the lowest charge, energy and voltage efficiencies.

It can be concluded that dividing the cell can lead to increased cycle life. This is because when solids start accumulating in the cell, and even when sludge collects at the bottom of the cell, shorting does not occur immediately, therefore the cell continues to cycle despite the presence of solids. Lowering the end-of-discharge voltage also increased cycle life. Cells that had the same electrolyte, the same inter-electrode gap as well as the same current density tended to have shorter cycle lives when compared to those with a lower end-of-discharge voltage. This is because the former would reach the end of discharge voltage before the allocated period of discharge, before they had fully discharged the stored capacity. Reaching the end-of-discharge voltage too soon also limited stripping of solids from the electrodes, hence leaving more material on the electrode, which caused quicker accumulation of solids in the cell and subsequent failure.

For the subsequent tests, the cells were divided and the end of discharge voltage was lowered to 0.1 V.

4.3.2 Comparison of Electrolytes in Flow Cells

Like with static cells, the flow cells initially had an end-of-discharge voltage of 0.5 V and an end-of-charge voltage of 2.6 V. The flow cell, shown in Figure 4-2, was charged at 20 $mA \cdot cm^{-2}$ for one hour to an EoCV of 2.6 V, allowed to rest on open circuit for two minutes, discharged at 20 $mA \cdot cm^{-2}$ to an EoDV of 0.5 V, and allowed another 2 minutes O/C rest. Cycles were repeated until charge efficiency fell below 60%, at which time they were deemed to have failed. The electrolyte flow was 4.58 $cm^{3} \cdot s^{-1}$ (2.29 $cm \cdot s^{-1}$). The flow cell, described in section 4.2.2, had VPX-20 anion membrane separator, which served to keep the two sides of the cells mechanically separated. The separator was chosen for its low electrical resistance at all Pb^{2+} concentrations [67]. Because the separator served mostly as a mechanical divider, the tank of the flow cells was kept the same, so that the same electrolyte was circulated to both sides of the cell, and the separator simply served to keep the two sides mechanical apart. This configuration is called semi-divided [67].

A comparison of charge discharge profiles when both electrolytes were cycled at 18 $mA \cdot cm^{-2}$ are shown in Figure 4-9. Over-potential starts high for both flow cells, indicating initially high losses. The difference between the charge and discharge voltages gradually lessens, improving voltage efficiency and the charge efficiency, which tends towards 90% for both electrolytes. Another noticeable feature of the curve in Figure 4-9 is that the over-potential for the RE is less than that of the RGE, even as they both decrease with cycling. This means less energy is required to charge the cell with RE than is required for that with RGE.

Figure 4-9 also indicates that the first cycle of the RE cell immediately displays almost equal charge and discharge times, while also being fairly flat, compared to the RGE flow cell. This signals the high charge efficiency at the onset of cycling, which was recorded as 90% in the first cycle, while the RGE cell charge efficiencies start at 70% and gradually increase. At failure, defined when charge efficiency fell below 60%, both cells had an average charge efficiency of 84%.

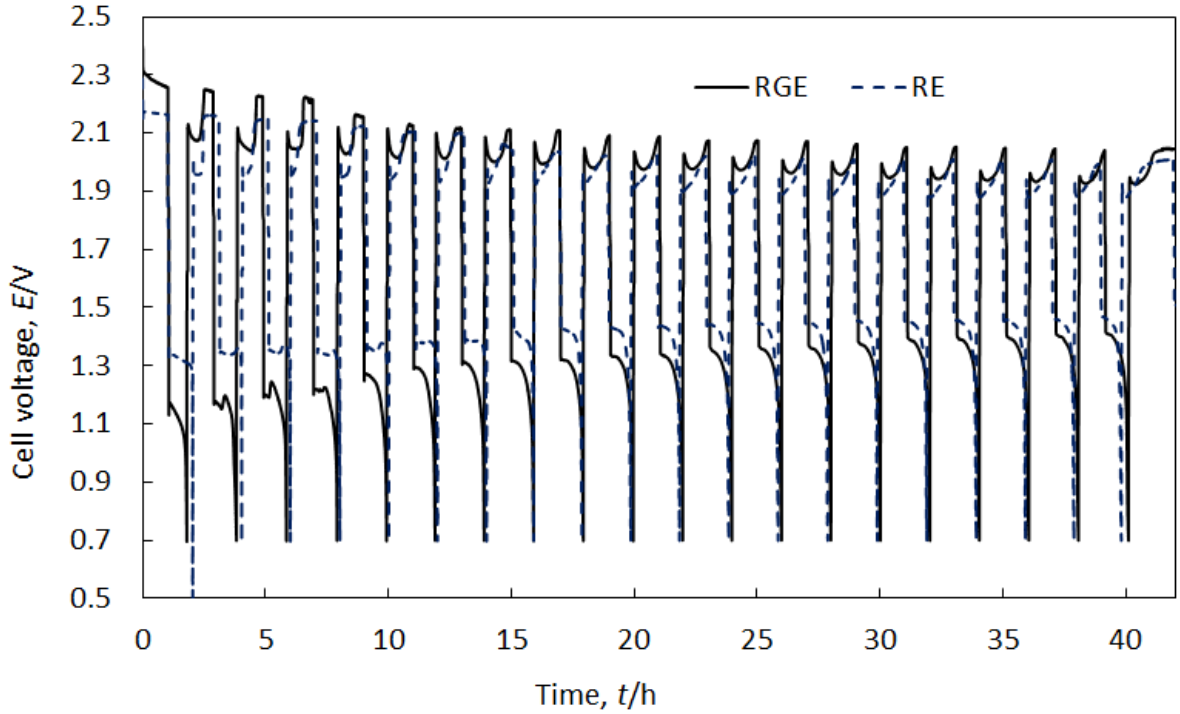

Figure 4-9: Comparison of recovered (RE) and reagent grade electrolytes (RGE) cycled in a RFC at 18 mA·cm^{-2}. The cell was charged for an hour, left on open circuit for 2 minutes, discharged for an hour, and allowed another 2 minutes. EoCV: 2.6 V & EoDV: 0.5 V. The curves show a gradual decrease in over-potentials, which occurs earlier for the recovered electrolyte.

As with static cell cycles, the graph indicates that subsequent charge occurs at two different voltages. In the second cycle, charge is initially at 2.1 V then at 2.3 V, similar to the static cell performance in section 4.3.1.

Performance of cells using RE and RGE at different concentrations and current densities is compared in Table 4-3.

Table 4-3: Average performance of recovered (RE) and reagent (RGE) grade electrolyte in a soluble lead redox flow cell charged at 10 $mA \cdot cm^{-2}$ for an hour to EoCV of 2.6V, 2 minutes OC and discharged at 10 $mA \cdot cm^{-2}$ to EoDV 0.5 V. Cell failure defined when charge efficiency fell below 60%.

Electrolyte	$[Pb^{2+}]$ /$mol \cdot dm^{-3}$	Current Density /$mA \cdot cm^{-2}$	Charge Efficiency /%	Energy Efficiency /%	Voltage Efficiency /%	Cycles before failure*
1 RE	0.9	10	88	68	77	47
2 RGE	0.9	10	88	65	74	56
3 RE	0.9	20	80	55	69	98
4 RGE	0.9	20	87	63	72	102
5 RE	0.7	10	90	65	72	205
6 RGE	0.7	10	78	63	81	101

* Failure is defined when the charge efficiency fell below 60%.

The charge efficiency displayed by the cell using RE is similar to that of the cell using RGE. The similarity can be seen in both the static cell (Table 4-1), and the flow cell (Table 4-3). It is also evident at different current densities. The voltage efficiency of cells with either electrolyte is also comparable. The number of cycles supported by the RE in a redox flow cell is significantly higher (86 cycles more) at a Pb^{2+} ion of 0.7 $mol \cdot dm^{-3}$ and 1.0 $mol \cdot dm^{-3}$ MSA, which was recommended for optimum electrochemical performance of a soluble lead cell [179].

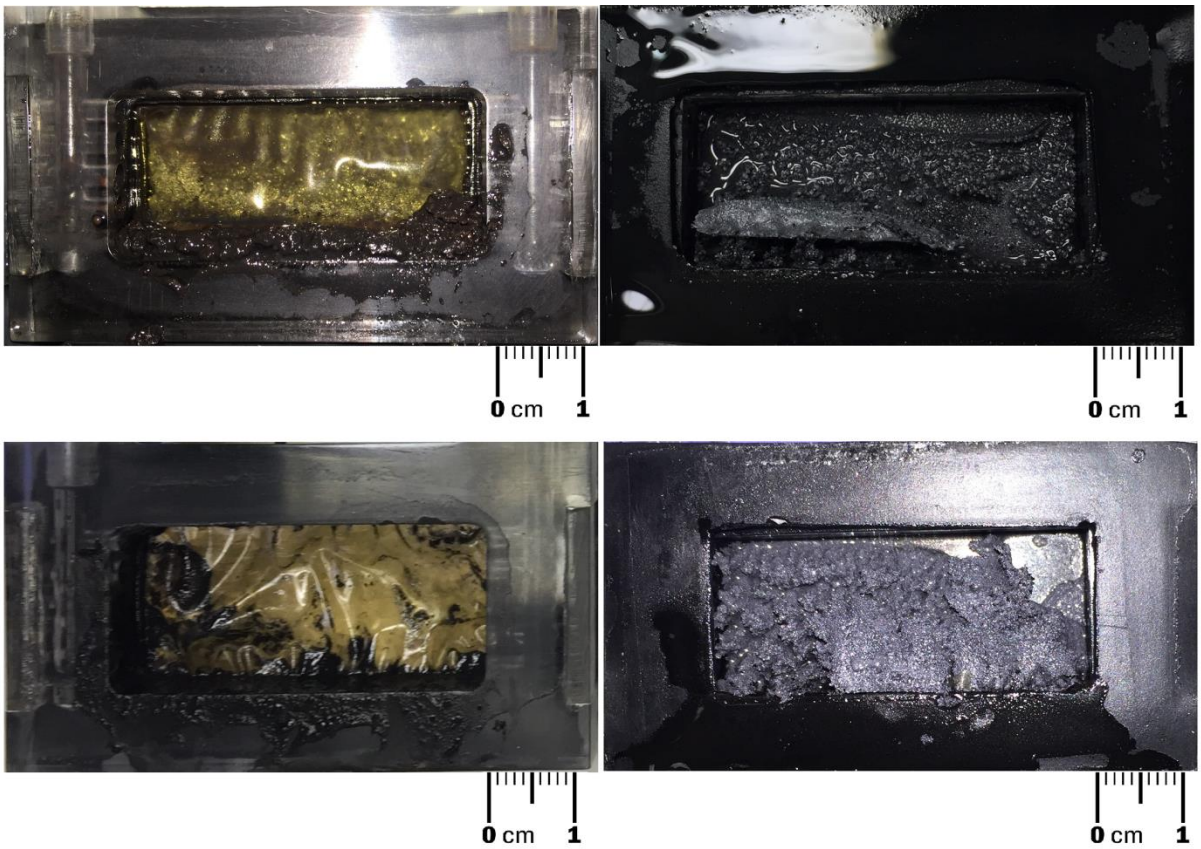

Figure 4-10: Solid build-up in positive (left) and negative (right) half cells of a soluble lead redox flow cell after 7 days of cycling at 10 $mA \cdot cm^{-2}$ on 1 hour charge and discharge cycles with 2 minutes of open circuit pauses between cycles. The top images depict deposit for a flow cell with RGE and the bottom images show deposit build-up for a cell using RE. On the left are images of accumulated slag in the positive half-cell, against the VPX-20 anion exchange membrane, on the right are images of the deposit on the negative electrode.

When left to continue to cycle, formation of solid deposit occurred in cells with either electrolyte, as shown in Figure 4-10. A spongy lead was deposited on the negative electrode while a sludgy and grainy deposit was formed in the positive half-cell. After seven days, not only had the deposit grown to fill the cell chamber, the surface of the deposit was no longer smooth. Inefficient reduction of lead dioxide, which started with deposition of the PbO_x during discharge, resulted on the accumulation of lead dioxide on the positive electrode. In turn lead started to accumulate on the negative electrode. In a divided cell, as long as there was no contact between the growing solids, the cell continued to operate at charge efficiencies above 80%, even as the black lead dioxide could be seen in the electrolyte tank. Similar results have been reported before [117]. However, with increased cycling the deposits grew until the negative side of the cell filled with soft spongy lead

(Figure 4-10) while the lead dioxide continued to travel with electrolyte to the tank. Eventually the Pb^{2+} concentration in the electrolyte fell as more lead was deposited and not stripped back into the electrolyte. In some instances, such as in Figure 4-10, the accumulated lead pushed against the dividing membrane, causing the membrane to shift and crinkle as shown. The lead dioxide deposit also clogged the electrolyte inlet, constricting the flow as seen in Figure 4-11.

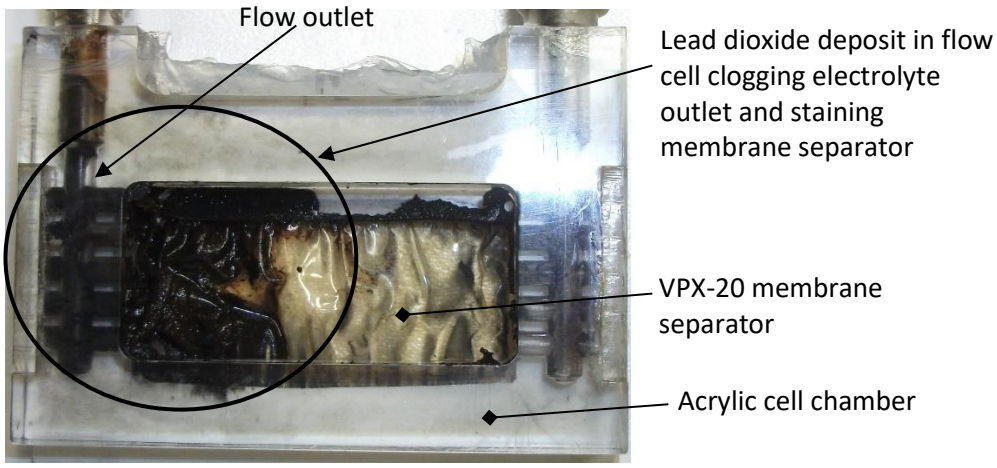

Figure 4-11: Built-up lead dioxide (right) deposit in a flow cell using RE at 0.7 mol·dm^{-3} Pb^{2+} and 1.0 mol·dm^{-3} MSA, cycled at 10 mA·cm^{-2} for 1 hour, left on O/C for 2 minutes, then discharged at the same current density. The lead dioxide is clogging the electrolyte outlet and has stained the membrane separator. The membrane is crinkled

Figure 4-11 is a picture of a flow cell after cycling, showing the clear acrylic chamber, the VPX-20 membrane separator stained on one side by lead dioxide deposit and the lead dioxide deposit, which has filled the electrolyte outlet, completely blacking it. Similar results were observed for both electrolytes, confirming the challenges that the soluble lead flow battery face.

In another cell that cycled over 200 time, the amount of deposit in the negative side of the cell was decidedly smaller. When dismantled after stopping the test, the lead dioxide deposit was strongly adhered to the positive electrode, while the lead in the negative side was not adhered, but had clumped into an agglomerate of lead metal. Figure 4-12 is a picture of the positive and negative electrode, showing the adhered lead dioxide and the lead agglomerate.

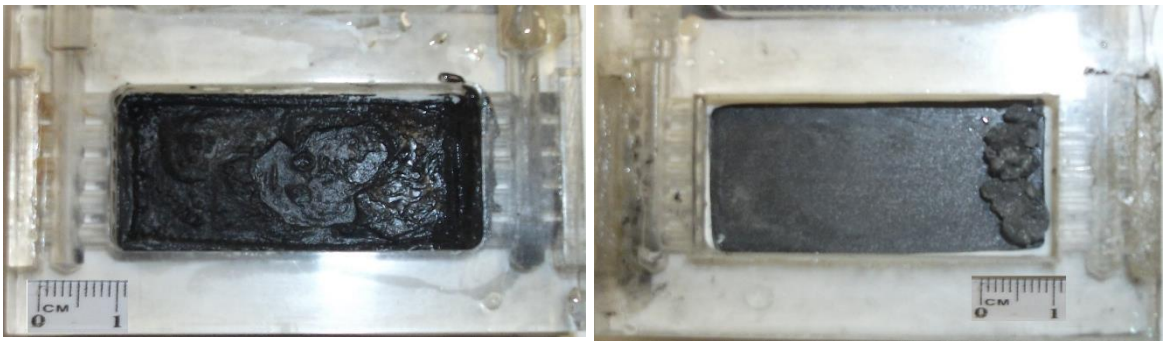

Figure 4-12: Flow cell chambers and the positive (left) and negative (right) electrodes, showing adhered lead dioxide on the positive electrode, and lead solids on the negative side. The flow cell cycled 205 times, and had 0.7 mol·dm^{-3} Pb^{2+} and 1.0 mol·dm^{-3} MSA RE, cycled at 10 mA·cm^{-2} for an hour with 2 min O/C rest, and 2.5 V EoCV and 0.1 V EoCV.

The deposit in the cell in Figure 4-12 was different from other deposit cells in that it was strongly adhered and only a small amount drifted to the electrolyte tank, and the lead deposit accumulated in the negative side was smaller in quantity than with other cells. Because of the smaller amount of deposit build-up, the electrolyte did not lose as much of the Pb^{2+} ions as other cells, and the cell continued to cycle beyond 200 cycles. The cell inlet and outlet also remained unblocked, which allowed for continued free flow of electrolyte between the cell and the tank. Below is a plot of cell voltage vs time for the first 10 cycles of charge/discharge.

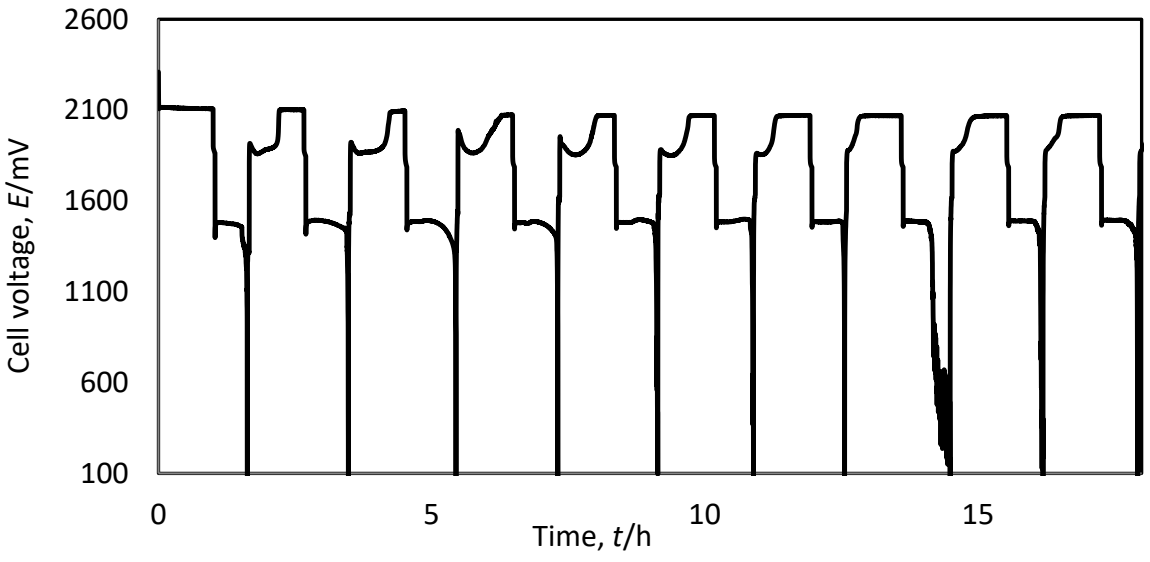

Figure 4-13: The first 10 cycles of a flow cell that cycled 0.7 mol·dm^{-3} Pb^{2+} and 1.0 mol·dm^{-3} MSA RE 205 times at 10 mA·cm^{-2} charge/discharge for an hour with 2 min O/C rest, and had 2.5 V EoCV and 0.1 V EoCV.

Initially the voltage started high at 2.3 V and reduced to 2.1 V for the duration of the rest of first charge cycle. In the next cycle, the typical two step charge was noticeable, where the voltage spiked to 1.9 V, then dropped immediately to 1. 8V while PbO_x was being converted to PbO_2, and then the voltage rose back to 2.1 V while Pb^{2+} was being converted to PbO_2. In this cell, the second peak voltage faded after the ninth cycle, and a gradual voltage increase profile from 1.8 V to 2.1 V was maintained for each charge cycle until the 139th cycle, when the peak charge voltage finally dropped to 2.0 V. At the 171st the maximum charge voltage fell to 1.9 V cycle and at that stage the charge efficiency rose back to 100%.

A possible explanation for this behaviour is that after the tenth cycle, where the 2-step charge voltage starts to fade, the cell was experiencing oxygen evolution, which was favoured over the formation of PbO_x. At a charge voltage of 2.0 V, this is a reasonable deduction. The results seem to suggest lowering of the formation of PbO_x from the smoothing of the voltage peak at the tenth cycle, shown in Figure 4-13, which was maintained for the rest of the 195 cycles. Since the formation of PbO_x was reduced compared to other cells, the deposited solids on the electrode was mostly adhered lead dioxide, which built-up at a lower rate than when there is unabated formation of PbO_x.

The amount of lead deposit in the negative half-cell also suggests that there was enough lead ion being dissolved back into the electrolyte that less lead accumulated than with other cells. Because of this, the accumulation of solids which would result in a constricted negative half-cell, clogged electrolyte outlets, reduced Pb^{2+} concentration in the electrolyte, and a sludgy accumulation in the positive half-cell did not occur, and the cell cycled over 200 times without failing. As a comparison RGE has been cycled a maximum of 164 at 10 mA·cm^{-2} [115]. Charging the soluble lead cell at 2.0 V or higher was recommended to increase the proportion of α-PbO_2 deposited and control the deposit size to nanoscale, which increased lead dioxide kinematics and improved cycle life [109]. This could explain the different morphology of deposited lead which tended to adhere more strongly than that seen with RE before.

4.3.3 Elemental Composition of Electrolyte

To investigate the superior results obtained in static cells, elemental analysis of both electrolytes was performed. Analysis on the RE and RGE revealed the presence of trace elements in both. The trace elements found in both electrolytes using ICP – Mass Spectroscopy were silver, arsenic, bismuth, cadmium, copper, nickel, tin, antimony, beryllium, chromium, cobalt, magnesium, manganese, molybdenum, selenium, strontium, and tellurium. The first eight elements listed, along with zinc, are common elements found in refined lead ingots that conform to BS EN 12659:1999 [192].

Figure 4-14 gives average quantities of three iterations of each sample for each element in the two electrolytes.

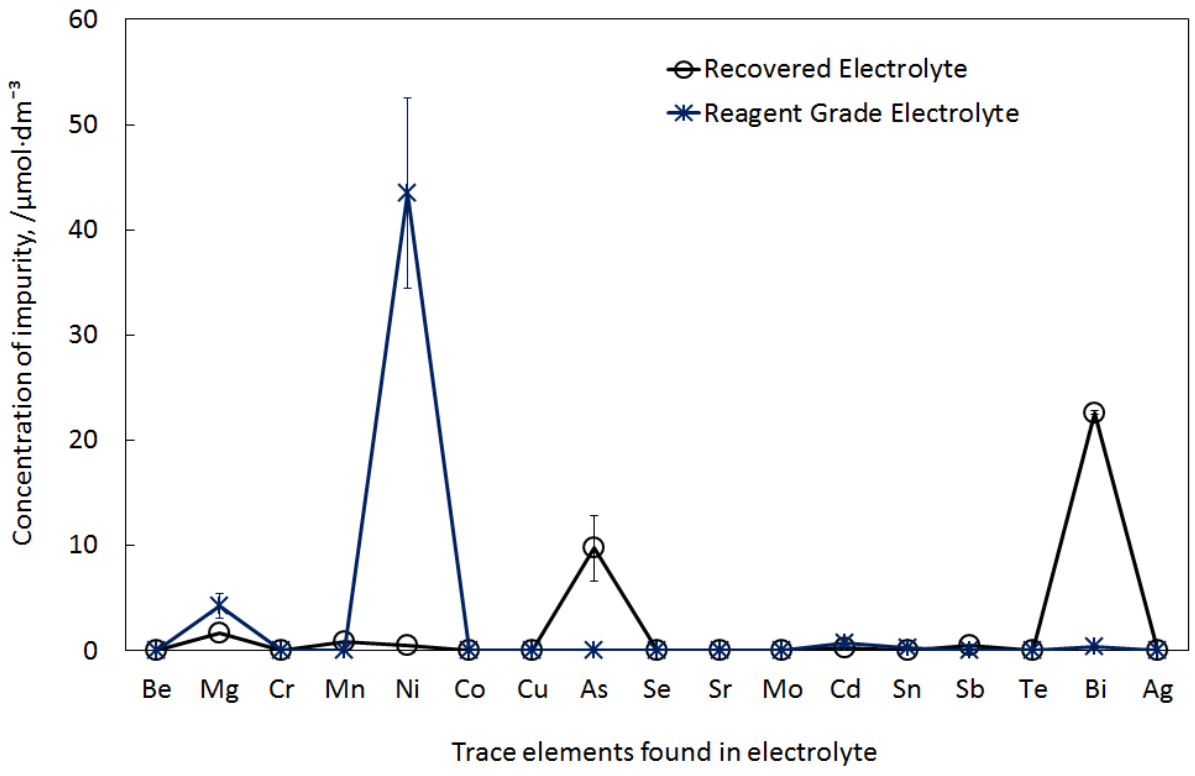

Figure 4-14: Trace elements found in samples of electrolyte made from lead acid battery electrodes. Samples were diluted and ionised using Argon plasma flame.

Figure 4-14 also shows that the highest concentrated impurity, nickel (43.5 µmol·dm^{-3}), is found in RGE, and is 48% higher in concentration than the highest concentrated impurity. Since the RGE is

made from as-is chemicals obtained from manufacturers, it would appear the presence of nickel is a result of the production process of lead methanesulfonate. On the other hand the RE is made from refined lead materials and the grids are deliberately alloyed to enhance the performance of the battery. Therefore the presence of nickel as an impurity in RE is understandably negligible.

The presence of nickel ions in a soluble lead cell is detrimental to performance of the cell. When using nickel foam as an electrode for the soluble lead cell, Hazza *et al.* [119] found that nickel leached into the electrolyte and caused a reduction in charge efficiency. Further investigation revealed a reduction of 12% at 0.1 $g \cdot dm^{-3}$ Ni^{2+} content. Cycling RE in static cells yielded an average of 30% better charge efficiency than using RGE, suggesting that nickel was hindering the performance of the cells using RGE.

Bismuth content for the RE was 22.7 $\mu mol \cdot dm^{-3}$ while the reagent grade contained 0.40 $\mu mol \cdot dm^{-3}$. A study found that the presence of bismuth aided in improvement of the stripping peak of lead dioxide, which tended to flatten and broaden with RGE [121]. The presence of Bi^{3+} improved the coulombic efficiency of the couple, by pushing the stripping peak of PbO_2 towards more positive values with continued cycling. These results were observed when 10 $mmol \cdot dm^{-3}$ Bi^{3+} in RGE resulted in a 20 fold improvement in cell cycle life, while 20 $mmol \cdot dm^{-3}$ Bi^{3+} resulted in a shift in the equilibrium potential for the PbO_2/Pb^{2+} couple from 1.440 V vs SCE at 0% content to 1.651 V vs SCE [121]. Bismuth is also used to improve contact and therefore conductivity between PbO_2 particles in the lead acid battery [173].

Other notable trace elements in both electrolytes were slightly elevated quantities of arsenic (12.0 $\mu mol \cdot dm^{-3}$) and magnesium (1.6 $\mu mol \cdot dm^{-3}$) in the RE and the highest concentration of magnesium, at 4.2 $\mu mol \cdot dm^{-3}$, found in the RGE. The effect of these trace elements does not seem to have adversely affected the RE nor the RGE. However further work is required to investigate the effect they have on the soluble lead.

4.3.4 Electrolyte Conductivity and Viscosity

The RE had a similar conductivity to that recorded for RGE at room temperature.

Table 4-4: Viscosity and conductivity of recovered electrolyte (0.7 mol·dm^{-3} Pb^{2+} and 1.0 mol·dm^{-3} MSA) measured at room temperature (294.15 K) using an Ostwald viscometer with C = 0.009236 C for the kinematic viscosity and Analytical Technology ATI Orion 162 (Pt electrode) for conductivity and electrolyte temperature.

Temperature T/K	Conductivity, C/mS·cm^{-1}	Dynamic viscosity, μ/ μPa·s
293.95	331	33.362
294.25	404	33.291
294.45	358	33.348
294.85	423	35.114
295.55	449	27.508
296.25	370	30.244

The average values for the 0.7 mol·dm^{-3} Pb^{2+} and 1.0 mol·dm^{-3} MSA RE are: Dynamic Viscosity: 0.319 mPa·s and conductivity: 401 C/mS·cm^{-1}, at room temperature. A RGE with the same concentration at 298 K was found to have 1.64 mPa·s dynamic viscosity and 275 C/mS·cm^{-1} conductivity, suggesting that the RE is less viscous than the RGE, while being more conductive, at a lower temperature.

A higher conductivity can potentially result in better migration, ensuring better kinetics for the electrolyte. A lower dynamic viscosity would result in lower friction, resulting in better fluid flow (topic for further research).

4.3.5 Voltammetry

Cyclic voltammetry was performed on RE for the Pb/Pb^{2+} and PbO_2/Pb^{2+} redox couples, using the three electrode cell shown in Figure 4-4, which had a 0.1257 cm² vitreous carbon working electrode, a Standard Calomel reference electrode and a 1.2 cm² Pt wire counter electrode. The scan rate was 25 mV·S^{-1}, and the working electrode rotational speed was 800 rpm, unless otherwise stated. All voltages are reported vs the SCE.

4.3.5.1 Lead/Lead (II) redox couple

For the Pb/Pb^{2+} couple, using an electrolyte containing 10 $mmol \cdot dm^{-3}$ Pb^{2+} RE in 1 $mol \cdot dm^{-3}$ MSA the potential sweep was applied between -0.7 V and -0.3 V. The first cycle for the couple is shown in Figure 4-15.

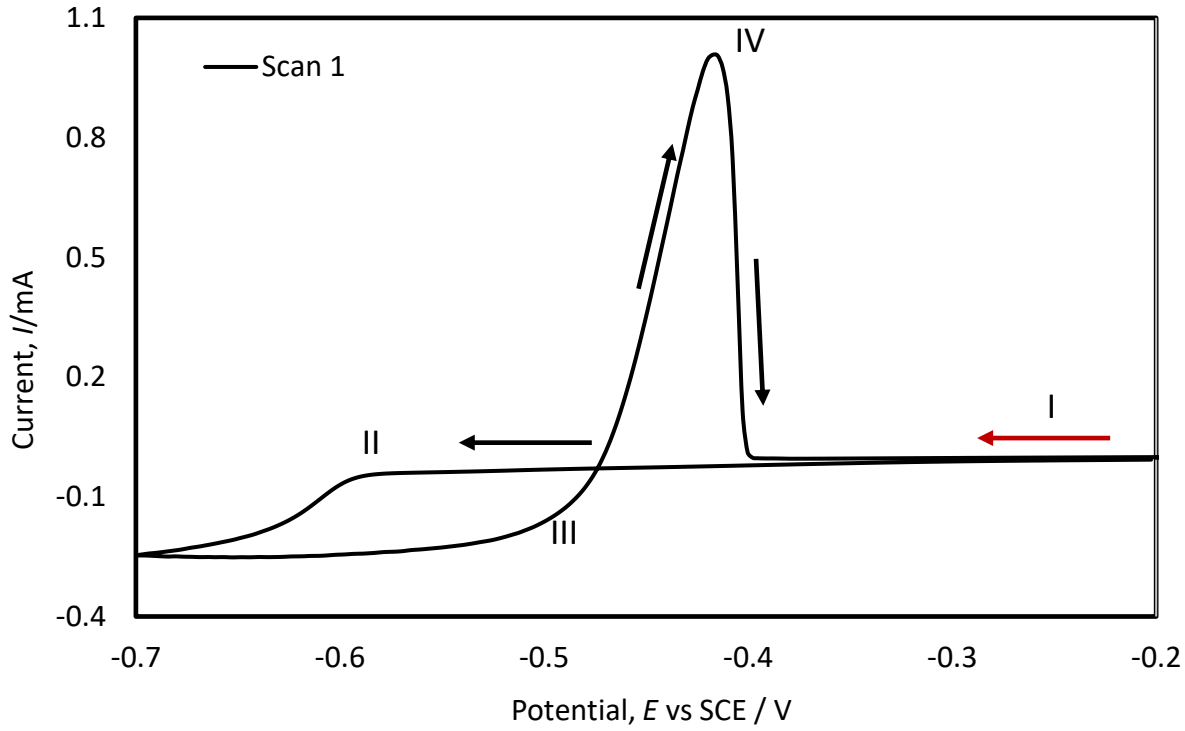

Figure 4-15: Voltammogram for the couple Pb/Pb^{2+} from CV carried out in a 3-electrode cell with a 0.1257 cm^2 vitreous carbon working electrode rotated at 800 rpm, a 1.2 cm^2 Pt-wire mesh counter electrode and a saturated calomel electrode. A potential sweep of 25 $mV \cdot s^{-1}$ was applied between -0.2 V and -0.7 V vs SCE. Concentration was 10 $mmol \cdot dm^{-3}$ Pb^{2+} RE in 1 $mol \cdot dm^{-3}$ MSA.

The potential was swept from -0.2 V towards negative potentials, as indicated by the red arrow at point **I**, until the applied voltage reached -0.55 V. A reduction peak was observed at -0.55 V (point **II**) corresponding to nucleation of lead on the electrode. A limiting current was observed at -0.7 V, indicating that reduction was limited by mass transport. Reduction continued on the return scan towards positive potentials, until -0.53 V (point **III**), when an oxidation wave commenced. A sharp anodic peak occurred at -0.41 V (point **IV**) and stripping continued rapidly until all the active species was depleted at -0.4 V. The reduction of Pb^{2+} and oxidation of Pb were rapid, characteristic of the deposition and stripping of a metal on a substrate, where the M^{2+}/M couple

kinetics are rapid and overpotentials are low [66]. The half-peak potential for RE Pb/Pb^{2+} in 1 $mol \cdot dm^{-3}$ MSA was -0.48 V. Similar findings have been observed where the nucleation and stripping of Pb/Pb^{2+} were repeatable for 200 scans with no loss of efficiency [121].

Further scanning of RE was carried out on 10 $mmol \cdot dm^{-3}$ of RE in 1 $mol \cdot dm^{-3}$ MSA. Similarly, the potential was swept towards negative potentials, between -0.2 V and -0.7 V, and the scan rate was 25 $mV \cdot s^{-1}$, and the working electrode was rotated at 800 rpm. The typical anodic deposition and stripping of metal described above was observed for the Pb/Pb^{2+} redox couple. The scans were repeated 25 times without cleaning the working electrode and some of the scans are shown in Figure 4-16.

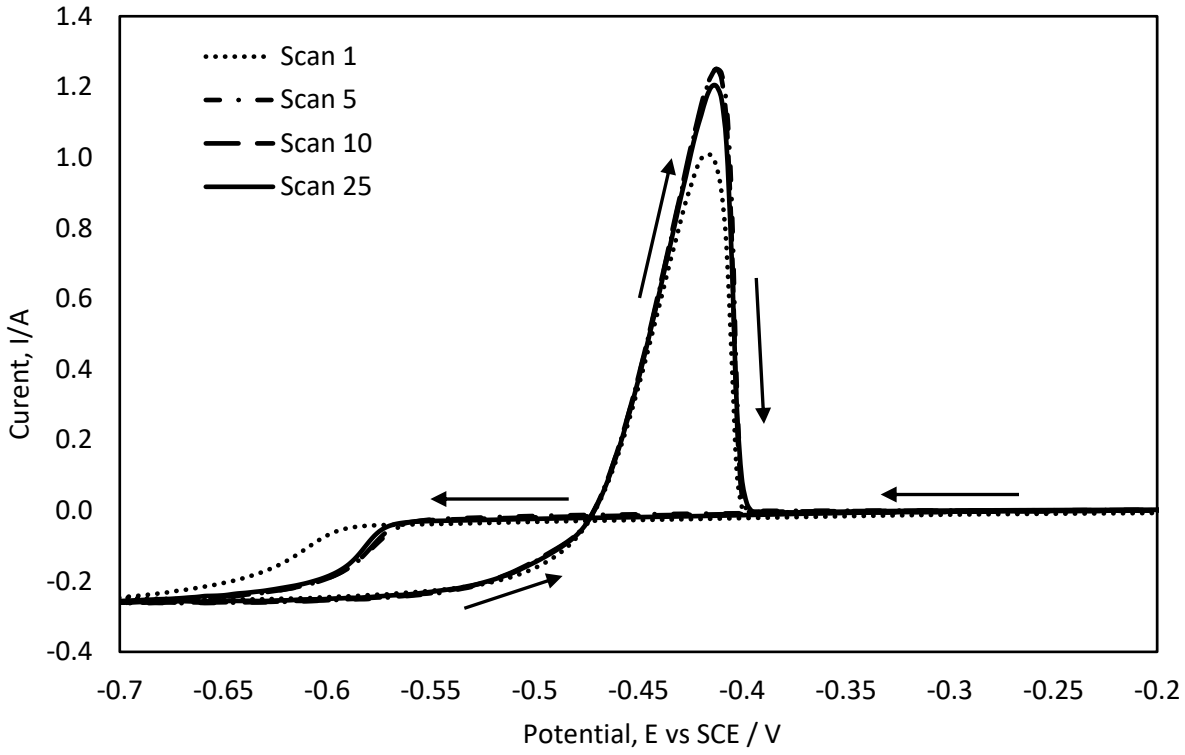

Figure 4-16: Scan 1, 5, 10 and 25 of 10 $mol \cdot dm^{-3}$ RE in 1 $mol \cdot dm^{-3}$ MSA in a 3-electrode cell with 0.1257 cm^2 vitreous carbon RDWE, SCE and Pt wire CE. Potential swept at 25 $mV \cdot s^{-1}$ between -0.7 V vs SCE and -0.2 V vs SCE. RDWE speed: 800 rpm.

The first scan has the lowest anodic and cathodic peaks, and a nucleation over-potential of 0.025 V higher than that of the 25th scan. The difference can be attributed to initial ionic resistance before stabilisation of electrolyte flow to the electrode surface. The rest of the cycles follow an almost identical path, with barely perceptible differences. For all scans nucleation and stripping

occur with low overpotentials and immediately after the equilibrium potential is exceeded, indicating a low overpotential above equilibrium, and high reversibility for all scans.

Scans of RGE in the same 3-electrode electrochemical cell were carried out to compare to RE. The 10 mmol·dm^{-3} of RGE was scanned in the same cell at 25 mV·s^{-1}, between -0.2 V and -0.7 V, with working electrode rotational speed of 800 rpm. The results for the second scan of both RE and RGE are presented in Figure 4-17.

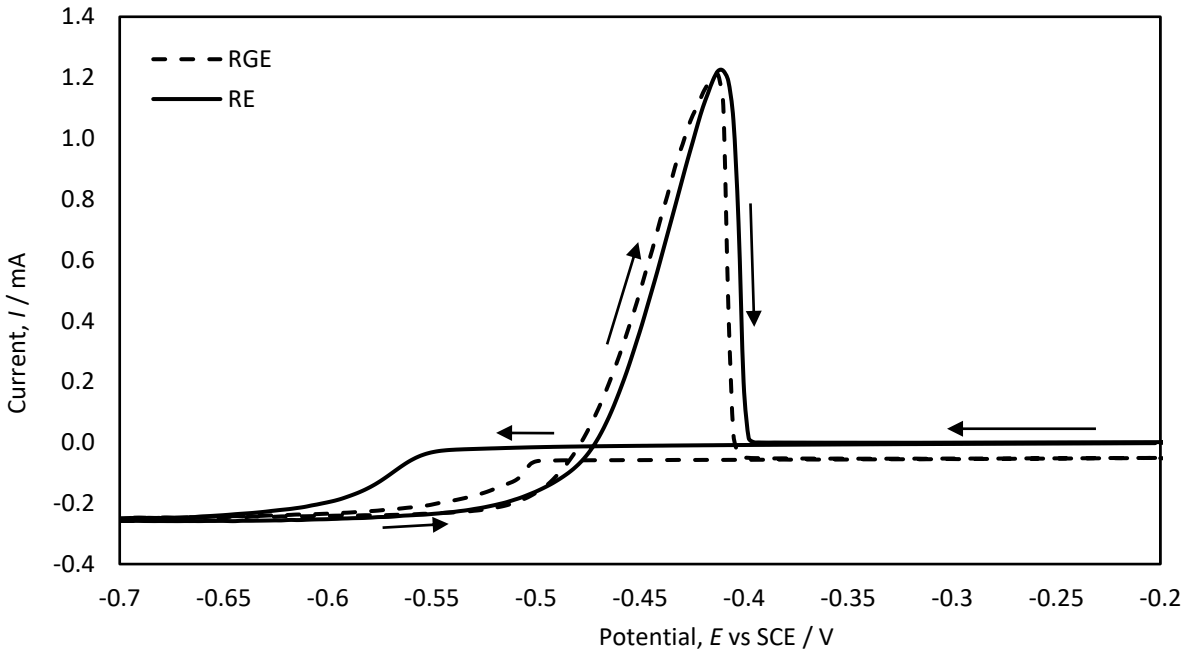

Figure 4-17: Scan 2 of 10 mmol·dm^{-3} RE and 10 mmol·dm^{-3} RGE in 1 mol·dm^{-3} MSA in a 3-electrode cells with 0.1257 cm² vitreous carbon RDWE, SCE and Pt wire CE. Potential swept at 25 mV·s^{-1} between -0.7 V vs SCE and -0.2 V vs SCE. RDWE rotational speed: 800 rpm.

Figure 4-17 shows the second scan for 0.25 mL RE in 1.0 mol·dm^{-3} MSA and another for 0.25 mL RGE in 1.0 mol·dm^{-3} MSA. The figure shows a consistent difference of 7 mV between the potential for the RE scan and that for the RGE, in favour of the RGE, except at the commencement of nucleation, where RGE has a lower over-potential by 46 mV to that of the RE.

Compared to RGE, nucleation of lead occurs at more positive potentials with RE, and the reduction occurs at a similar potentials. This suggests that in this scan the RGE is performing better, with a lower reduction overpotential, while RE lags behind. The following voltammograms

indicates that this does not stay true with longer cycling. Figure 4-11A is the voltammograms of both electrolytes overt 25 cycles, and figure 4-11B is the voltammogram for both electrolytes at scan 25.

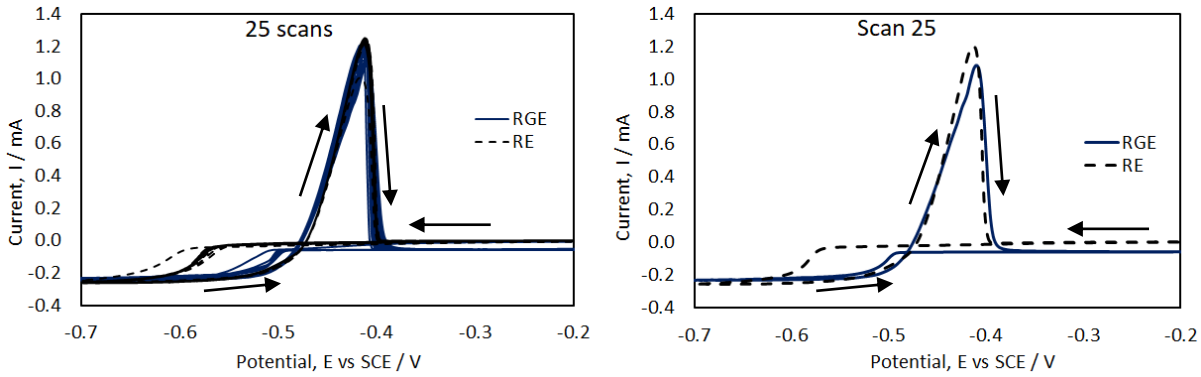

A B

Figure 4-18: Cyclic voltammograms of 0.25 mL RGE and RE electrolytes in 1 mol·dm^{-3} MSA each, at 800 rpm, 25 mV·s^{-1} between -0.7 V and -0.2 V, in a 3 electrode cell with 0.1257 cm^2 WE, SCE, and Pt wire CE. On the left is the 25 scans and on the right is the 25th scan, for both electrolytes.

The voltammogram on left in Figure 4-18 shows that the two electrolytes have fast kinetics for lead stripping. They both also start at higher overpotential for nucleation, compared to subsequent scans, even though the RE overpotential is higher, as seen in Figure 4-17. However, subsequent scans show that the RE continues to have high current efficiency between nucleation and stripping, while RGE capacity for nucleation declines gradually, until the 25th scan shows a much smaller deposition mass than the second (and first) scans. This behaviour mirrors the one observed in galvanic cycling, and suggests that the Pb/Pb^{2+} current efficiencies contribute to galvanic cell inefficiencies.

In the next Figure 4-19 , deposition and stripping of lead Pb and Pb^{2+} was carried out for RE at a rotating disc electrode at different rotational speeds. As expected, the anodic peak current increased with rotational speed, due to an increase in the concentration gradient of Pb^{2+} ions at the electrode surface [194].

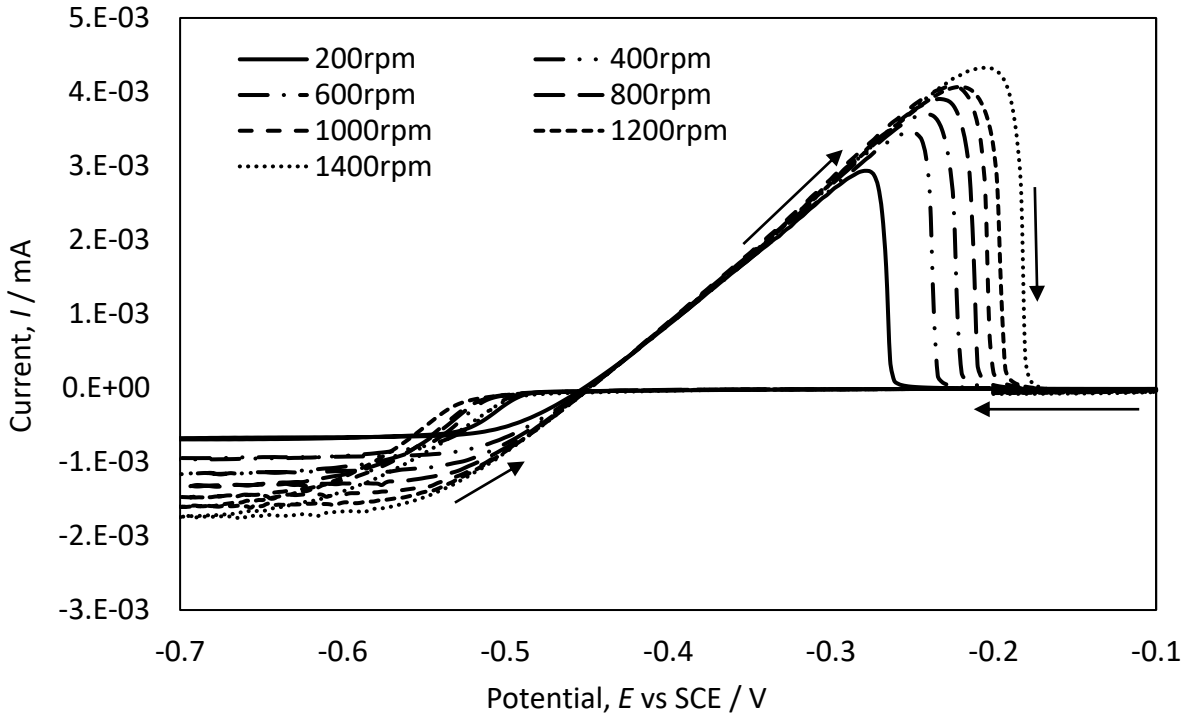

Figure 4-19: 11mmol·dm^{-3} Pb^{2+} recovered electrolyte [$Pb(CH_3SO_3)_2$] in 1 mol·dm^{-3} MSA, sweeping potential at 25 mV·s^{-1} from -0.7 V to -0.1 V, varying WE electrode rotational speeds. 3Electrode cell: 0.1257 cm² vitreous carbon WE, Calomel RE & Pt wire mesh CE.

The increasing anodic peak with increasing scan rate suggests limited reversibility of the Pb/Pb^{2+} couple. The limiting current also increases with rotational speed, in response to the faster transport of active species to the electrode surface, as well as the shrinking diffusion layer at the electrode surface. The strong dependence of the anodic peak on change in the rotational speed suggests that the reduction of lead is mass transport controlled, and the Levich plot in Figure 4-20 of the limiting current vs square root of the rotational speed confirms this [194, 196]

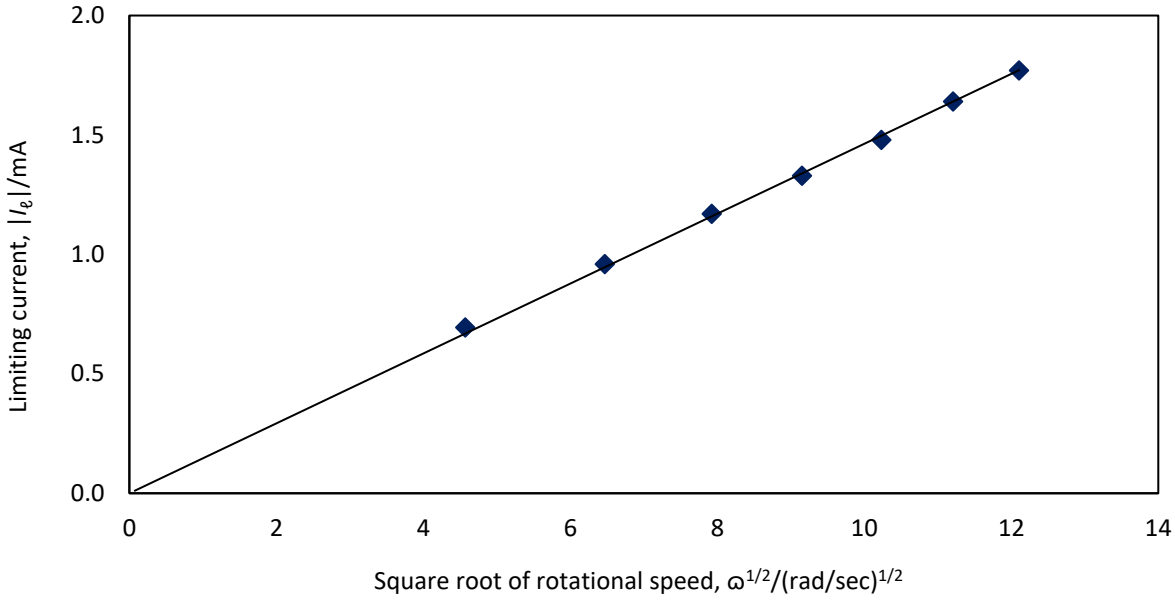

Figure 4-20: Limiting current, I_ℓ vs square root of rotational speed, $\omega^{1/2}$ of voltammograms when potential is swept from -0.1 to -0.7 V vs SCE, at 25 mV·s^{-1} in a cell made of vitreous carbon WE, Pt wire CE and SCE, containing RE at 11 mmol·dm^{-3} Pb^{2+} in 1 mol·dm^{-3} MSA electrolyte. The rotational speed was changed from 200 rpm to 1400 rpm, in steps of 200 rpm.

The Levich equation below relates the limiting current to the diffusion coefficient of the electrolyte [194, 196]. The limiting current, I_ℓ, is given by;

$$I_\ell = 0.62\mathrm{nFAD}^{2/3}w^{1/2}\upsilon^{-1/6}\mathrm{C}_{\mathrm{Pb}^{2+}} \qquad 30$$

Where n is number of electrons transferred, F is Faraday's constant, 96,845 C·mol^{-1}, A is electrode area, w is the electrode rotational speed / rad/s, v is the kinematic viscosity of the solution, $C_{Pb^{2+}}$ is the concentration of Pb^{2+} in bulk electrolyte.

4.3.5.2 Lead oxide/Lead (II) redox couple

For the PbO_2/Pb^{2+} redox couples, an electrolyte of 1 mol·dm^{-3} MSA containing 0.1 mmol·dm^{-3} Pb^{2+} RE was cycled in the same 3-electrode cell. Potential was swept at 25 mV·s^{-1} between 0.2 V and 1.9 V, from the left to more positive potentials and the working electrode was rotated at 800 rpm.

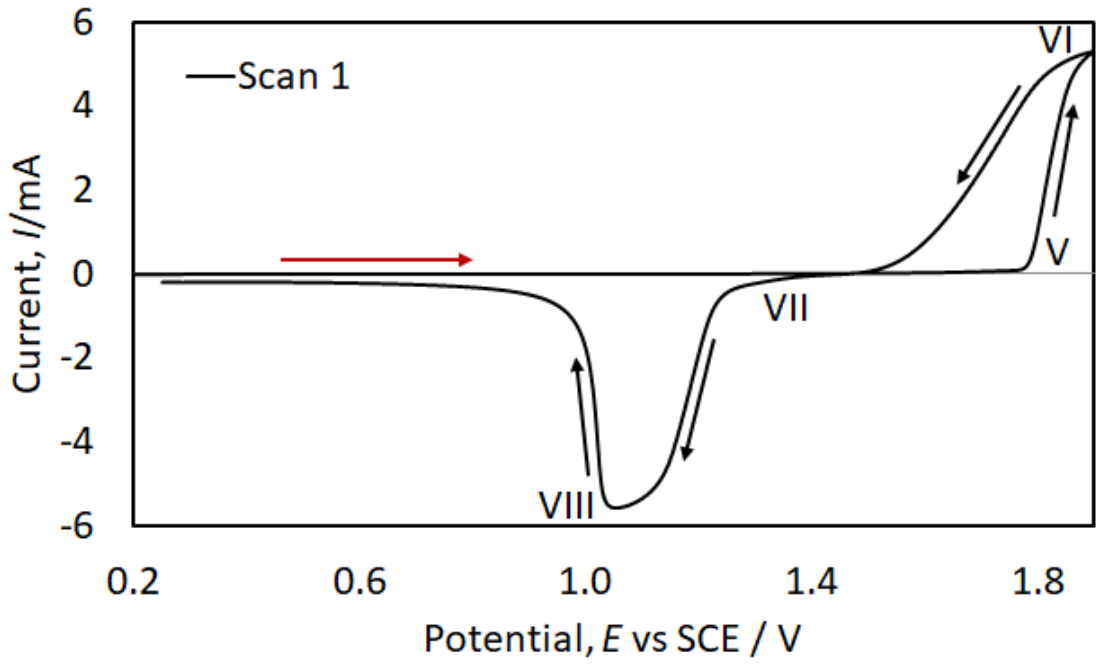

Figure 4-21: Voltammogram for the couple PbO_2/Pb^{2+} from CV carried out in a 3-electrode cell with a 0.1257 cm^2 vitreous carbon working electrode rotated at 800 rpm, a 1.2 cm^2 Pt-wire mesh counter electrode and a saturated calomel electrode. A potential sweep of 25 $mV \cdot s^{-1}$ was applied between 0.2 V and 1.8 V vs SCE. Concentration was 1 $mmol \cdot dm^{-3}$ Pb^{2+} RE in 1 $mol \cdot dm^{-3}$ MSA

Figure 4-21 shows a single voltammogram of 1 $mmol \cdot dm^{-3}$ Pb^{2+} RE in 1 $mol \cdot dm^{-3}$ MSA. The red arrow indicates the direction of applied potential sweep. For this voltammogram nucleation of lead dioxide commenced at 1.77 V vs SCE (point **V**) and continued until an anodic peak of 5 mA at 1.9 V vs SCE (**VI**). The return sweep commenced just before oxygen evolution, and on the return scan, nucleation continued until 1.5 V vs SCE. Reduction of lead dioxide to Pb^{2+} did not occur until potentials more negative than 1.4 V vs SCE (VII). A wide cathodic peak was observed at 1.05 V (**VII**), characteristic of RGE lead dioxide stripping [ref]. Stripping continued until 0.5 V when the current tapered off towards a constant current close to zero. The formal potential for the PbO_2/Pb^{2+} couple in 1 $mol \cdot dm^{-3}$ MSA was 1.475 V.

The voltammogram shows large overpotentials for both lead dioxide nucleation and reduction. This indicated poor reversibility of the reduction of PbO_2/Pb^{2+} couple and poor current efficiency, characteristic of the RGE PbO_2/Pb^{2+} couple.

Figure 4-22 shows voltammograms of the same RE electrolyte with further scanning. In the second scan anodic deposition starts earlier at 1.5 V, which suggests that it is easier to deposit lead dioxide on the second scan. Similar results have been observed with RGE elsewhere, and a black powder residue observed on the electrode after dissolution of lead dioxide was identified as lead monoxide, on which lead dioxide got deposited on subsequent scans [198]. The lower nucleation overpotential indicates that it is easier to deposit lead dioxide on this layer than on a clean electrode for RE as it is for RGE.

The second scan also had two anodic peaks, one at the switching potential, 1.9 V, and another on the backward scan at 1.7 V. The first anodic peak current was 5.4 mA and the second 4.6 mA. Therefore, the second peak yielded a lower conversion rate of Pb^{2+} to PbO_2. Three scans of 0.25 $mol \cdot dm^{-3}$ Pb^{2+} RE in 1 $mol \cdot dm^{-3}$ MSA are shown in Figure 4-23 to highlight and discuss the two-step deposition peak of lead dioxide. This tendency to a two-step anodic current is more pronounced in the subsequent cycles and can also be observed in voltage vs time plot when charging a storage cell, shown in 4.3.1.

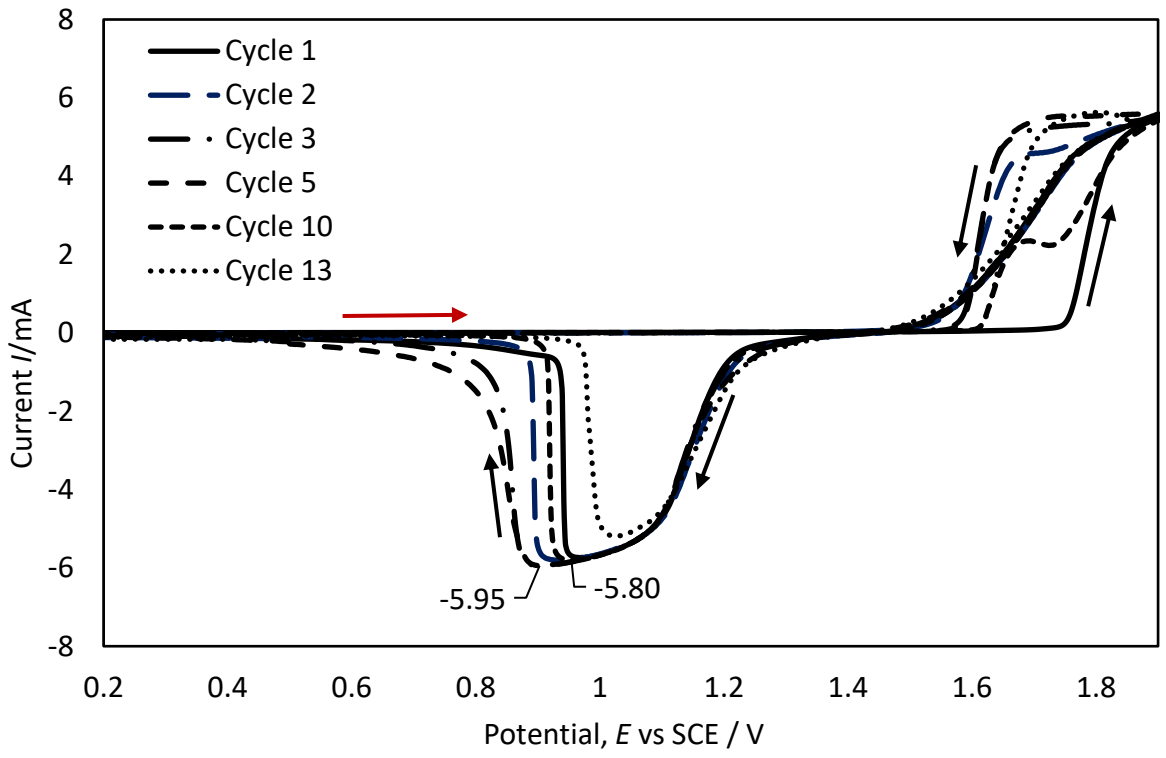

Figure 4-22: 1 mmol·dm^{-3} Pb^{2+} RE in 100 mL 1 mol·dm^{-3} MSA in a 3-electrode cell with 0.1257 cm^2 vitreous carbon rotating disc working electrode, saturated calomel electrode, and Pt wire counter electrode. Potential swept at 25 mV·s^{-1} between 0.2 V and 1.9 V vs SCE. RDWE rotational speed = 800 rpm.

The reduction wave of the second and subsequent scans in Figure 4-22 commence around the same potential (1.4 V) as the first scan, however the reduction peak gradually broadens for cycles two to five, as the amount of deposit on the electrode accumulates. At the same time the cathodic peak increases only by small steps, changing from 5.8 mA at the first scan to 5.95 mA at the fifth. From the tenth scan the amount of deposit on the electrode became dislodged, and the stripping peak became narrower. The final scan had the lowest cathodic peak, possibly because of the accumulated insoluble solids on the electrode which limit the amount of lead dioxide available to strip back to Pb^{2+}. The stripping efficiency gradually improved in the later scans compared to the initial scans, even as the amount of lead dioxide deposited and dissolved reduced with increased scanning.

Three scans of 0.25 mol·dm^{-3} Pb^{2+} RE in 1 mol·dm^{-3} MSA are shown in Figure 4-23 to highlight the two-step deposition peak of lead dioxide. A typical first scan indicates the beginning of oxidation at 1.7 V, and a rapidly increasing anodic current to a peak of 5.4 mA. A reduction wave starts at 1.4 V and continues until a cathodic peak current of -5.3 mA at 0.9 V. The cathodic current then rapidly decreases and tapers to zero from 0.87 V vs SCE to 0.6 v vs SCE. The second and third scans show more clearly the effect of the residual deposit on the working electrode, which is more readily oxidised back to PbO_2, before the oxidation of Pb^{2+} to PbO_2. For both the second and third scans, deposition commences at 1.6 V and an anodic peak is reached at 1.9 V. On the backward scan, the second anodic peaks occur at 1.73 V and 1.75 V for the second and third scans, respectively. The second peak is due to the conversion of PbO_x to PbO_2, which occurs at lower voltages than conversion of Pb^{2+} to PbO_2 [198]. Once the insoluble solid on the electrode surface has been depleted, the conversion of Pb^{2+} to PbO_2 resumes until it stops at 1.53 V.

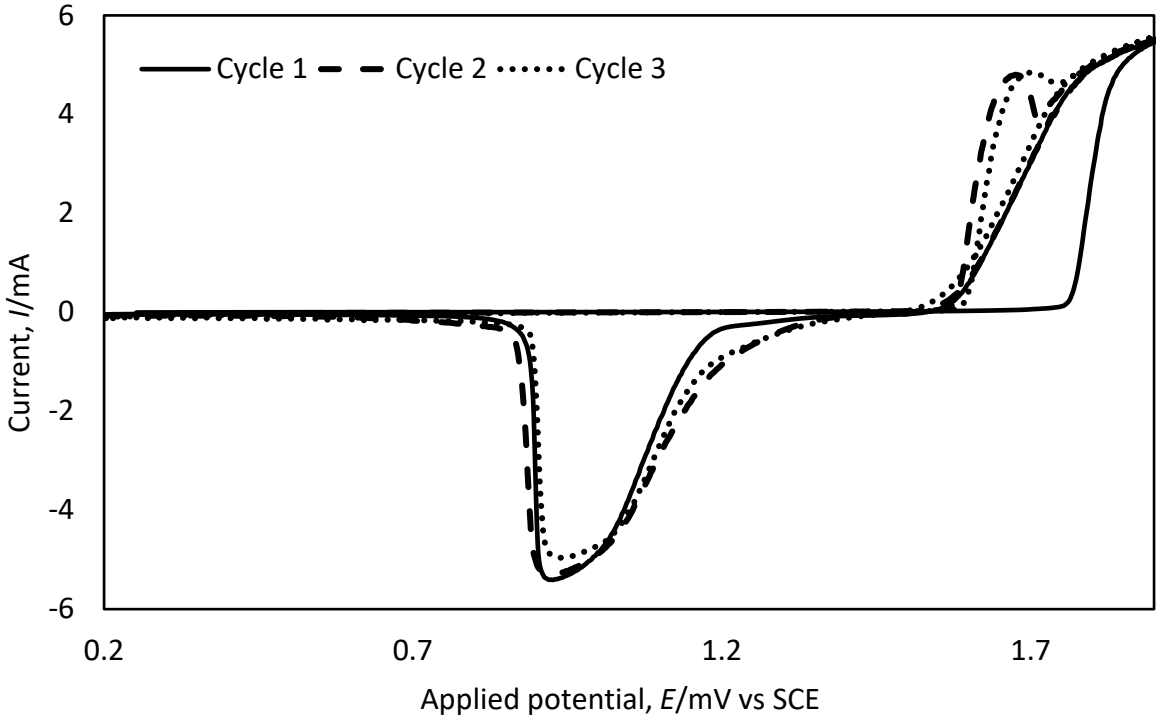

Figure 4-23: Three scans of 0.25 mol·dm^{-3} Pb^{2+} RE in 1 mol·dm^{-3} MSA, cycled in a 3-electrode cell with a 0.1257 cm² vitreous carbon rotating disc WE, Pt wire CE and SCE. Potential swept at 25 mV·s^{-1} from 0.2 V to 1.9 V. WE speed: 800 rpm.

Beyond 1.53 V, a cathodic wave commences and there is an observed cathodic peak of 5.3 mA at 0.9 V, which changes slightly to 4.9 mA on the third scan. The cathodic peaks did not change nor increase appreciably, and they remained sharp. Therefore the main differences between the first scan and the two subsequent scans is the lead dioxide deposition, which had two peaks because of the presence of insoluble solids on the electrode. The presence of insoluble solids on the positive electrode, and the subsequent two peak deposition of lead dioxide is a feature of the SLFB which contributes to battery inefficiency and limits cycle life [111, 117, 118]. Both RGE and RE show the same limitations.

The effect of increasing RE active species concentration was studied for the PbO_2/Pb^{2+} couple. Similar cyclic voltammetry experiments were carried for with 0.1 mol·dm^{-3}, 0.25 mol·dm^{-3}, and 0.5 mol·dm^{-3} RE in 1.0 mol·dm^{-3} MSA. The voltammograms shown in Figure 4-24 indicate a shift to more positive nucleation potentials as the concentration of active species increased, while the reduction over-potentials required to strip lead dioxide from the electrode increased in the negative direction. This resulted in a larger potential difference between the commencement of the anodic and cathodic waves, reducing the current efficiency. The peak cathodic current also reduced with increase in active species concentration.

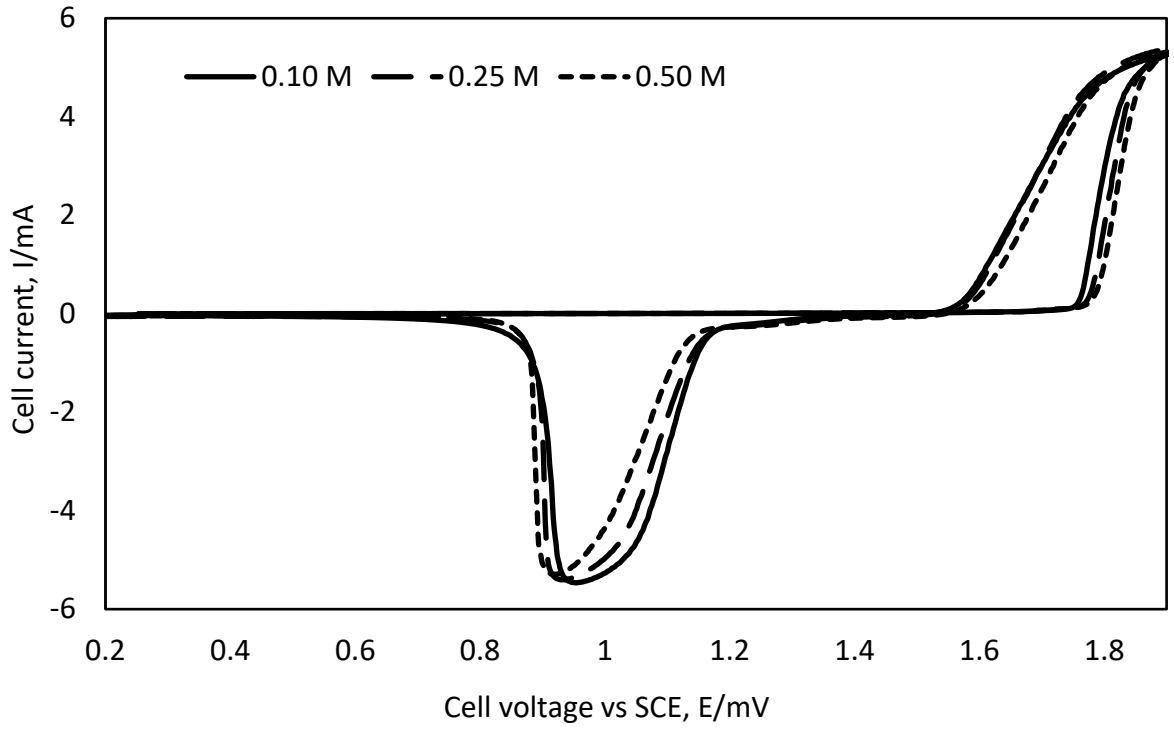

Figure 4-24: CVs of different concentrations of Pb^{2+} in 1 mol·dm^{-3} MSA using 3 electrode cell; 0.1257 cm² VC WE, Saturated Calomel E & Pt wire mesh CE. 800rpm, 0.2V to 1.9V. 25 mV/s

The cyclic voltammetry results confirm that the PbO_2/Pb^{2+} couple for RE has poor reversibility, similar to reported RGE results [111, 117, 118]. This manifests as undissolved solids at the electrodes and inside a storage cell, which causes shorting, depletes Pb^{2+} ions in the electrolyte, and limits cell cycle life.

4.3.6 Scanning Electron Microscopy with EDX

Scanning Electron Microscopy was used to analyse powder samples of both the positive and negative electrodes of an expended, YUASA NP Series: NP7-12 valve regulated lead acid battery.

Results show presence of lead, sulfur and oxygen in the electrode material scans, consistent with composition of lead acid battery pastes [173]. The first sample was the ground powder of the negative electrode of from a YUASA NP Series: NP7-12 lead acid battery. It had small particle sizes measuring micron to tens of micros. The powder from both electrodes also had similar particle

sizes. The RE, which was dried and crushed, but not ground to powder showed the crystalline structure of lead methane sulfonate.

<table>
<tr><td> 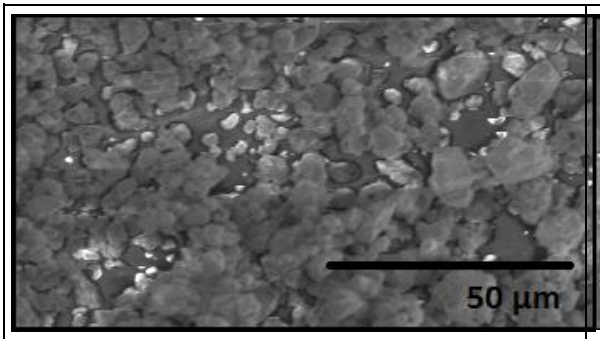
</td><td> 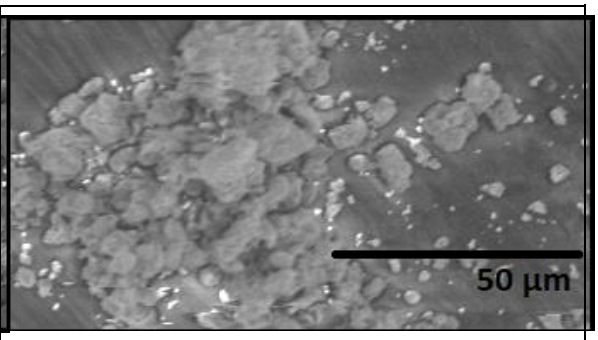
</td></tr>
<tr><td>Negative electrode powder</td><td>Negative & Positive electrode powder</td></tr>
<tr><td> 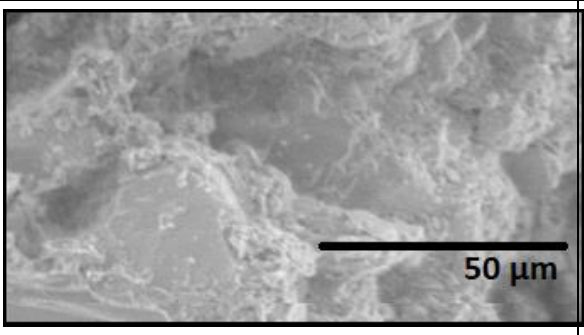
</td><td> 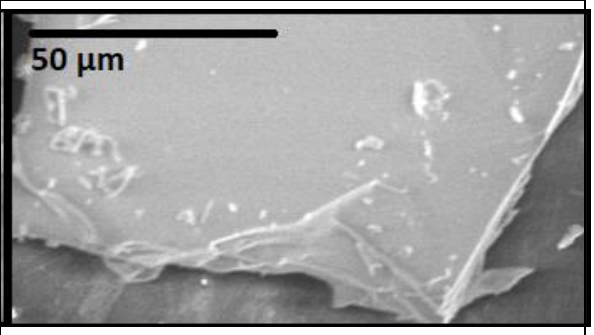
</td></tr>
<tr><td>Dried recovered electrolyte</td><td>Dried lead methanesulfonate</td></tr>
</table>

Figure 4-25:

None of the samples revealed the presence of trace elements, as shown by the figures below.

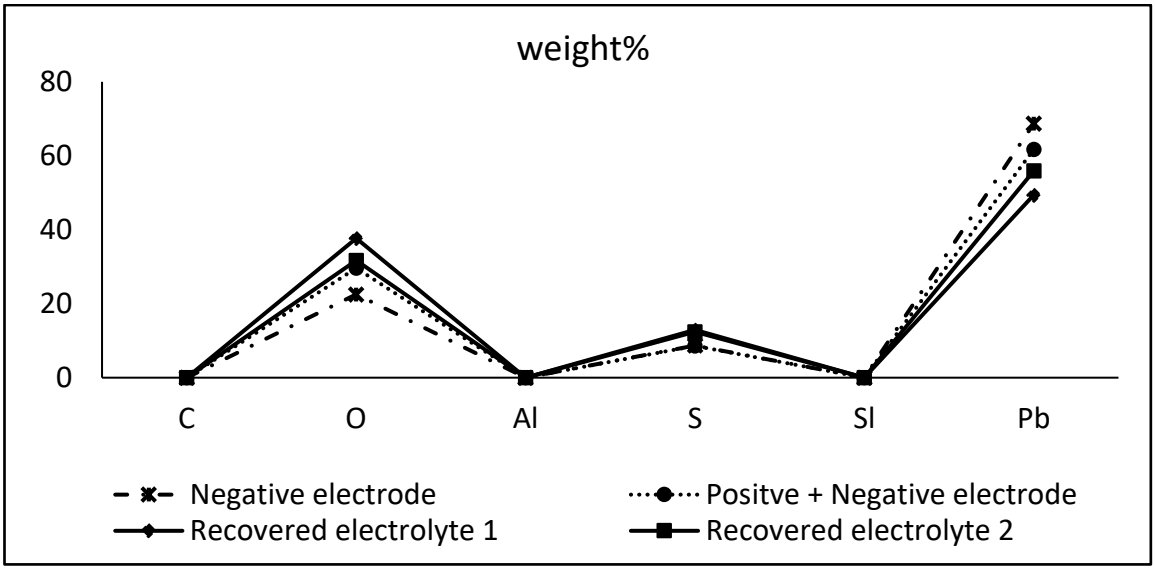

Figure 4-26: The percentage weight contribution of components of four samples under SEM. The samples were: powder from the negative electrode of a YUASA NP Series: NP7-12 VRLA; a mixed powder from both the negative and positive electrode of the same battery; 2 mol·dm^{-3} Pb^{2+}recovered electrolyte made from the same battery electrode.

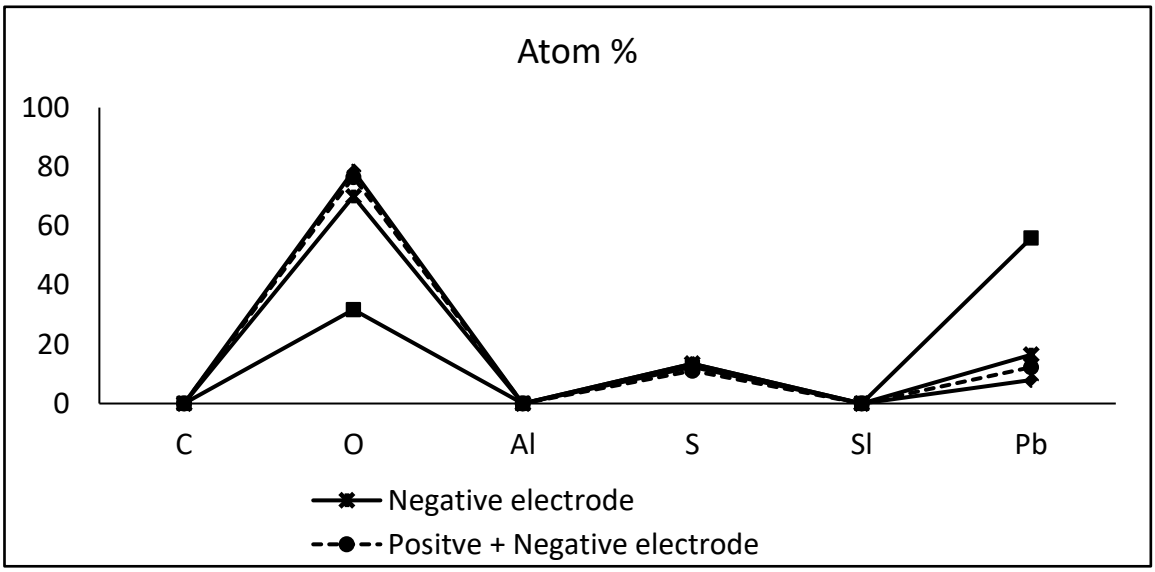

Figure 4-27: The percentage atom contribution of components of four samples under SEM. The samples were: powder from the negative electrode of a YUASA NP Series: NP7-12 VRLA; a mixed powder from both the negative and positive electrode of the same battery; 2 mol·dm^{-3} Pb^{2+}recovered electrolyte made from the same battery electrode.

Both Figure 4-26 and Figure 4-27 confirm the presence of Pb, S, and O as expected. The atomic ratios are also as expected. However, the presence of aluminium and silicon are a result of equipment error and were unfortunately expected with the equipment used. The detection limit of the method was not enough to reveal the presence of trace elements, which were expected to be present in the recovered electrolyte because of the refining processes during manufacture of lead acid batteries.

Similar analysis was carried out for dried electrolyte samples. Samples were dried and analysed under a Scanning Electron Microscope with EDX to determining sample composition at a different resolution.

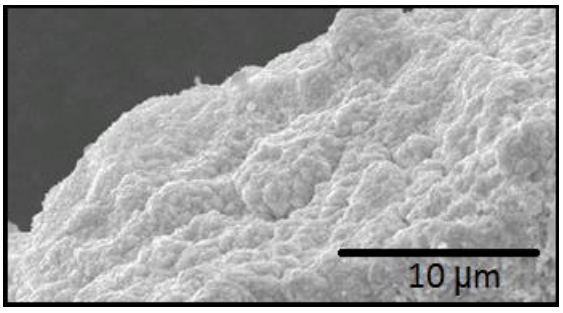

Sample A(i) – negative electrode powder

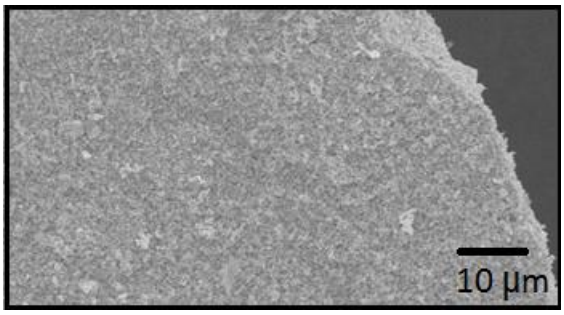

Sample A(ii) – negative electrode powder

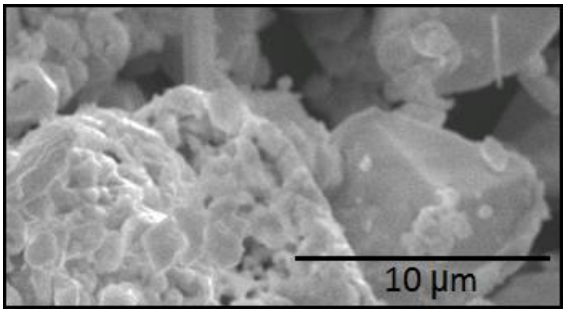

Sample B(i) – RE electrolyte

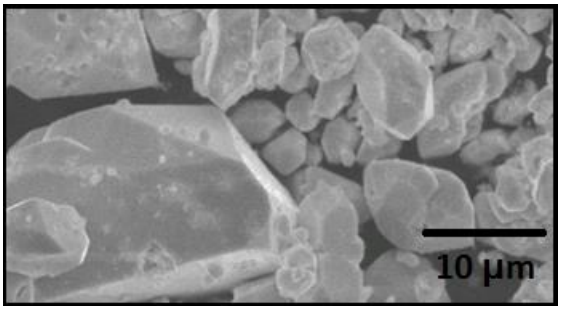

Sample B(ii) – RE electrolyte

Figure 4-28: SEM/EDX images of dried samples of electrolyte made from spent lead acid batteries. Images on the right are scaled images of those on the left. Sample A is a dried sample of electrolyte made from the negative electrode of a spent lead acid battery. Sample B is the dried electrolyte made from both the negative and positive electrodes.

Sample A is solid mass with a rough surface and an undefinable structure at this resolution. The result showed that the sample contained 80% Pb. Sample B is better identifiable as a crystal, indicating the presence of lead methanesulfonate. The EDX method detection limit was still not

sufficient to show trace elements. Nonetheless elemental Analysis using ICP – Mass Spectroscopy was enough to identify and quantify the trace elements in the electrolyte.

4.4 Chapter Conclusions

In this chapter RE was cycled in static and flow cells and compared to RGE in the same cells. The electrolyte viscosity, density and conductivity was also measured and compared to literature. Scanning Electron Microscopy was used to identify the trace elements in the lead acid battery electrodes as well as in the RE. Finally, cyclic voltammetry was used to characterise the RE's electrochemistry.

The RE performs better than the RGE in both the static and flow cells. Section 4.3.1 indicates that, in the static cell with 1.0 mol·dm^{-3} Pb^{2+}, the RE had 89% charge, 86% energy and 96% voltage efficiency compared to 63%, 49% and 78% charge, energy and voltage efficiencies, respectively, for the RGE. Cells with either electrolyte have columbic efficiencies close to or above 80%. For the RE flow cell, high coulombic efficiencies above 90% are reached at the first cycle. This implies that the battery can potentially be used to deliver most of its rated capacity instantaneously. This would be useful for grid applications as well as medium (kWh) to large (MWh) stationery energy storage applications.

The tendency towards two-stage charge voltage after the first cycle was observed for both electrolytes in both the static and the flow cells. This behaviour is due to formation of solid PbO or PbO_x at the positive electrodes during charge [66, 102, 111, 115, 198]. During discharge, solid PbO/PbO_x is converted to Pb^{2+} ions at 1.8 V first, before PbO_2 is at 2.0 V. This creates the two discharge voltage levels. This phenomenon contributes to the eventual build-up of solids on both electrodes and affects cells with both electrolytes. It evidences the similarity of the two electrolytes and confirms that the two can be used interchangeably.

The conductivity of the RE was higher than that of RGE reported in literature, at lower temperatures. The viscosity was lower comparatively, suggesting lower flow resistance. At the scale of the cells under investigation, the differences are insignificant, however for scaled batteries, the lower viscosity could have a cumulative positive effect of reducing pumping needs.

To investigate the presence of trace elements in the electrolyte, which could influence the performance of the electrolyte, SEM was performed on the electrode material of a YUASA NP 7: 12 V VRLA. The scans did not reveal any trace elements, instead confirming the presence of lead, oxygen and sulfur, which make up the paste material of a lead acid battery. The SEM detection limit

was too low to reveal the presence of the trace elements, hence another method was sought to identify and quantify the trace elements.

To investigate the cause of the superior performance of the RE over RGE, never before-done elemental analysis was performed on both electrolytes. The results revealed that both electrolytes contained trace quantities of impurities:

The RE contained 22.7 $\mu mol \cdot dm^{-3}$ bismuth (III) ions. Bismuth aids in the stripping efficiency of lead dioxide, which improved the coulombic efficiency of the PbO_2/Pb^{2+} couple, by pushing the stripping peak of PbO_2 towards more positive values with continued cycling [121]. The overall effect was an improvement in cycle life for a cell containing bismuth compared to one that didn't. In this study, static cells using RE had at least double the cycle life of RGE, while flow cells using 0.7 $mol \cdot dm^{-3}$ Pb^{2+} and 1 $mol \cdot dm^{-3}$ MSA RE had 85% more cycles than those using RGE with the same concentration.

Bismuth also promotes growth of smoother lead dioxide deposit, thereby improving conduction between particles and to the current collector. It is because of the latter reason that bismuth additive is used to aid conductivity between PbO_2 particles in lead acid batteries. The presence of bismuth clearly benefits soluble lead cells, and it is desirable to have it in the electrolyte. The RE already contains bismuth from the preparation of lead acid batteries, and therefore the electrolyte has an inbuilt advantage.

This study revealed the presence of the nickel impurity in RGE, which was not been highlighted before. It has been reported that nickel affects charge efficiency negatively even at 0.1 $g \cdot dm^{-3}$. This study quantified nickel in RGE, and revealed that even at 43.5 $\mu mol \cdot dm^{-3}$ nickel is detrimental to the operation of the soluble lead battery. Based on the findings of this project, it is therefore recommended that the soluble lead battery should not contain nickel ions.

In commercial lead acid batteries, additives are used to enhance the performance of the batteries. The RE already contains some if not all of the additives added to batteries to enhance performance. Just as important, lead acid battery electrodes are also made from lead materials refined during recycling, where the elements detrimental to the performance of the battery are removed. This means the electrolyte made out of the spent lead acid batteries benefits not only from the refining, but also the addition of helpful elements that enhance performance.

On the other hand, RGE, which has been revealed to contain nickel, does not benefit from such treatments. If the same performance of RE is to be obtained, as a minimum, then the reagent grade lead methanesulfonate has to be pre-processed to remove nickel. The other option would be to change the production process of lead methanesulfonate to remove nickel during

processing. Both these options are expensive and could be energy intensive. However, using RE not only presents an electrolyte that performs better, it also eliminates the extra cost and effort associated with pre-processing. It is recommended then that, at a minimum, the soluble lead battery should use RE, which is cheaper and is made sustainably out of spent lead acid batteries.

The electrochemical properties of the RE were investigated using cyclic voltammetry. The results show that the RE has better reversibility at the anode than does the RGE. Similar results are seen at the cathode, where reduction of lead dioxide to Pb^{2+} occurs at more positive potentials than with the RGE.

Just like RGE, the RE shows poor reversibility at the PbO_2/Pb^{2+} couple, where undissolved solids are preferentially converted to PbO_2 before Pb^{2+} during deposition, and the insoluble solids accumulate on the electrode, further reducing the efficiency of the couple.

With the Pb/Pb^{2+} couple, RE experiences an initial overpotential 46 mV vs SCE larger than RGE for the deposition of lead onto the electrode. However, subsequent scans had a similar overpotential as RGE and the RE electrolyte cycled for longer with no loss in efficiency. This supports the better cycle life exhibited by both the static and the flow cells.

The results of this chapter are supported by the published paper below:

Orapeleng, K., Wills, R.G.A., and Cruden, A., Performance of recovered and reagent grade electrolyte in a soluble lead redox cell. Journal of Energy Storage, 2018. 20: p. 49-56.DOI: https://doi.org/10.1016/j.est.2018.08.017

Chapter 5 Further Investigations on the Effect of Cycling on Cell Performance

5.1 Introduction

The challenge to the soluble lead cell remains the tendency for electrode deposit to build up in the cell, constricting the electrolyte flow, causing short-circuits, and gradually depleting Pb^{2+} ions in the electrolyte [117, 120, 198], all of which limit the cycle life of the cell. Use of additives in reagent grade electrolyte (RGE) has been suggested to improve deposit particle smoothness and compactness in an attempt to reduce deposit build-up on the electrodes and improve cell cycle life [67, 104, 119, 121]. HDMA in RGE was found to significantly improve the lead deposit morphology without adversely affecting the positive electrode [104]. A bismuth additive in RGE added to the positive half-cell in a divided cell improved cell cycle life twenty-fold [121]. Therefore, some additives have been found to improve the performance of a soluble lead cell that uses RGE.

However, chapter 3 shows that RGE contains nickel, which is detrimental even at trace quantities. In fact the recommendation from that finding is to use RE as a minimum instead of RGE. Not only does RE have negligible amounts of nickel due to the refinement process during lead acid battery recycling, it also already contains additives beneficial to performance of the soluble lead battery [185]. This chapter investigates the effect of cycling recovered electrolyte in different regimes as an alternative method to improve charge efficiency and cycle life of the soluble lead battery.

Control of cycling conditions has been employed to enhance battery cycle life and ensure safe operation of lithium-ion batteries [200]. In the $LiCoO_2$ battery charging at >0.2C at –20 °C results in plating of lithium onto the graphitised carbon negative electrode surface, reducing battery cycle life. If the battery is then operated at room temperature, the loss of capacity is permanent and the battery cycle life declines [201]. The study of Li_xC_6 in 1.0 mol·dm^{-3} $LiPF_6$ /EC + DEC electrolyte showed commencement of SEI (Solid Electrolyte Interface) decomposition at an average 61°C, which enabled the electrolyte to penetrate the broken SEI and reach the edge of lithiated graphite and react with lithium, resulting in formation of another SEI until all the lithium was depleted or the lithium was converted to Li_2CO_3 or LiF that blocked the edge planes and exacerbated thermal runaway [202]. Prevention of this damage can be achieved by imposing relevant minimum and maximum operating temperatures using battery management systems to ensure safe operation of the lithium ion as well as prevent permanent capacity loss and enhance cycle life [200].

Over-discharge or low voltage causes cathode lattice collapse in lithium ion batteries, which is detrimental to battery performance. At 0.521 V vs SHE the copper current collector dissolves, and then forms dendrites when the battery is recharged, which causes short-circuits [200]. Over-discharge also causes a reduction in electrolyte and production of combustible gas, and subsequent thermal runaway. Over-discharge in lithium ion batteries causes the positive electrode to decompose, resulting in production of heat as well as deposition of metallic lithium on the negative electrode, and subsequent capacity loss and internal short circuits, all of which lead to thermal runaway [203]. Therefore, battery management systems have been employed in commercial lithium ion batteries to prevent both over-charge and over-discharge.

Electronic battery charge controllers have also been employed to integrate batteries and other energy storage technologies into the grid or to regulate operation in isolated electricity supply systems. Charge cycle control is employed to facilitate synchronisation of the vanadium redox flow battery with the PV generation system it is connected to [29]. Similar controls are credited with reducing generation costs by between 1.35% and 25.3% for isolated grid systems, dependent on the type of system and renewable energy penetration level [204].

Failure modes of the lead acid battery:

For lead acid batteries, charge regulators have been employed to control charge and discharge, to maintain float charge, prevent heat runaway and cell drying, and to equalise charge in stacked cells [62, 126, 131, 132]. These controls improve cycle life and ensure safe operation of lead acid batteries. The softening and loss of Positive Electrode Material (PAM) in a lead acid battery is a natural failure mode that progresses with battery use [126]. With continued cycling coherence between the materials of the positive electrode lessens and eventually the material disintegrates and no longer participates in electrochemical activity [133]. Use and abuse of the battery can accelerate this failure mode, when the battery is over-charged [126]. Charge regulators impose an End of Charge Voltage (EoCV) to prevent overcharge and premature PAM loss. Float charge at high current also improves cycle life by increasing the cell internal temperature, which promotes coherence in PAM and promotes $PbSO_4$ dissolution to PbO_2 [126]. However, cell temperatures need to stay under 60°C to prevent sulfation, therefore temperature monitoring and control is also necessary in battery management. Sulfation also occurs when VRLA are subjected to high rates of charge (~ 18C) and discharge under partial charge conditions. High rates of discharge lead to rapid formation of lead sulfate on the surface of the negative electrode plate, which does not penetrate the plate, but instead accumulates on the surface. This reduces the effective area for electrochemical activity and blocks diffusion of H^+ into the electrode plate. This reduces the capacity of the battery. Partial charge results incomplete conversion of lead sulfate to lead,

therefore the lead sulfate becomes a site for hydrogen evolution, which is exacerbated at high charge currents [132]. Charge regulators ensure that the charge and discharge rates for lead acid batteries is kept low enough to enhance battery life and protect battery capacity.

Using charge controllers to force a full charge for VRLA used in conjunction with PV energy restored the batteries' full capacity, which was otherwise lost when the batteries were operated under constant partial charge [134].

The lead acid battery requires charge control to prevent battery state-of-charge falling below a set value due to self-discharge, which if allowed could result in sulfation. Sulfation occurs when the sulfate ions of a discharged battery form large crystals which are difficult to convert back to lead and lead dioxide during charge. Discharging at high current rates cause sulfation, as does operation at temperatures above 60°C, for VRLAs. By supplying a float charge, charge controllers prevent self-discharge of stored batteries and prevent permanent damage to battery capacity.

When a cell is allowed to rest after charge, mass transport is the only mechanism by which the cell is allowed to discharge, in this case, carrying the Pb^{2+} ions from both the anode and the cathode into the electrolyte. Forcing the cell to discharge further by drawing a current from it forces the cell to relinquish whatever charge is still available on the electrodes, potentially discharging more energy out of the cell.

The SLFB battery degradation mechanisms are incomplete reduction of PbO_2, which results in build-up of both Pb and PbO_2 on the electrodes, and subsequent detachment of PbO_2 from the positive electrode, and consequent reduction of Pb^{2+} ions and increase in acid concentration in the electrolyte. An investigation of the mechanism of degradation revealed that at high acid concentration [> 1M], PbO_2 reduction tended to occur at progressively more negative potentials, and eventually stopped while deposition occurred at more positive potentials [111]. At 2.2 $mol \cdot dm^{-3}$ MSA, PbO_2 reduction occurred even earlier, after the 2nd cycle. At lower acid concentration, 0.2M [H^+], cycling continued for more than a hundred cycles at high charge efficiency. Change in [Pb^{2+}] did not have an effect on the reduction potential nor the deposition potential, but it did lower the charge efficiency from 94% at 1.2 $mol \cdot dm^{-3}$ Pb^{2+} to 90% at 0.6 $mol \cdot dm^{-3}$ and finally 83% at 0.2 $mol \cdot dm^{-3}$ Pb^{2+}. A higher impedance was also recorded for low reduction potentials. It was also observed that less deposit mass was recovered from reduction that was deposited. And that open circuit relaxation was characterised by gradual mass loss, indicating that some deposit was being converted to a soluble species.

Deposition of non-stoichiometric PbO_x occurred above $[H^+] > 1M$, and the PbO_x passivates the electrode. The PbO_x has poor solubility and a high electric resistance, which explains the SLFB's low (2 compared to 15 in above example) cycle life.

At low current density, 2 $mA \cdot cm^{-2}$, the mass of deposited PbO_2 almost equals that of dissolved deposit. With higher current density, the deposited mass reduces even when there is no undissolved residue. This confirms a competing OER, where the partial current for deposition of PbO_2 reduces by the same amount as increase in OER partial current. The higher the current density the higher the OER. However, increase in OER declines with increasing current density.

5.2 Methodology

Galvanic Cycles

The static cell shown in Figure 4-1 was cycled at constant current under different conditions and the effect on cycle life and charge, voltage and energy efficiencies noted.

The cell had 5 cm x 5 cm 2D electrodes made of Sigracell carbon polymer material. The current collectors were made of 0.1 mm nickel foil and the cell chamber was made of silicone rubber material. Parafilm was used to cover the cell to limit electrolyte evaporation. The cells were connected to an MTI multi-analyser that controlled the experiments and recorded the data. Each experiment was repeated three times and an average of the data was used.

All experiments were conducted at approximately 298 K. The following conditions were changed to monitor the effect on performance and cycle life for the cells:

- Cycling regimes
- Current density
- End-of-discharge voltage
- Open Circuit (OC) periods imposed on the cells (Self-discharge)
- Whether or not cells were divided
- Inter-electrode gap

5.2.1 Cycling Regimes

The static cell shown in Figure 4-1 was cycled using recovered electrolyte made using the method described in 4.2.1. The cells were all charged and discharge for 20 minutes each, unless otherwise

stated. Each cell was first charged for 20 minutes at the stated current density before cycling commenced. The table below differentiates the cycling regimes used on the cells.

Table 5-1: Cycling regimes used to investigate the effect of different conditions on operation of static cell using recovered electrolyte at approx. 298 K.

Cycling Regime Ref.	**Cycling regime after 1st charge**	**Open Circuit Rest time, O/C Time/h**	
A	Rest 2 min, discharge 20 min, rest 2 min, charge 20 min, repeat 5 times. Then Open Circuit rest.	0.1, 0.25, 0.5, 1, 2, 5, 10, 24	Open Circuit rest time altered after every 6 cycles.
B	Rest 2 min, discharge 20 min, rest 2 min, charge 20 min, Open Circuit rest. Repeat 5 times.	0.1, 0.25, 0.5, 1, 2, 5, 10, 24	Open Circuit rest time altered after every 6 cycles.
C	Open Circuit rest, discharge 20 min, Open Circuit rest, charge 20 min. Repeat until failure*.	0.1, 0.25, 0.5, 0.75, 1, 24	Open Circuit rest time maintained for all cycles.
D	Open Circuit rest, discharge 20 min, 2 min Open Circuit rest, charge 20 min. Repeat until failure*.	0.1, 0.25, 0.5, 0.75, 1, 24	Open Circuit rest time maintained for all cycles.

*Failure defined when charge efficiency fell below 60%.

5.3 Results and Discussion

Static cells made of 5 cm x 5 cm by 2.1 mm thick Sigracell electrodes, 0.1 mm nickel foil current collectors, and covered with parafilm were cycled at constant current under different conditions to ascertain effect on cycle life, charge, energy and voltage efficiencies. The effects are documented below.

5.3.1 Effect of different cycling regimes

Krishna et al. [179] have found that a soluble lead redox flow battery that operates with a Pb^{2+} ion concentration of 0.7 mol.dm^{-3} and an acid concentration of 1.0 mol.dm^{-3} gives the best cycling life. Using this electrolyte, I investigated the effect of different cycling regimes on static cells. The cycle regime involves cycling electrolyte at a constant flow rate and maintaining the same current density while changing the length of time the cell is allowed to stand at open circuit. The aim was to determine whether withdrawing the applied voltage from the electrodes, and letting the electrolyte sit undisturbed would cause a decrease in electrolyte polarisation, and hence result in a lower discharge voltage than when the electrodes were recently charged, and the electrolyte still polarised. Therefore the time the cells were left on open circuit was gradually increased and the effect on cycle efficiency noted.

For the following experiments a recovered electrolyte of 0.7 mol·dm^{-3} Pb^{2+} and 1.0 mol·dm^{-3} MSA was used. The same static cells specified above were used.

5.3.1.1 Cycle Regime A

The static cells were initially charged for 20 mins, left on open circuit for 2 minutes, and then cycled between discharge and charge at the same rate, 5 more times. Between each six iterations of cycling, the cells were allowed to rest fully charged for 0.1, 0.25, 0.5, 1, 2, 5, 10, and finally, 24 hours. This type of cycling was called Cycle Regime A.

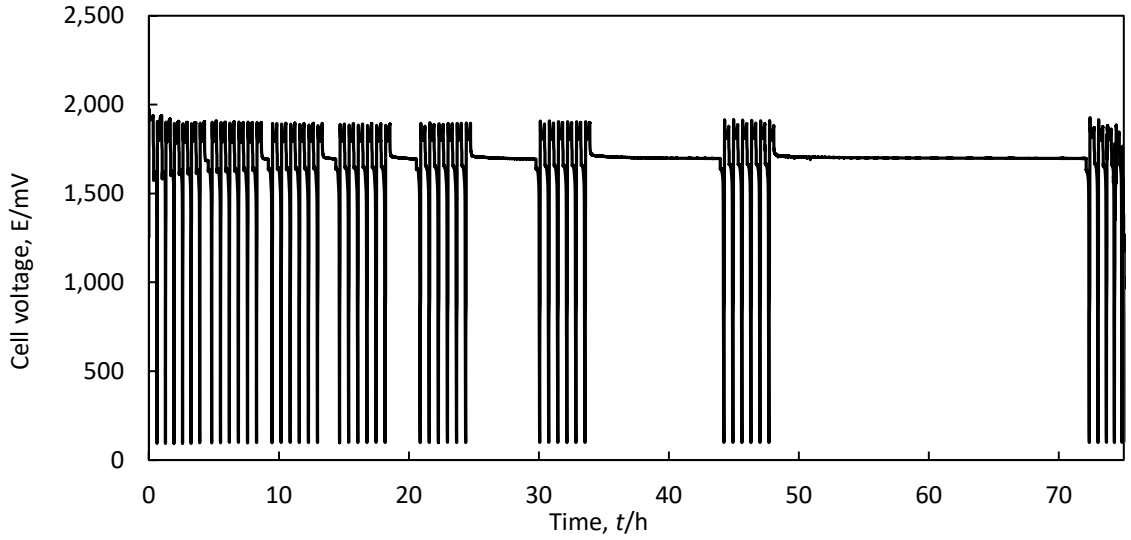

Figure 5-1: Typical Cycle Regime A where static cell were cycled at 5 $mA \cdot cm^{-2}$ between 2.5 V end-of-charge voltage and 0.1 V end-of-discharge voltage with an 8 mm inter-electrode gap.

Figure 5-1 above indicates typical cycles for Cycle Regime A, where the open circuit rest time is progressively increased. The cell shown cycled 42 times in over 70 hours and had an overall average charge, energy and voltage efficiency of 88%, 74% and 80%. The cell did not fail over all the 42 cycles, and it had cycled through 10 hours Open Circuit rest period. Before the experiment was stopped, the cell had rested for five hours, and its open circuit had not decayed, indicating little to no effect on open circuit. This confirms that the cell is unlikely to self-discharge even when left to sit on open circuit for long periods.

The table below gives average efficiencies for each six cycles before the open circuit rest time was changed, for the three iterations.

Table 5-2: Performance of static cells cycled using Regime A. The efficiency shown is averaged over 6 cycles at each rest period and the cycle I.D. is at the end of each 6 iterations.

Cycle I.D.	**O/C rest period**	**Average charge efficiency**	**Average energy efficiency**	**Average voltage efficiency**
6	2 min	83%	68%	83%
18	30 min	90%	74%	82%
24	1 hr	90%	72%	81%
30	2 hr	89%	71%	81%
36	5 hr	82%	66%	80%
42	10 hr	78%	64%	81%
48	24 hr	19%	15%	23%

From Table 5-2 above, the average charge efficiency stayed above 80% for at least 36 cycles for all cells. Charge efficiency peaked at 90% when the rest period was 0.5 hours and 1 hour long. This

appears to suggest that rest period of 30 minutes and one hour give optimum performance of the cells. The data also shows that the cells' performance remained good even when the cells were left on open circuit for 10 hours. Considering the size of the cell, 5 cm x 5 cm electrodes and 0.8 cm inter-electrode gap, the volume of the electrolyte was small enough to be indicative of possible electrolyte polarisation decay, or even loss of solubility of ions which would affect performance negatively. Therefore, the electrolyte performance was excellent over 10 hours.

Rapid deterioration in performance was observed after the cell had been left on open circuit for 24 hours. The charge, energy and voltage efficiencies fell to 19%, 15% and 23%, respectively. Even though the cells were covered, but not sealed, precipitation of lead methanesulfonate was observed at the top edge of the electrodes, indicating that the cells were losing moisture at the unsealed side. However, it is important to note that the method ignored the accumulated effect of cycle life on the cell. Therefore this exaggerated the effect on the cells. This means the cells could potentially perform better even at 24 hours open circuit.

5.3.1.2 Cycle Regime B

To check the effect of open circuit on the cell after a single charge, another set of cells were cycled, where, after an initial charge was applied, the cells were left on open circuit, and then discharged afterwards. Each cell was cycled six times before the open circuit period was increased from 0.1, 0.25, 0.5, 1, 2, 5, 10, and finally to 24 hours. By grouping the different open circuit periods into six iterations, the effect of each open circuit period could be estimated. This method was called Cycle Regime B. However, it is important to note that the method also ignored the accumulated effect of cycle life on the cell, and therefore the effect of cycling with open circuit is also exaggerated.

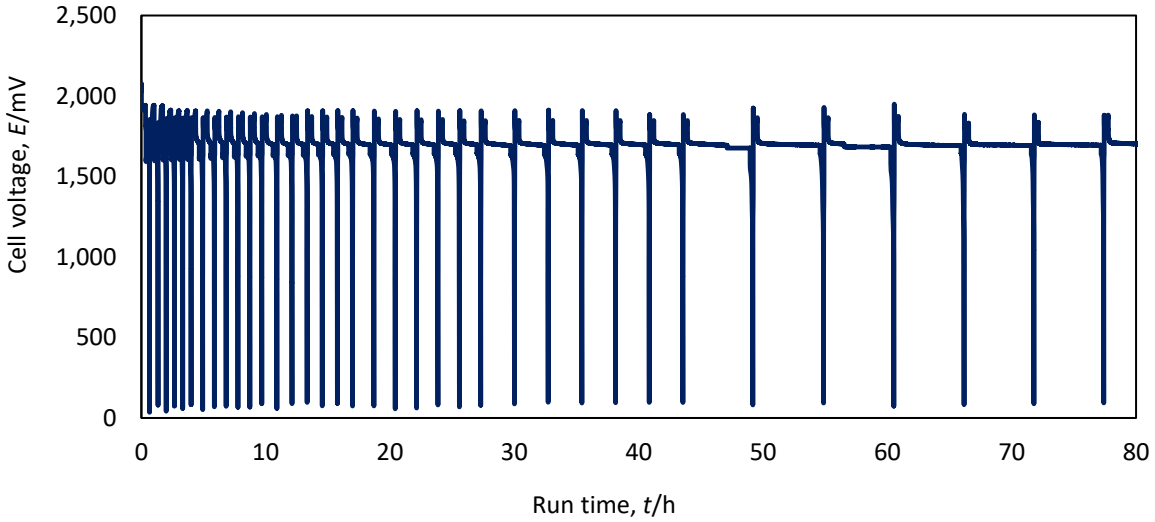

Figure 5-2: Static Cell cycled using Cycle Regime B charged and discharged at 5 mA·cm^{-2}, between 2.5 V and 0.1 V end-of-charge and end-of-discharge voltages. The cells had an inter-electrode gap of 8 mm.

Figure 5-2 shows that once again, the open circuit voltage remained approximately 1.7 V, whether the cell was held at open circuit for 20 minutes, or for 10 hours. That meant that the equilibrium potential was maintained for the length of time the cell was allowed to rest. In the first 35 hours average charge, energy, and voltage efficiencies were 87%, 74% and 85%, respectively and the cell had cycled 36 times. After then charge efficiency fell below 60%. Figure 5-3 compares the charge efficiency of cells type A and type B when an average of the charge efficiency is recorded for each six cycles at specific open circuit periods.

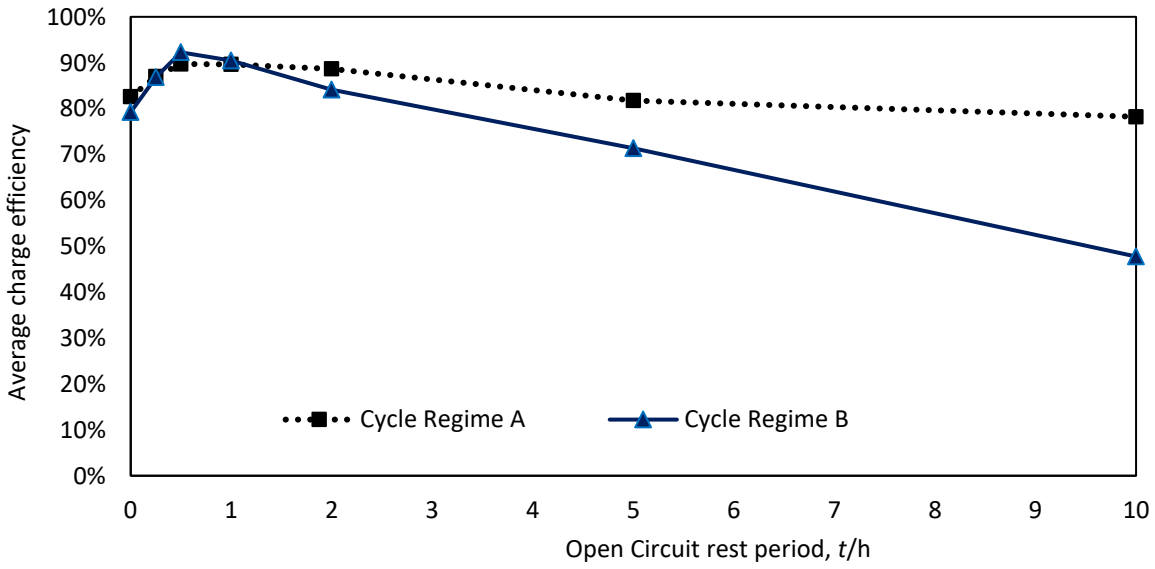

Figure 5-3: Comparison of average charge efficiencies for cells under Cycle Regimes A and B over the imposed open circuit periods.

In the initial cycles, Cycle Regime cells outperformed Cycle Regime A cells, when the former's charge efficiency peaked at 92% at the 30 minutes Open Circuit rest period. However, the charge efficiency fell to 90% when Open Circuit period was one hour. At the same time, Cycle Regime A cells also had the same average charge efficiency. Cells Cycle Regime B lost their competitive advantage in the next 6 cycles at the two hour O/C period. By the 10 hour O/C period, during cycles 37 - 42, the average charge efficiency of Cycle Regime B cells had deteriorated to 48%. This rapid fall in performance is consistent with growth of deposit inside the cells.

Cycle Regime A cells outperformed Cycle Regime B cells. Their average charge efficiency stayed consistently high, dipping to 78% only when the cells had cycled 42 times, at the 10 hour Open Circuit rest period. This suggests that when cells are cycled at least six times without resting, they perform better than if they sit at open circuit after every cycle.

Cycle Regime A cells had an average charge efficiency of 90% when O/C period was 30 minutes, which was maintained when the O/C rest period was increased to one hour. Since both cells had a peak charge efficiency at 30 minutes Open Circuit period, it appears 30 minutes rest period after charging is an optimum rest time for charge efficiency. However, t Cycle Regime A cells maintained a stable charge efficiency through different O/C periods and for a longer period and over more cycles, suggesting that with this type of cycles, the effect of changing open circuit period has a less significant effect.

5.3.1.3 Cycle Regime C

In cycle regimes A and B the effect of different open circuits on cell performance was carried out consecutively on the same cells, therefore, the cell cycle life could not be determined because of an accumulation of effect over time. To determine cycle life at these different open circuit periods, experiments were set up where the open circuit was unvaried throughout the life of the cell.

In this cycle regime, cells were allowed the same amount of O/C relaxation time before and after charge, and the relaxation time was maintained until the cells failed. Different cells were then tested at 20 min O/C, 30 min, 1 hr, 2 hr, 5hr, 10 hr, and 24 hr O/C rest time. This also allowed comparison of the 30 minute O/C rest time with other O/C rest time. It also allowed comparison

between cells that had open circuit rest time after charge and those that had O/C relaxation before and after charge/discharge. Similar experiments have been done for the lithium ion and it was found that the lithium ion cycle life improved when allowed to relax on open circuit after charge and there was no effect from relaxation time applied after discharge. The improvement in cycle life was attributed to lessening of effect of charge current on the battery electrodes [205].

This cycle regime also allowed investigation of whether indeed the 30 minute rest period yielded the best results, where different cells were allowed to rest for a specific rest period and the rest period was maintained until failure, and the performance of the different cells compared. After an initial charge, Cycle Regime C cells were cycled through discharge, OC, charge, and O/C rest until they failed. A typical voltage curve for cells type C with 30 minutes Open Circuit between charge and discharge, is shown in Figure 5-4. The cell above failed after 56 cycles, having run for 92 hours. Just before failure the average charge efficiency was 90%, and the average energy and voltage efficiencies were 76% and 84% respectively.

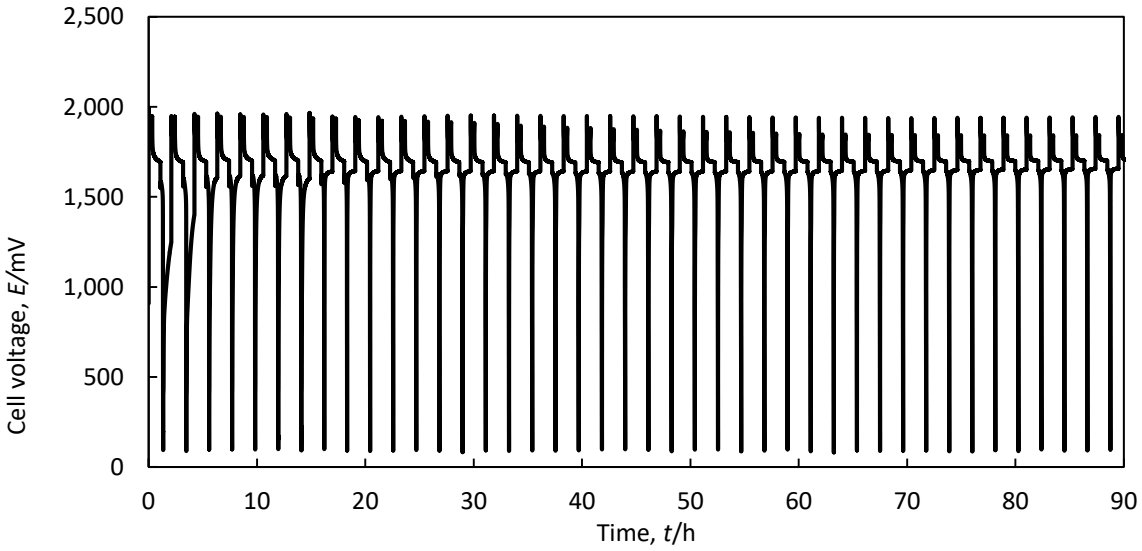

Figure 5-4: Voltage vs time curve for cells type C with 0.7 mol·dm^{-3} Pb^{2+} and 1.0 mol·dm^{-3} MSA recovered electrolyte, cycled between 2.5 V and 0.1 V at 5 mA·cm^{-2} for 20 minutes each, and with an O/C period of 45 minutes between charge and discharge.

This cell however was not the best performing in the range of cells tested using Cycle Regime C. Table 5-3 compares cells cycled using Regime C, indicating the t Open Circuit period, average number of cycles before failure, and average charge, energy and voltage efficiencies.

Table 5-3: Average charge, energy and voltage efficiency and number of cycles before failure for static cells cycled with Regime C, using 0.7 mol·dm^{-3} Pb^{2+} and 1.0 mol·dm^{-3} MSA recovered electrolyte. The cells were charged and discharged at 5 mA·cm^{-2} for 20 minutes each, between 2.5 V and 0.1 V and had different Open Circuit periods after charge. The inter-electrode gap was 8 mm.

O C time min	**# cycles before failure**	**Average Charge efficiency**	**Average Energy efficiency**	**Average Voltage efficiency**
6	26	84	70	83
12	17	75	63	84
15	40	84	70	83
20	39	82	67	82
30	42	84	70	84
35	8	81	68	84
40	26	81	67	82
45	40	78	63	80
60	123	83	64	78

Cells with 15, 20, 30, and 45 minutes O/C rest periods had an average number of cycles around 40. Cells with 60 minutes rest period had the highest number of cycles at 123, while the rest had fewer than 30. Cells with Open circuit periods 6 minutes, 15 minutes, and 30 minutes had the maximum charge efficiency of 84%, marginally higher than that of the 60 min O/C period cells. From Table 5-4 we can conclude that cells with 60 minutes O/C rest period performed best and that the 30 minute rest period is not necessarily the best for cycle life. This cell represents the highest achieved number of cycles for all three cell Cycling Regimes A, B and C.

The next table compares the best performing cells in Regime C at each open circuit rest time, averaged over the life of the individual cell before failure.

Table 5-4: Best performing cells at different O/C rest periods for Regime C, using 0.7 mol·dm^{-3} Pb^{2+} and 1.0 mol·dm^{-3} MSA recovered electrolyte. The cells were charged and discharged at 5 mA·cm^{-2} for 20 minutes each, between 2.5 V and 0.1 V and had different Open Circuit periods after each charge. Inter-electrode gap = 8 mm.

O/C rest period /min	**# cycles before failure**	**Average Charge efficiency**	**Average Energy efficiency**	**Average Voltage efficiency**
15	40	84	70	83
20	50	87	73	83
30	56	90	76	84
45	60	85	70	82
60	123	83	64	78

This table indicates more clearly that cells with 30 minutes O/C rest periods have the best charge efficiency, even if they do not have the longest cycle life. The average charge efficiency for Cycle Regime C cells remained above 80% at 15, 20, 30, 45 and 60 minutes O/C rest periods. In practical terms this means cells with a type C operation regime can supply a high surge of energy, if they are allowed to rest for 60 minutes after charge, and they can be cycled many times before significant deposit build-up.

A comparison of the best performing cells from the three Cycling Regimes based on their charge, energy and voltage efficiencies and on length of operation, is shown in the Table 5-5.

Table 5-5: Best performing cells at different O/C rest periods for Regime C, using 0.7 mol·dm^{-3} Pb^{2+} and 1.0 mol·dm^{-3} MSA recovered electrolyte. The cells were charged and discharged at 5 mA·cm^{-2} for 20 minutes each, between 2.5 V and 0.1 V and had different Open Circuit periods after each charge. Inter-electrode gap = 8 mm.

Cycling Regime	**Number of cycles**	**Average Charge efficiency**	**Average Energy efficiency**	**Average Voltage efficiency**	**Length of operation, /days**
A	42	88	74	85	3
B	44	88	72	81	8
C	123*	83	64	78	13

*The cell failed

The operation times indicated are a feature of the cycling regimes, where Cycle Regime A has a typically shorter operation time because the cell cycled for twenty minutes on charge and discharge with two minutes O/C times between charge and discharge, and only rested for longer periods after six cycles. Cycle Regime B resulted in longer operation type because the cells were allowed progressively longer O/C rest periods after each charge. With continued cycling, the cells spent more time resting than charging or discharging. The cell on Cycle Regime C, remains the one with the longest time of operation as well as the highest cycle life. The cell had 60 minutes O/C rest periods every time after charge and after discharge. This contributed to the long operation time of 13 days. Nevertheless, the charge efficiency of the cell remained above 80%, indicating that even after several days of operation, the cell was still able to perform well. The other two cells had the higher charge, energy and voltage efficiencies, which was expected because of the lower cycle numbers and associated lower deposit build-up. Other iterations of the same regimes resulted in failure at 36 cycles.

5.3.1.4 Cycle Regime D

Another set of experiments was performed to investigate if shortening the time between discharge and charge would have any effect on the cell performance, which gave rise to cell types D. These cells were cycled through: Charge/OC period/Discharge/2 min OC/Repeat.

Table 5-6: Cells type D, using 0.7 mol·dm^{-3} Pb^{2+} and 1.0 mol·dm^{-3} MSA recovered electrolyte. The cells were charged and discharged at 5 mA·cm^{-2} for 20 min each, between 2.5 V and 0.1 V and each had a consistent Open Circuit period after charge while the O/C after discharge was 2 min in all cases. The inter-electrode gap was 8 mm.

O/C time /min	**# cycles before failure**	**Average Charge efficiency**	**Average Energy efficiency**	**Average Voltage efficiency**
20/2	25	78	64	83
45/2	41	82	66	81
1440/2	5	98	80	82

Table 5-6 shows that type D cells did not have competitive advantages over other cell types. On the other hand, the cells that were allowed to sit in Open Circuit for 24 hours had 100% charge efficiency for the first four cycles, and 88% for the fifth. The energy and voltage efficiencies also stayed consistently above 80% for the first four cycles. However the cell failed immediately after the fifth cycle, the charge efficiency falling to 46% on the sixth cycle. Thereafter the cell performance deteriorated until charge efficiency was 27% at cycle number 17, when the cell was stopped.

In comparison none of the type A or B cells cycled long enough to reach the 24 hour rest period. Type C cells were not tested at 24 hours O/C rest period.

5.3.2 Effect of different current densities

The experiments in this section were conducted to further investigate the effect of conditions on the recovered electrolyte. The effect of increasing current density was investigated on cells cycled using Regime A, by changing the current density to 10 mA·cm^{-2} and comparing with cells cycled at 5 mA·cm^{-2}. A comparison of their charge efficiency at the different O/C rest time is shown in Figure 5-5 below.

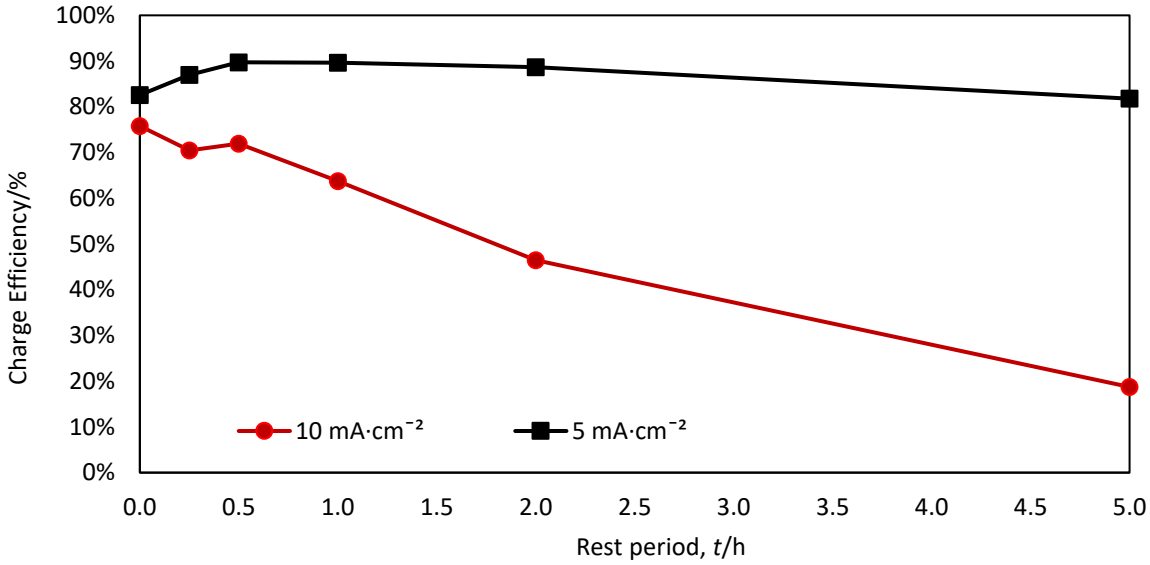

Figure 5-5: Comparison of Cycle Regime A cells cycled at 5 mA·cm^{-2} and at 10 mA·cm^{-2}. The cells had 0.7 mol·dm^{-3} Pb^{2+} and 1.0 mol·dm^{-3} MSA RE.

The average energy efficiency of Cell A cycled at 10 mA·cm^{-2} peaked at 79%, when the O/C period was 30 minutes. This peak occurs at a similar period as for type A and B cells mentioned earlier. The average charge efficiency of type A cells cycled at 10 mA·cm^{-2} subsequently dropped to 64% at O/C periods of one hour. The charge efficiency fell rapidly, and the cells reached failure before the two-hour O/C period was over.

Figure 5-5 shows that high current density adversely affects the cycle life as well as the charge efficiency of type A cells by reducing the cycle life and lowering the initial charge efficiency. Not only that, cell failure occurred more quickly. This is consistent with others findings where higher current density results in less compact deposits on the negative electrode and less smooth deposit on the positive electrode [198]. The latter results in poor stripping of the lead dioxide deposit from the positive electrode and rapid build-up of deposit inside the cell. Since the test cells for these experiments were undivided, short-circuiting occurred faster and the cells failed sooner than at lower current density.

Also highlighted by Figure 5-5 is that when cycled at 10 mA·cm^{-2}, type A cells performed worse than type B cells cycled at the lower current density of 5 mA·cm^{-2}. This is despite the fact that type A cells initially outperformed type B cells. It is clear that the effect of high current density in these experiments is the significant reason for failure rather than the cycling regime. This makes sense since at higher current density the deposit smoothness and compactness is affected at the positive electrode, and so is lead dioxide stripping efficiency, resulting in deposit build-up on both electrodes and subsequent shorting.

Charge efficiency for all three sets of cells peaked when O/C period was 30 minutes. Again this suggests that a 30 minute rest period after charging is ideal. To further investigate this, another cycling regime was introduced. This time the O/C period for a specific cell remained unchanged, and the cells were cycled until they failed.

The effect of current density was investigated further in the static cells below, which had an inter-electrode gap of 5 mm, and used recovered electrolyte of 0.8 mol·dm^{-3} Pb^{2+} and 0.9 mol·dm^{-3} MSA. Cells with 7.5 mA·cm^{-2} had the highest charge efficiency at 100%, but performance dropped sharply by the 6th cycle, resulting in a total average efficiency of 78%. The cells with 10 mA·cm^{-2} performed the worst. Even though the charge efficiency started high at 80%, by the sixth cycle the cell had failed, charge efficiency falling below 60% and by the eighth it was trailing at 0%.

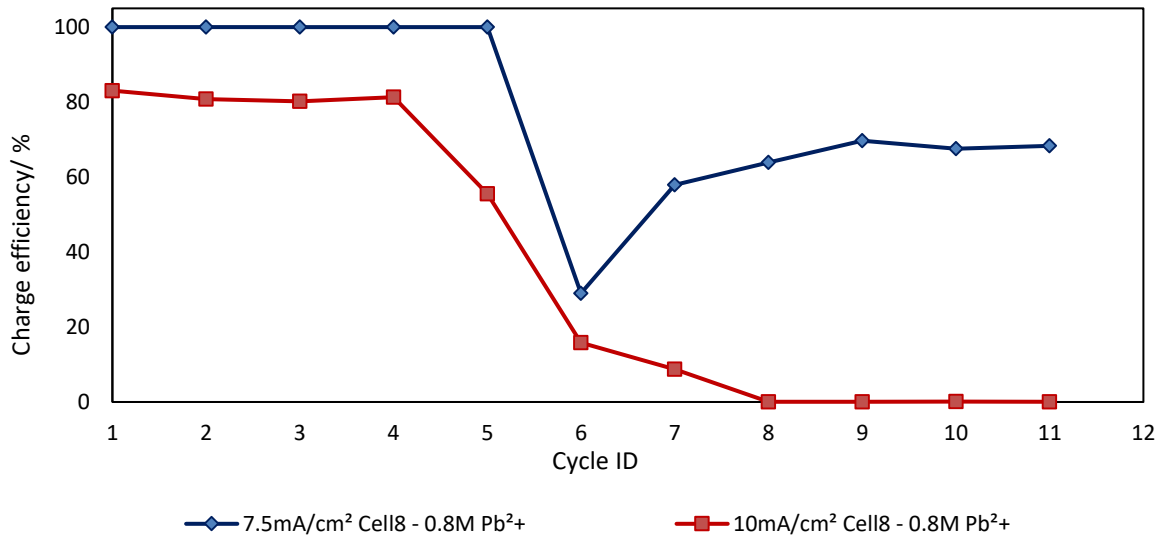

Figure 5-6: Static cells with 0.8 mol·dm^{-3} Pb^{2+} and 0.9 mol·dm^{-3} MSA, cycled at different current densities.

High current density results in quicker deterioration of cell capacity. Cycles that maintain the same rest period also indicate this. The sudden deterioration here is not necessarily indicative of worse performance at longer rest periods. The next table indicates the effect of current density on cell charge efficiency and cycle life. It also compares static cells that are divided and those that are not. It also indicates effect current density has on cycle life, as well as the effect of end-of-discharge voltage.

5.3.3 Effect of Configuration

Some static cells were assembled in a divided configuration with a permeable membrane separating the two sides. The static cells were cycled at different current densities and also with different end-of-discharge voltages to compare the effect on the performance. The table below gives a summary of the effect of the different conditions on cycle life and efficiency.

Table 5-7: Comparison of divided and undivided static cells with different end-of-charge voltages and current densities. O/C rest period was 2 min. Electrolyte: 0.8 mol·dm^{-3} [Pb^{2+}], 0.9 mol·dm^{-3} MSA.

Current density / mA·cm^{-2}	**Config-uration**	**Inter-Electrode gap/mm**	**EoDV - EoCV**	**# cycles before failure**	**Average Charge efficiency**	**Average Energy efficiency**	**Average Voltage efficiency**
5	Divided	4 + 4	0.1 – 3.0	83	83	87	65
5	Divided	4 + 4	0.5 – 3.0	145	145	90	71
20	Divided	4 + 4	0.1 – 3.0	4	4	63	66
5	Undivided	8	0.1 – 3.0	22	22	77	62
5	Undivided	8	0.5 – 3.0	28	28	84	67

In the table above, cells with the same recovered electrolyte and the same cycling regime are compared when some are divided and some are not. It is clear that divided cells cycle longer than those without a separating membrane. A divided cell with 0.1 V end-of-discharge voltage lasted 145 cycles compared to an undivided one's 22 cycles with the same end-of-discharge voltage. Another divided cell lasted 83 cycles when its end-of discharge voltage was raised to 0.5 V. This means its charge efficiency fell below 60% before the one with a lower end-of-charge voltage. Compounding the effect of a high current density (20 mA·cm^{-2}) and a high end-of-discharge voltage (0.5 V) severely limited the cycle life to 4. In this instance the division of the cell did not help. The cell also had the lowest charge, energy and voltage efficiencies

The end-of-discharge voltage also limits the performance of cells. Cells that had the same electrolyte, the same inter-electrode gap as well as the same current density tended to have shorter lives when compared to those with a lower end-of-discharge voltage. This is because the cells would start charging before they had fully discharged the stored capacity, also limiting the

stripping of solids from the electrodes, hence leaving more material on the electrode, which caused quicker growth of build-up and hence faster failure.

5.4 Conclusions and Recommendations for Future Work

Static cells with recovered electrolyte were subjected to different cycling regimes to investigate the effect on cycle life and charge efficiency. The cycling regimes were achieved by changing the length of time the cells were left on open circuit when fully charged, as well as varying the sequence in which the charging and the open circuit periods occurred. The effect of other conditions such as current density and over-charging the cells were also investigated. Based on the work reported in this chapter, the following findings were made:

1. When left on open circuit fully charged, a soluble lead cell that uses recovered electrolyte maintains equilibrium voltage for at least 24 hours. The cell voltage stays around 1.7 V, whether the cell is held at open circuit voltage for 20 minutes, 10 hours, or for 24 hours.
2. Even though the same electrolyte is used in both sides of the static cell, dividing the cell increases cycle life two-fold.
3. Lowering the end-of-discharge voltage increases the cycle life as well as the charge efficiency by elongating the length of discharge and hence allowing recovery of deposited capacity.
4. Forcing over-discharge on a soluble cell by increasing the amount of discharge time compared to charge time can increase cycle life. Since acid concentration reduces during discharge for the soluble lead battery, losses due to oxygen evolution are not expected to be of significant value.

Based on these results we can infer that a battery that has excess electrolyte, compared to its electrode surface area and that operates at a low enough current density will maintain a high charge and energy efficiency, making ancillary losses the main losses the battery has. Since these are constant, the battery can be designed to deliver constant energy with each discharge, as long as the current density is low enough.

Chapter 6 Conclusions and Recommendations for Future Work

6.1 Conclusions

Improvements to the soluble lead cell have been achieved through several novel approaches.

1. A method has been developed to make electrolyte for the soluble lead battery directly from spent lead acid batteries, effectively using discarded material and preventing the use of laboratory grade and potentially expensive materials for the production of electrolyte.
2. Through cycling in 10 cm^2 flow cell and 25 cm^2 electrode area static cells, the electrolyte has been shown to perform better than reagent grade electrolyte, achieving twice the cycle life of flow cells using reagent grade and three times that of static cells using reagent grade electrolyte. The charge efficiency achieved in cells using recovered electrolyte was higher for all static cells while it was comparable for flow cells, except for those using electrolyte with a concentration of 0.7 $mol \cdot dm^{-3}$ Pb^{2+} and 1.0 $mol \cdot dm^{-3}$ MSA, in which case the recovered electrolyte outperformed the reagent grade electrolyte.
3. By conducting never-before done elemental analysis using Inductively Coupled Plasma Mass Spectroscopy on reagent grade electrolyte, it has been established that the reagent grade electrolyte contains nickel than does the recovered electrolyte, and that the nickel, though at trace quantities, is detrimental to the performance of the soluble lead battery. based on this finding, it is recommended here that the soluble lead battery should only use recovered electrolyte, since recovered electrolyte has fewer impurities that are detrimental to cell operation, and contains additives that are beneficial to operation. This is because the recovered electrolyte benefits from the refining process used to recycle lead for lead acid batteries through the removal of harmful impurities and the addition of useful additives.
4. Through extensive cycling of recovered electrolyte, it has been established that:
    a. High current density is detrimental to cycle life and to charge, energy and voltage efficiency.
    b. Using a divider elongates cell life by up to five times the life of undivided cells and therefore it is recommended that soluble lead cells operate divided rather than undivided. Even though there is a 25% loss in voltage efficiency due to resistance introduced by the least conductive membrane available commercially, the losses

introduced by the membrane are negligible when compared to the gains in cycle life.

5. A soluble lead cell can stand for 24 hours charged with little to no effect on charge efficiency. If allowed to stand for five days, a flow cell will recover its capacity after one full charge.
6. A high end-of-discharge voltage limits the amount of solids that can be dissolved back into electrolyte during discharge, therefore, the end-of-discharge voltage needs to be as low as possible. Lowering the end-of-discharge voltage does not adversely affect the soluble lead cell, which implies that the cell can be deeply discharged with no effect on long term operation.
7. Over-discharging by increasing the time it takes to discharge a soluble lead compared to the time it takes to charge does not damage cell operation nor does it have long term effects. Instead, it enhances discharge so that deposit that was otherwise not dissolved is stripped back in to the electrolyte, improving the overall performance of the cell. Again this confirms that the soluble lead is robust enough to withstand over-discharge.

6.2 Confirming Claims to Novelty

The conclusions above are supported by the following publications:

1. Orapeleng, K., Wills, R., and Cruden, A., Developing Electrolyte for a Soluble Lead Redox Flow Battery by Reprocessing Spent Lead Acid Battery Electrodes. Batteries, 2017. 3(2): p. 15. DOI: https://doi.org/10.3390/batteries3020015.
   Which covers conclusion 1.

2. Orapeleng, K., Wills, R.G.A., and Cruden, A., Performance of recovered and reagent grade electrolyte in a soluble lead redox cell. Journal of Energy Storage, 2018. 20: p. 49-56.DOI: https://doi.org/10.1016/j.est.2018.08.017.
   Which covers the conclusions 2 and 3.

3. “Improvement of performance of the soluble lead redox cells through optimised cycling.” The paper is intended for the Journal of Energy Storage, and will present data from chapter 5, which shows that certain operating conditions are favourable for the performance of the soluble lead cell, while others are detrimental. The paper will recommend the most favourable for improving performance of the soluble lead cell.

6.3 Recommendations to Further Work

Several questions arose that were not fully addressed in this work, that are worth pursuing further:

1. Experiments to establish the amount of residue left when battery electrodes are used to make recovered electrolyte were inconclusive since the residue contained carbon. It would be interesting to find out how much of the residue contains lead.
2. Further analysis of the recovered electrolyte is required to establish what organic additives are in the electrolyte and what their effect is on performance. Studies on the additives already in the electrolyte need to establish what tandem benefits, if any, there are due to the presence of different additives, organic and non-organic.
3. A flow cell using recovered electrolyte at the recommended concentration of 0.7 $mol \cdot dm^{-3}$ Pb^{2+} and 1.0 $mol \cdot dm^{-3}$ MSA cycled 205 times without failing. Because of limitation in the equipment it was not possible to cycle the cell before it failed. It is therefore not known what the cycle life of such is. More experiments using a similar electrolyte need to be conducted to establish the cell cycle life. Also of particular interest with the same cell is why the lead dioxide was strongly adhered to the electrode, rather than being a loose powder that drifts to the electrolyte tank, as has been observed with other cells. What conditions, apart from oxygen evolution, caused the deposit to adhere that strongly and how that affected discharging in the long run.
4. Cycling of the soluble lead cells at longer charge and discharge times is required to ascertain the effect of depleting the active ions in the electrolyte between charging and discharge.

List of References

1. IPCC, *WG1 IV Assessment Report. Summary for Policymakers*, in *Climate Change 2007: The Physical Science Basis*, S. Solomon, et al., Editors. 2007, Cambridge University Pres: Cambridge, New York.

2. Canadell, J.G., C. Le Quéré, M.R. Raupach, C.B. Field, E.T. Buitenhuis, P. Ciais, T.J. Conway, N.P. Gillett, R.A. Houghton, and G. Marland, *Contributions to accelerating atmospheric CO_2 growth from economic activity, carbon intensity, and efficiency of natural sinks.* Proceedings of the National Academy of Sciences, 2007. **104**(47): p. 18866-18870.DOI: 10.1073/pnas.0702737104.

3. IPCC, *Global Warming of 1.5°C- Summary for Policymakers*, in *Secondary Global Warming of 1.5°C- Summary for Policymakers*, Secondary IPCC, Editor. 2018, W.M. Organization: Geneva, Switzerland. p. 32.[cited 20/01/2015]; Available from: http://srren.ipcc-wg3.de/report.

4. IPCC, W.G.I., *Special report on renewable energy sources and climate change mitigation (SRREN)*, in *Secondary Special report on renewable energy sources and climate change mitigation (SRREN)*, Secondary IPCC, W.G.I., Editor. 2012, C.U. Press: New York.

5. Commission, E., *The future role and challenges of energy storage*, in *Secondary The future role and challenges of energy storage*, Secondary Commission, E., Editor. 2013, E. COMMISSION: EU Commission.[cited 07/12/2015]; Available from: https://ec.europa.eu/energy/sites/ener/files/energy_storage.pdf.

6. Das, A., L. Emele, F. Meinke-Hubeny, I. Moorkens, C. Nissen, and M. Tomescu, *Renewable energy in Europe — 2018, Recent growth and knock-on effects*, in *Secondary Renewable energy in Europe — 2018, Recent growth and knock-on effects*, Secondary Das, A., L. Emele, F. Meinke-Hubeny, I. Moorkens, C. Nissen, and M. Tomescu, Editors. 2018, E. Union: Luxembourg.[cited 21/04/2019]; Available from: eea.europa.eu.

7. Government, S. *2020 Routemap for Renewable Energy in Scotland. Executive summary*. [Scottish Government publications] 2011 16/02/2015 [cited 2015 16 Feb]; Routemap]. Available from: http://www.gov.scot/Publications/2011/08/04110353/2.

8. Burger, B., *Net Public Electricity Generation in Germany in 2018*, in *Secondary Net Public Electricity Generation in Germany in 2018*, Secondary Burger, B., Editor. 2019, F. ISE: Freiburg.[cited 21/04/2019]; Available from: www.energy-charts.de/index.htm.

9. REN21, *Renewables 2014 global status report*, in *Secondary Renewables 2014 global status report*, Secondary REN21, Editor. 2014, R. Secretariat: Paris.

10. Bahaj, A.S., *Delivering developing country growth: A new mechanistic approach driven by the photovoltaic industry.* Renewable and Sustainable Energy Reviews, 2009. **13**(8): p. 2142-2148.DOI: http://dx.doi.org/10.1016/j.rser.2009.01.029.

11. Cust, J., A. Singh, and K. Neuhoff, *Rural electrification in India: economic and institutional aspects of renewables*, in *Secondary Rural electrification in India: economic and institutional aspects of renewables*, Secondary Cust, J., A. Singh, and K. Neuhoff, Editors. 2007.

12. *The Electricity (Amendment) Bill, 2014*, in *Bill No. 191 of 2014*. 2014, Ministry of Law and Defence: New Delhi, India.

13. GNESD, *Renewable energy-based rural electrification: The Mini-Grid Experience from India.*, in *Secondary Renewable energy-based rural electrification: The Mini-Grid Experience from India.*, Secondary GNESD, Editor. 2014, G.N.o.E.f.S.D. (GNESD): New Delhi.

14. Sawin, J.L., J. Rutovitz, and F. Sverrisson, *Renewables 2018 Global Status*, in *Secondary Renewables 2018 Global Status*, Secondary Sawin, J.L., J. Rutovitz, and F. Sverrisson, Editors. 2018, Renewables21: Paris.[cited 23/04/2019]; Available from: http://www.ren21.net/status-of-renewables/global-status-report/.

15. Ahammed, F. and D.A. Taufiq, *Applications of solar PV on rural development in Bangladesh.* Journal of Rural Community Development, 2008. **3**(1): p. 93-103.

16. UN. *7 - Affordable and Clean Water*. Sustainable Development Goals [Online report] 2018 [cited 2019 2/06/2019]; Available from: https://unstats.un.org/sdgs/report/2018/goal-07/.

17. San Martín, J.I., I. Zamora, J.J. San Martín, V. Aperribay, and P. Eguia. *Energy storage technologies for electric applications*. in *International Conference on Renewable Energies and Power Quality*. 2011.

18. Rodrigues, E.M.G., R. Godina, S.F. Santos, A.W. Bizuayehu, J. Contreras, and J.P.S. Catalão, *Energy storage systems supporting increased penetration of renewables in islanded systems.* Energy, 2014. **75**: p. 265-280.DOI: https://doi.org/10.1016/j.energy.2014.07.072.

19. Ibrahim, H., A. Ilinca, and J. Perron, *Energy storage systems—Characteristics and comparisons.* Renewable and Sustainable Energy Reviews, 2008. **12**(5): p. 1221-1250.DOI: http://dx.doi.org/10.1016/j.rser.2007.01.023.

20. Dunn, B., H. Kamath, and J.-M. Tarascon, *Electrical Energy Storage for the Grid: A Battery of Choices.* Science, 2011. **334**(6058): p. 928-935.DOI: 10.1126/science.1212741.

21. Yang, Z., J. Zhang, M.C.W. Kintner-Meyer, X. Lu, D. Choi, J.P. Lemmon, and J. Liu, *Electrochemical Energy Storage for Green Grid.* Chemical Reviews, 2011. **111**(5): p. 3577-3613.DOI: 10.1021/cr100290v.

22. EUROBAT, *Battery Energy Storage for Smart Grid Applications*, in *Secondary Battery Energy Storage for Smart Grid Applications*, Secondary EUROBAT, Editor. 2013, EUROBAT; Available from: https://eurobat.org/images/news/position-papers/eurobat_smartgrid_publication_may_2013.pdf.

23. Ulaganathan, M., V. Aravindan, Q. Yan, S. Madhavi, M. Skyllas-Kazacos, and T.M. Lim, *Recent Advancements in All-Vanadium Redox Flow Batteries.* Advanced Materials Interfaces, 2016. **3**(1): p. 1500309-n/a.DOI: 10.1002/admi.201500309.

24. Xiaoli, W. and Z. Yu, *Applications of Flow Battery Energy Storage*, in *Redox Flow Batteries. Fundamentals and Applications*. 2017, CRC Press: Boca Raton. p. 444.ISBN: 9781315152684.

25. Gyuk, I., M. Johnson, J. Vetrano, K. Lynn, W. Parks, R. Handa, L. Kannberg, S. Hearne, K. Waldrip, and R. Braccio, *Grid Energy Storage*, in *Secondary Grid Energy Storage*, Secondary Gyuk, I., M. Johnson, J. Vetrano, K. Lynn, W. Parks, R. Handa, L. Kannberg, S. Hearne, K. Waldrip, and R. Braccio, Editors. 2013.[cited 25/06/2014]; Available from: http://energy.gov/sites/prod/files/2014/09/f18/Grid%20Energy%20Storage%20December%202013.pdf.

26. SANDIA, *DoE global energy storage database*. 2019, SANDIA National Laboratories: [Online].

27. Gitis, A., M. Leuthold, and Dirk U. Sauer, *Chapter 4 - Applications and Markets for Grid-Connected Storage Systems*, in *Electrochemical Energy Storage for Renewable Sources and Grid Balancing*, P.T. Moseley and J. Garche, Editors. 2015, Elsevier: Amsterdam. p. 33-52.ISBN: 978-0-444-62616-5.

28. Bindner, H., C. Ekman, O. Gehrke, and F. Isleifsson, *Characterization of Vanadium Flow Battery*, in *Secondary Characterization of Vanadium Flow Battery*, Secondary Bindner, H., C. Ekman, O. Gehrke, and F. Isleifsson, Editors. 2010, N.L.f.S. Energy: Roskilde, Denmark. p. 27.[cited 25/04/2019]; Available from: http://orbit.dtu.dk/files/5889861/ris-r-1753.pdf.

29. Yano, K., S. Hayashi, T. Kumamoto, T. Shibata, K. Yamanishi, and K. Fujikawa, *Development and Demonstration of Redox Flow Battery System*, in *Sei Technical Review*. 2017, Sumitomo Electric: online. p. 22-28.

30. Bryans, D., B. G. McMillan, M. Spicer, A. Wark, and L. Berlouis, *Complexing Additives to Reduce the Immiscible Phase Formed in the Hybrid ZnBr 2 Flow Battery.* Journal of The Electrochemical Society, 2017. **164**(13): p. A3342-A3348.DOI: 10.1149/2.1651713jes.

31. Lowell, H., *ViZn Energy Systems Announces Zinc/Iron Flow Battery Installation at Flathead Electric Cooperative* in *ViZn's Z20, a 160kwh proprietary energy storage technology, has been installed at Flathead Electric Cooperative for utility integration and testing.* 2014, Cision PRWeb: Kalispell. p. 1.

32. Waldrip, K.E., *An Overview of the US Department of Energy's Flow Battery Program Under the Office of Electricity Delivery and Energy Reliability*, in *Secondary An Overview of the US Department of Energy's Flow Battery Program Under the Office of Electricity Delivery and Energy Reliability*, Secondary Waldrip, K.E., Editor. 2011, S.N. Laboratories; Available from: https://www.osti.gov/servlets/purl/1108234.

33. Imergy, *Energy Savings using Flow Batteries, Telecom Base Station Application*, in *Secondary Energy Savings using Flow Batteries, Telecom Base Station Application*, Secondary Imergy, Editor. 2015, IMERGY: online.[cited 12/05/2019]; Available from: https://covertelpower.com.au/wp-content/uploads/2015/05/IMERGY_GeneralTelecom_CaseStudies_Paper_-12000001007-003_B.pdf.

34. Conca, J., *Vanadium-Flow Batteries: The Energy Storage Breakthrough We've been Waiting For*, in *Forbes*. 2016, Forbes Media LLC: online.

35. Ketlogetswe, C. and T.H. Mothudi, *Solar home systems in Botswana—Opportunities and constraints.* Renewable and Sustainable Energy Reviews, 2009. **13**(6): p. 1675-1678.DOI: https://doi.org/10.1016/j.rser.2008.08.007.

36. Karekezi, S. and W. Kithyoma, *Renewable energy strategies for rural Africa: is a PV-led renewable energy strategy the right approach for providing modern energy to the rural poor of sub-Saharan Africa?* Energy Policy, 2002. **30**(11–12): p. 1071-1086.DOI: http://dx.doi.org/10.1016/S0301-4215(02)00059-9.

37. IEE, *Overview of key energy interventions in the DEA partner countries*, in *Secondary Overview of key energy interventions in the DEA partner countries*, Secondary IEE, Editor. 2013, I.E. Europe: Amsterdam.

38. Anderson, P.G.O. *The role, reliability and limitations of solar photo-voltaic systems in Botswana*. in *Ninth International Conference on Harmonics and Quality of Power, 2000. Proceedings.* 2000. Orlando, FL: IEEE.

39. Loka, P., S. Moola, K. Polsani, S. Reddy, S. Fulton, and A. Skumanich, *A case study for micro-grid PV: lessons learned from a rural electrification project in India.* Progress in Photovoltaics: Research and Applications, 2014. **22**(7): p. 733-743.DOI: 10.1002/pip.2429.

40. Chaurey, A. and T.C. Kandpal, *Assessment and evaluation of PV based decentralized rural electrification: An overview.* Renewable and Sustainable Energy Reviews, 2010. **14**(8): p. 2266-2278.DOI: http://dx.doi.org/10.1016/j.rser.2010.04.005.

41. Lysen, E.H., *Pico solar PV systems for remote homes*, in *Secondary Pico solar PV systems for remote homes*, Secondary Lysen, E.H., Editor. 2013, I.E. Agency.[cited 16/02/2015]; Available from: https://www.iea.org/media/openbulletin/Pico_Solar_PV_System.pdf.

42. GmbH, *Solar Photovoltaic Systems for Social Infrastructure and Village Electrification in Mozambique: Study of Existing Systems in two Provinces*, in *Secondary Solar Photovoltaic Systems for Social Infrastructure and Village Electrification in Mozambique: Study of Existing Systems in two Provinces*, Secondary GmbH, Editor. 2010.

43. Wamukonya, N., *Solar home system electrification as a viable technology option for Africa's development.* Energy Policy, 2007. **35**(1): p. 6-14.DOI: http://dx.doi.org/10.1016/j.enpol.2005.08.019.

44. Ketlogetswe, C., T.H. Mothudi, and J. Mothibi, *Effectiveness of Botswana's policy on rural electrification.* Energy Policy, 2007. **35**(2): p. 1330-1337.DOI: https://doi.org/10.1016/j.enpol.2006.04.002.

45. Barry, M.-L., H. Steyn, and A. Brent, *Selection of renewable energy technologies for Africa: Eight case studies in Rwanda, Tanzania and Malawi.* Renewable Energy, 2011. **36**(11): p. 2845-2852.DOI: http://dx.doi.org/10.1016/j.renene.2011.04.016.

46. Wiemann, M., E.M.C. Gómez, and L.-C.M. Baz, *Best practices for the alliance for rural electrification*, in *Secondary Best practices for the alliance for rural electrification*, Secondary Wiemann, M., E.M.C. Gómez, and L.-C.M. Baz, Editors. 2013: Brussels.[cited 16/04/2015]; Available from: http://www.ruralelec.org/fileadmin/DATA/Documents/06_Publications/ARE_Best_Practises_2013_FINAL.pdf.

47. Nygaard, I., U.E. Hansen, and T.H. Larsen, *The emerging market for pico-scale solar PV systems in Sub-Saharan Africa: From donor-supported niches toward market-based rural electrification*, in *Secondary The emerging market for pico-scale solar PV systems in Sub-Saharan Africa: From donor-supported niches toward market-based rural electrification*, Secondary Nygaard, I., U.E. Hansen, and T.H. Larsen, Editors. 2016, U.D. Partnership: Copenhagen Ø, Denmark.[cited 25/04/2019]; Available from: http://orbit.dtu.dk/files/127508197/Market_Pico_Solar_WEB.pdf.

48. Daly, H. and M.A. Walton, *Energy Access Outlook - From Poverty to Prosperity*, in *Secondary Energy Access Outlook - From Poverty to Prosperity*, Secondary Daly, H. and M.A. Walton, Editors. 2017, I.E. Agency: www.iea.org; Available from: https://www.iea.org/publications/freepublications/publication/WEO2017SpecialReport_EnergyAccessOutlook.pdf.

49. Daly, H. and M.A. Walton, *Energy Access Outlook - From Poverty to Prosperity: Box 1.1*, in *Secondary Energy Access Outlook - From Poverty to Prosperity: Box 1.1*, Secondary Daly,

H. and M.A. Walton, Editors. 2017, I.E. Agency: www.iea.org; Available from: https://www.iea.org/publications/freepublications/publication/WEO2017SpecialReport_EnergyAccessOutlook.pdf.

50. Chen, X. and Y. Gao, *Research and development of solar cookers in China.* Biomass, 1989. **20**(1): p. 113-123.DOI: https://doi.org/10.1016/0144-4565(89)90025-5.

51. Bhattacharya, S.C. and C. Jana, *Renewable energy in India: Historical developments and prospects.* Energy, 2009. **34**(8): p. 981-991.DOI: http://dx.doi.org/10.1016/j.energy.2008.10.017.

52. Ahmad, B., *Users and disusers of box solar cookers in urban India- Implications for solar cooking projects.* Solar Energy, 2001. **69**(6): p. 209-215.DOI: 10.1016/S0038-092X(01)00037-8.

53. Adelmann, P., *Chapter 5 - Existing Markets for Storage Systems in Off-Grid Applications*, in *Electrochemical Energy Storage for Renewable Sources and Grid Balancing*, P.T. Moseley and J. Garche, Editors. 2015, Elsevier: Amsterdam. p. 53-60.ISBN: 978-0-444-62616-5.

54. IRENA, *Electricity storage and renewables: Cost and Markets to 2030*, in *Secondary Electricity storage and renewables: Cost and Markets to 2030*, Secondary IRENA, Editor. 2017, I.R.E. Agency: Abu Dhabi.[cited 26/04/2019].

55. Spiers, D.J. and A.A. Rasinkoski, *Limits to battery lifetime in photovoltaic applications.* Solar Energy, 1996. **58**(4–6): p. 147-154.DOI: http://dx.doi.org/10.1016/S0038-092X(96)00085-0.

56. Butler, P., J. Dunleavey, M. Farber-DeAnda, and P. Moseley, *Performance of valve-regulated lead-acid batteries in real-world stationary applications — utility installations.* Journal of Power Sources, 2001. **96**(1): p. 94-101.DOI: http://dx.doi.org/10.1016/S0378-7753(01)00713-3.

57. Berndt, D., *VRLA batteries, advances and limitations.* Journal of Power Sources, 2006. **154**(2): p. 509-517.DOI: http://dx.doi.org/10.1016/j.jpowsour.2005.10.083.

58. Albright, G., J. Edie, and S. Al-Hallaj, *A Comparison of Lead Acid to Lithium-ion in Stationary Storage Applications*, in *Secondary A Comparison of Lead Acid to Lithium-ion in Stationary Storage Applications*, Secondary Albright, G., J. Edie, and S. Al-Hallaj, Editors. 2012, A.T. LLC; Available from: file:///C:/SOTON 2014-2018/Batteries/Lead-acid-white-paper.pdf

http://www.batterypoweronline.com/main/wp-content/uploads/2012/07/Lead-acid-white-paper.pdf.

59. Zhang, C., T.S. Zhao, Q. Xu, L. An, and G. Zhao, *Effects of operating temperature on the performance of vanadium redox flow batteries.* Applied Energy, 2015. **155**: p. 349-353.DOI: http://dx.doi.org/10.1016/j.apenergy.2015.06.002.

60. Butler, P.C., P.A. Eidler, P.G. Grimes, C. Butler, P.A. Eidler, P.G. Grimes, S.E. Klassen, and R.C. Miles, *Zinc/Bromine batteries*, in *Handbook of batteries*, D. Linden and T. Reddy, Editors. 2002, McGraw-Hill: New York. p. 39.1 - 39.22.ISBN: 0-07-135978-8.

61. Rose, M.D. and R.S. Ferreira, *Performance Testing of Zinc-Bromine Flow Batteries for Remote Telecom Sites*. 2013, Sandia National Laboratories: Albuquerque.

62. Wagner, R., *Failure modes of valve-regulated lead/acid batteries in different applications.* Journal of Power Sources, 1995. **53**(1): p. 153-162.DOI: http://dx.doi.org/10.1016/0378-7753(94)01983-3.

63. Rand, D.A.J. and P.T. Moseley, *Chapter 13 - Energy Storage with Lead–Acid Batteries*, in *Electrochemical Energy Storage for Renewable Sources and Grid Balancing*, P.T. Moseley and J. Garche, Editors. 2015, Elsevier: Amsterdam. p. 201-222.ISBN: 978-0-444-62616-5.

64. Alotto, P., M. Guarnieri, and F. Moro, *Redox flow batteries for the storage of renewable energy: A review.* Renewable and Sustainable Energy Reviews, 2014. **29**(0): p. 325-335.DOI: http://dx.doi.org/10.1016/j.rser.2013.08.001.

65. Leung, P., X. Li, C. Ponce de Leon, L. Berlouis, C.T.J. Low, and F.C. Walsh, *Progress in redox flow batteries, remaining challenges and their applications in energy storage.* RSC Advances, 2012. **2**(27): p. 10125-10156.DOI: http://dx.doi.org/10.1039/C2RA21342G.

66. Hazza, A., D. Pletcher, and R. Wills, *A novel flow battery: A lead acid battery based on an electrolyte with soluble lead(ii) Part I. Preliminary studies.* Physical Chemistry Chemical Physics, 2004. **6**(8): p. 1773-1778.DOI: http://dx.doi.org/10.1039/B401115E.

67. Krishna, M., R.G.A. Wills, A.A. Shah, D. Hall, and J. Collins, *The separator-divided soluble lead flow battery.* Journal of Applied Electrochemistry, 2018. **48**(9): p. 1031-1041.DOI: https://doi.org/10.1007/s10800-018-1230-2.

68. Pillot, C., *Battery Market Developmentfor Consumer Electronics, Automotive, and Industrial: MaterialsRequirements& Trends*, in *Batteries 2014*. 2014, Avicenne Energy: Nice, France.

69. Kurzweil, P., *Gaston Planté and his invention of the lead–acid battery—The genesis of the first practical rechargeable battery.* Journal of Power Sources, 2010. **195**(14): p. 4424-4434.DOI: http://dx.doi.org/10.1016/j.jpowsour.2009.12.126.

70. Zakeri, B. and S. Syri, *Electrical energy storage systems: A comparative life cycle cost analysis.* Renewable and Sustainable Energy Reviews, 2015. **42**(0): p. 569-596.DOI: http://dx.doi.org/10.1016/j.rser.2014.10.011.

71. Group, S.S., *National recycling rate study*, in *Secondary National recycling rate study*, Secondary Group, S.S., Editor. 2014, S.S. Group.

72. ILA. *Lead facts*. [Internet] 2019 [cited 2015 14/05.2019]; Available from: https://www.ila-lead.org/publications.

73. Group, S.S., *National recycling rate study*, in *Secondary National recycling rate study*, Secondary Group, S.S., Editor. 2017, S.S. Group: Chicago, Illinois.[cited 10/01/2017]; Available from: http://c.ymcdn.com/sites/batterycouncil.org/resource/resmgr/Recycling_Rate/BCI_2012 12-17_FinalRecycling.pdf.

74. Moodley, S., *Battery manufacturer sets up recycling unit*, in *Engineering News*. 2014, Creamer Media: Johannesburg, South Africa.

75. Zhang, Q., *The current status on the recycling of lead-acid batteries in China.* Int J Electrochem Sci, 2013. **8**: p. 6457-6466.

76. Sun, Z., H. Cao, X. Zhang, X. Lin, W. Zheng, G. Cao, Y. Sun, and Y. Zhang, *Spent lead-acid battery recycling in China – A review and sustainable analyses on mass flow of lead.* Waste Management, 2017. **64**: p. 190-201.DOI: https://doi.org/10.1016/j.wasman.2017.03.007.

77. Manhart, A., T. Amera, G. Kuepouo, D. Mathai, S. Mng'anya, and T. Schleicher, *The deadly business – Findings from the Lead Recycling Africa Project*, in *Lead Recycling Africa Project*. 2016, Oeko-Institut e.V.: Freiburg, Germany.

78. Tür, M., A. Manhart, and T. Schleicher, *Generation of used lead-acid batteries in Africa – estimating the volumes*, in *Secondary Generation of used lead-acid batteries in Africa – estimating the volumes*, Secondary Tür, M., A. Manhart, and T. Schleicher, Editors. 2016, O.-I. e.V.: Freiburg, Germany.[cited 18/12/2017]; Available from: http://www.econet.international/index.php?id=3.

79. Linden, D., *Basic components*, in *Handbook of batteries*, D. Linden and T. Reddy, Editors. 2002, McGraw-Hill: New York. p. 1.3-1.18.ISBN: 0-07-135978-8.

80. Tretkoff, E., *March 20, 1800: Volta describes the Electric Battery*, in *American Physical Society News*. 2006, American Physical Society.

81. Linden, D. and T. Reddy, *Handbook of batteries*. 3rd ed, ed. D. Linden and T. Reddy. 2002, New York: McGraw-Hill.ISBN: ISBN: 0-07-135978-8.

82. Spiers, D., *IIIb-2 - Batteries in PV Systems*, in *Practical Handbook of Photovoltaics*, T. Markvart and L. Castañer, Editors. 2003, Elsevier Science: Amsterdam. p. 587-631.ISBN: 978-1-85617-390-2.

83. Ponce de León, C., A. Frías-Ferrer, J. González-García, D.A. Szánto, and F.C. Walsh, *Redox flow cells for energy conversion.* Journal of Power Sources, 2006. **160**(1): p. 716-732.DOI: http://dx.doi.org/10.1016/j.jpowsour.2006.02.095.

84. Shibata, T., T. Kumamoto, Y. Nagaoka, and K. Kawase, *Redox flow batteries for the Stable Supply of Renewable Energy*, in *Sei Technical Review*. 2013, Sumitomo Electric: online. p. 14-22.

85. Weber, A., M. Mench, J. Meyers, P. Ross, J. Gostick, and Q. Liu, *Redox flow batteries: a review.* Journal of Applied Electrochemistry, 2011. **41**(10): p. 1137-1164.DOI: 10.1007/s10800-011-0348-2.

86. Alotto, P., M. Guarnieri, and F. Moro, *Redox flow batteries for the storage of renewable energy: A review.* Renewable and Sustainable Energy Reviews, 2014. **29**: p. 325-335.

87. Kazacos, M., M. Cheng, and M. Skyllas-Kazacos, *Vanadium redox cell electrolyte optimization studies.* Journal of Applied Electrochemistry, 1990. **20**(3): p. 463-467.DOI: 10.1007/BF01076057.

88. Rydh, C.J., *Environmental assessment of vanadium redox and lead-acid batteries for stationary energy storage.* Journal of Power Sources, 1999. **80**(1-2): p. 21-29.DOI: 10.1016/S0378-7753(98)00249-3.

89. Leung, P.K., C. Ponce de León, and F.C. Walsh, *An undivided zinc–cerium redox flow battery operating at room temperature (295 K).* Electrochemistry Communications, 2011. **13**(8): p. 770-773.DOI: http://dx.doi.org/10.1016/j.elecom.2011.04.011.

90. Wang, K., P. Pei, Y. Wang, C. Liao, W. Wang, and S. Huang, *Advanced rechargeable zinc-air battery with parameter optimization.* Applied Energy, 2018. **225**: p. 848-856.DOI: https://doi.org/10.1016/j.apenergy.2018.05.071.

91. Skyllas-Kazacos, M., G. Kazacos, G. Poon, and H. Verseema, *Recent advances with UNSW vanadium-based redox flow batteries.* International Journal of Energy Research, 2010. **34**(2): p. 182-189.DOI: 10.1002/er.1658.

92. Imergy, *Imergy Power Systems Achieves Technological Breakthrough in Energy Storage: Flow Batteries Made from Recycled Vanadium*. 2015.

93. Skyllas-Kazacos, M., M.H. Chakrabarti, S.A. Hajimolana, F.S. Mjalli, and M. Saleem, *Progress in Flow Battery Research and Development.* Journal of The Electrochemical Society, 2011. **158**(8): p. R55-R79.DOI: 10.1149/1.3599565.

94. Wen, Y., Y. Xu, J. Cheng, G. Cao, and Y. Yang, *Investigation on the stability of electrolyte in vanadium flow batteries.* Electrochimica Acta, 2013. **96**(0): p. 268-273.DOI: http://dx.doi.org/10.1016/j.electacta.2013.02.091.

95. Clarke, R.L.O., CA, US), Dougherty, Brian (Menlo Park, CA, US), Harrison, Stephen (Benicia, CA, US), Millington, Peter J. (Weaverham, GB), Mohanta, Samaresh (Fremont, CA, US), *Cerium batteries*. 2009, Plurion Limited Company (GB): United States.

96. Leung, P.K., C. Ponce-de-León, C.T.J. Low, A.A. Shah, and F.C. Walsh, *Characterization of a zinc–cerium flow battery.* Journal of Power Sources, 2011. **196**(11): p. 5174-5185.DOI: http://dx.doi.org/10.1016/j.jpowsour.2011.01.095.

97. Xu, Q. and T.S. Zhao, *Fundamental models for flow batteries.* Progress in Energy and Combustion Science, 2015. **49**: p. 40-58.DOI: https://doi.org/10.1016/j.pecs.2015.02.001.

98. Yu, B., R. Xu, Y. He, Y. Li, and J. Zhang, *Study of methanesulfonic acid effect on electrosynthesis of lead dioxide to provide more environmentally electrolyte selection.* International Journal of Hydrogen Energy, 2017. **42**(31): p. 19597-19603.DOI: https://doi.org/10.1016/j.ijhydene.2017.05.239.

99. Amunátegui, B., A. Ibáñez, M. Sierra, and M. Pérez, *Electrochemical energy storage for renewable energy integration: zinc-air flow batteries.* Journal of Applied Electrochemistry, 2018. **48**(6): p. 627-637.DOI: 10.1007/s10800-017-1133-7.

100. Mainar, A.R., E. Iruin, L.C. Colmenares, A. Kvasha, I. de Meatza, M. Bengoechea, O. Leonet, I. Boyano, Z. Zhang, and J.A. Blazquez, *An overview of progress in electrolytes for secondary zinc-air batteries and other storage systems based on zinc.* Journal of Energy Storage, 2018. **15**: p. 304-328.DOI: https://doi.org/10.1016/j.est.2017.12.004.

101. Bartolozzi, M., *Development of redox flow batteries. A historical bibliography.* Journal of Power Sources, 1989. **27**(3): p. 219-234.DOI: https://doi.org/10.1016/0378-7753(89)80037-0.

102. Pletcher, D. and R. Wills, *A novel flow battery: A lead acid battery based on an electrolyte with soluble lead(ii) Part II. Flow cell studies.* Physical Chemistry Chemical Physics, 2004. **6**(8): p. 1779-1785.DOI: http://dx.doi.org/10.1039/B401116C.

103. Wills, R.G.A., *A lead acid flow battery for utility scale energy storage and load levelling*, in *Faculty of Chemistry*. 2004, University of Southampton: EThOS Online Database. p. 153.

104. Pletcher, D., H. Zhou, G. Kear, C.T.J. Low, F.C. Walsh, and R.G.A. Wills, *A novel flow battery - A lead-acid battery based on an electrolyte with soluble lead(II) V. Studies of the lead negative electrode.* Journal of Power Sources, 2008. **180**(1): p. 621-629.DOI: https://doi.org/10.1016/j.jpowsour.2008.02.024.

105. Akhil, A.A., G. Huff, A.B. Currier, B.C. Kaun, D.M. Rastler, M.C. Chen, A.L. Cotter, D.T. Bradshaw, and W.D. Gauntlett, *DOE/EPRI 2013 Electricity Storage Handbook in Collaboration with NRECA*, in *Secondary DOE/EPRI 2013 Electricity Storage Handbook in Collaboration with NRECA*, Secondary Akhil, A.A., G. Huff, A.B. Currier, B.C. Kaun, D.M. Rastler, M.C. Chen, A.L. Cotter, D.T. Bradshaw, and W.D. Gauntlett, Editors. 2013, SANDIA.

106. Cunha, Á., J. Martins, N. Rodrigues, and F.P. Brito, *Vanadium redox flow batteries: a technology review.* International Journal of Energy Research, 2015. **39**(7): p. 889-918.DOI: 10.1002/er.3260.

107. Teller, O., J.-P. Nicolai, M. Lafoz, D. Laing, R. Tamme, A.S. Pedersen, M. Andersson, C. Folke, C. Bourdil, M. Conte, G. Gigliucci, I. Fastelli, M. Vona, M.R. Porto, T. Hackensellner, R. Kapp, H.J. Seifert, M. Noe, M. Sander, J. Lugaro, M. Lippert, P. Hall, R. Saliger, A. Harby, M. Pihlatie, N. Omar, J.-M. Durand, M.J. Duarte, and P. Clerens, *Joint EASE/EERA recommendations for a European energy storage technology development roadmap towards 2030*, in *Secondary Joint EASE/EERA recommendations for a European energy storage technology development roadmap towards 2030*, Secondary Teller, O., J.-P. Nicolai, M. Lafoz, D. Laing, R. Tamme, A.S. Pedersen, M. Andersson, C. Folke, C. Bourdil, M. Conte, G. Gigliucci, I. Fastelli, M. Vona, M.R. Porto, T. Hackensellner, R. Kapp, H.J. Seifert, M. Noe, M. Sander, J. Lugaro, M. Lippert, P. Hall, R. Saliger, A. Harby, M. Pihlatie, N. Omar, J.-M. Durand, M.J. Duarte, and P. Clerens, Editors. 2013, EASE/EERA: Brussels, Belgium. p. 1-226.[cited 17/08/2018]; Available from: https://www.eera-set.eu/wp-content/uploads/148885-EASE-recommendations-Roadmap-04.pdf.

108. Ding, C., H. Zhang, X. Li, T. Liu, and F. Xing, *Vanadium Flow Battery for Energy Storage: Prospects and Challenges.* The Journal of Physical Chemistry Letters, 2013. **4**(8): p. 1281-1294.DOI: 10.1021/jz4001032.

109. Verde, M.G., K.J. Carroll, Z. Wang, A. Sathrum, and Y.S. Meng, *Achieving high efficiency and cyclability in inexpensive soluble lead flow batteries.* Energy & Environmental Science, 2013. **6**(5): p. 1573-1581.DOI: http://dx.doi.org/10.1039/C3EE40631H.

110. Laitinen, A., *Industrial Battery Market Outlook*, in *Secondary Industrial Battery Market Outlook*, Secondary Laitinen, A., Editor. 2017, EnerSys: Zug, Switzerland.

111. Oury, A., A. Kirchev, Y. Bultel, and E. Chainet, *PbO_2/Pb^{2+} cycling in methanesulfonic acid and mechanisms associated for soluble lead-acid flow battery applications.* Electrochimica Acta, 2012. **71**(0): p. 140-149.DOI: http://dx.doi.org/10.1016/j.electacta.2012.03.116.

112. Krishna, M., *The soluble lead redox flow battery (SLFB)*, in *jpg*, T.s.l.f. battery, Editor. 2015, NREL: Energy technology research page, University of Southampton website.

113. Gernon, M., M. Wu, T. Buszta, and P. Janney, *Environmental benefits of methanesulfonic acid . Comparative properties and advantages.* Green Chemistry, 1999. **1**(3): p. 127-140.DOI: 10.1039/A900157C.

114. Wills, R.G.A., J. Collins, D. Stratton-Campbell, C.T.J. Low, D. Pletcher, and F. Walsh, *Developments in the soluble lead-acid flow battery.* Journal of Applied Electrochemistry, 2010. **40**(5): p. 955-965.DOI: 10.1007/s10800-009-9815-4.

115. Collins, J., G. Kear, X. Li, C.T.J. Low, D. Pletcher, R. Tangirala, D. Stratton-Campbell, F.C. Walsh, and C. Zhang, *A novel flow battery: A lead acid battery based on an electrolyte with soluble lead(II) Part VIII. The cycling of a 10 cm x 10 cm flow cell.* Journal of Power Sources, 2010. **195**(6): p. 1731-1738.DOI: https://doi.org/10.1016/j.jpowsour.2009.09.044.

116. Collins, J., X. Li, D. Pletcher, R. Tangirala, D. Stratton-Campbell, F.C. Walsh, and C. Zhang, *A novel flow battery: A lead acid battery based on an electrolyte with soluble lead(II). Part IX: Electrode and electrolyte conditioning with hydrogen peroxide.* Journal of Power Sources, 2010. **195**(9): p. 2975-2978.DOI: 10.1016/j.jpowsour.2009.10.109.

117. Li, X., D. Pletcher, and F.C. Walsh, *A novel flow battery: A lead acid battery based on an electrolyte with soluble lead(II) Part VII. Further studies of the lead dioxide positive electrode.* Electrochimica Acta, 2009. **54**(20): p. 4688-4695.DOI: https://doi.org/10.1016/j.electacta.2009.03.075.

118. Krishna, M., E.J. Fraser, R.G.A. Wills, and F.C. Walsh, *Developments in soluble lead flow batteries and remaining challenges: An illustrated review.* Journal of Energy Storage, 2018. **15**: p. 69-90.DOI: https://doi.org/10.1016/j.est.2017.10.020.

119. Hazza, A., D. Pletcher, and R. Wills, *A novel flow battery - A lead acid battery based on an electrolyte with soluble lead(II) - IV. The influence of additives.* Journal of Power Sources, 2005. **149**: p. 103-111.DOI: https://doi.org/10.1016/j.jpowsour.2005.01.049.

120. Pletcher, D., H. Zhou, G. Kear, C.T.J. Low, F.C. Walsh, and R.G.A. Wills, *A novel flow battery - A lead-acid battery based on an electrolyte with soluble lead(II) Part VI. Studies of the lead dioxide positive electrode.* Journal of Power Sources, 2008. **180**(1): p. 630-634.DOI: https://doi.org/10.1016/j.jpowsour.2008.02.025.

121. Wallis, L.P.J. and R.G.A. Wills, *Membrane divided soluble lead battery utilising a bismuth electrolyte additive.* Journal of Power Sources, 2014. **247**: p. 799-806.DOI: http://dx.doi.org/10.1016/j.jpowsour.2013.09.026.

122. Plante, G., *Storage of electrical energy and researches in the effects created by currents combining quantity with high tension* - 1859, Internet Archive. 296.

123. Salkind, A.J., A.G. Cannone, and F.A. Trumbure, *Lead-acid batteries*, in *Handbook of batteries*, D. Linden and T. Reddy, Editors. 2002, McGraw-Hill: New York.ISBN: 0-07-135978-8.

124. Salkind, A.J., C. Fennie, P. Singh, T. Atwater, and D.E. Reisner, *Determination of state-of-charge and state-of-health of batteries by fuzzy logic methodology.* Journal of Power Sources, 1999. **80**(1-2): p. 293-300.DOI: 10.1016/s0378-7753(99)00079-8.

125. Dell, R.M., *Batteries: fifty years of materials development.* Solid State Ionics, 2000. **134**(1–2): p. 139-158.DOI: http://dx.doi.org/10.1016/S0167-2738(00)00722-0.

126. Ruetschi, P., *Aging mechanisms and service life of lead–acid batteries.* Journal of Power Sources, 2004. **127**(1–2): p. 33-44.DOI: http://dx.doi.org/10.1016/j.jpowsour.2003.09.052.

127. Smaniotto, A., A. Antunes, I.d.N. Filho, L.D. Venquiaruto, D. de Oliveira, A. Mossi, M. Di Luccio, H. Treichel, and R. Dallago, *Qualitative lead extraction from recycled lead–acid batteries slag.* Journal of Hazardous Materials, 2009. **172**(2–3): p. 1677-1680.DOI: http://dx.doi.org/10.1016/j.jhazmat.2009.07.026.

128. ESC, *Global Energy Storage Market Overview & Regional Summary Report*, in *Secondary Global Energy Storage Market Overview & Regional Summary Report*, Secondary ESC, Editor. 2015: Mawson.[cited 10/04/2016]; Available from: http://neca.asn.au/sites/default/files//media/state_nsw/News%20&%20Views/ESC%20Global%20Energy%20Storage%20Report_2015.pdf.

129. Nakamura, K., M. Shiomi, K. Takahashi, and M. Tsubota, *Failure modes of valve-regulated lead/acid batteries.* Journal of Power Sources, 1996. **59**(1–2): p. 153-157.DOI: http://dx.doi.org/10.1016/0378-7753(95)02317-8.

130. Barry, M.L., H. Steyn, and A. Brent. *Determining the most important factors for sustainable energy technology selection in Africa: Application of the focus group*

technique. in *Management of Engineering & Technology, 2008. PICMET 2008. Portland International Conference on*. 2008.

131. Balakrishnan, P.G. and J. Rethinam, *Failures of VRLA - Causes and Remedial Measures*, in *Developments in Valve-Regulated Lead-Acid (VRLA) Batteries*. 2008, Nova Science Publishers, Incorporated: New York, US. p. 63-70.ISBN: 9781608762989.

132. Lam, L.T., N.P. Haigh, C.G. Phyland, and A.J. Urban, *Failure mode of valve-regulated lead-acid batteries under high-rate partial-state-of-charge operation.* Journal of Power Sources, 2004. **133**(1): p. 126-134.DOI: http://dx.doi.org/10.1016/j.jpowsour.2003.11.048.

133. Yang, J., C. Hu, H. Wang, K. Yang, J.B. Liu, and H. Yan, *Review on the research of failure modes and mechanism for lead–acid batteries.* International Journal of Energy Research, 2017. **41**(3): p. 336-352.DOI: https://doi.org/10.1002/er.3613.

134. Wagner, R. and D.U. Sauer, *Charge strategies for valve-regulated lead/acid batteries in solar power applications.* Journal of Power Sources, 2001. **95**(1–2): p. 141-152.DOI: http://dx.doi.org/10.1016/S0378-7753(00)00614-5.

135. ABRI, *Lead Acid Battery Recycling - The Battery Recycling Process*, A.B.R. Initiative, Editor. 2014, ABRI: online. p. 2.

136. Turner, J.M., *Following the Pb: An Envirotechnical Approach to Lead-Acid Batteries in the United States.* Environmental History, 2015. **20**(1): p. 29-56.DOI: 10.1093/envhis/emu128.

137. Eckel, W.P., M.B. Rabinowitz, and G.D. Foster, *Discovering unrecognized lead-smelting sites by historical methods.* American journal of public health, 2001. **91**(4): p. 625-627.

138. EU, *Batteries and accumulators and waste batteries and accumulators*, in *Directive 2006/66/EC* 2006, EU Commission: EU. p. 28.

139. Thornton, I., R. Rautiu, and S. Brush, *Recycling of lead*, in *Lead, the facts*. 2001, Ian Allan Printing Ltd: Hersham, Surrey. p. 71-80.ISBN: 0-9542496-0-7.

140. van der Kuijp, T., L. Huang, and C. Cherry, *Health hazards of China's lead-acid battery industry: a review of its market drivers, production processes, and health impacts.* Environmental Health, 2013. **12**(1): p. 61.DOI: https://doi.org/10.1186/1476-069X-12-61.

141. WHO, *Recycling used lead acid batteries: health considerations*, in *Secondary Recycling used lead acid batteries: health considerations*, Secondary WHO, Editor. 2017, W.H. Organization: Geneva.[cited 14/05/2019]; Available from: https://apps.who.int/iris/bitstream/handle/10665/259447/9789241512855-eng.pdf;jsessionid=3DB26C92267AFC7C499A14B52BAA0A1D?sequence=1.

142. Haefliger, P., M. Mathieu-Nolf, S. Lociciro, C. Ndiaye, M. Coly, A. Diouf, A. Faye, A. Sow, J. Tempowski, J. Pronczuk, A. Filipe, R. Bertollini, and M. Neira, *Mass lead intoxication from informal used lead-acid battery recycling in Dakar, Senegal.* Environ Health Perspect, 2009. **117**.DOI: 10.1289/ehp.0900696.

143. Ericson, B., P. Landrigan, M.P. Taylor, J. Frostad, J. Caravanos, J. Keith, and R. Fuller, *The Global Burden of Lead Toxicity Attributable to Informal Used Lead-Acid Battery Sites.* Annals of Global Health, 2016. **82**(5): p. 686-699.DOI: https://doi.org/10.1016/j.aogh.2016.10.015.

144. Fink, C.G. and L. Greenspan, *Electrolytic Recovery of Lead from Lead Sulfate Waste.* Transactions of the American Electrochemical Society, 1930. **58**(1): p. 465-473.DOI: 10.1149/1.3493763.

145. Habashi, F., *A short history of hydrometallurgy.* Hydrometallurgy, 2005. **79**(1): p. 15-22.DOI: https://doi.org/10.1016/j.hydromet.2004.01.008.

146. Ramus, K. and P. Hawkins, *Lead/acid battery recycling and the new Isasmelt process.* Journal of Power Sources, 1993. **42**(1): p. 299-313.DOI: https://doi.org/10.1016/0378-7753(93)80159-M.

147. Battery, F.N. *Recycling Process*. [website] 2019 [cited 2018 11/03/2019]; Available from: https://www.battery.co.za/recycling/recycling-process/.

148. Ellis, T.W. and A.H. Mirza, *The refining of secondary lead for use in advanced lead-acid batteries.* Journal of Power Sources, 2010. **195**(14): p. 4525-4529.DOI: http://dx.doi.org/10.1016/j.jpowsour.2009.12.118.

149. ECOBAT. *ECOBAT´s Closed Recycling Loop*. [website] 2019 [cited 2018 11/03/2019]; Available from: http://ecobatgroup.com/ecobatgroup-en/technologies/recycling_technology.php.

150. Joseph, K. and W. Verwey. *An overview of lead recycling in South Africa*. in *United Nations Conference on Trade And Development*. 2001. Bangkok.

151. Government, U.F., *Non-bulk Packaging for Hazardous Materials Other Than Class 1 and Class 7*, in *General Requirements for Shipment and Packagings*. 2009.

152. Department of Labour, R., *Lead Regulations*, in *Occuptional Health and Safety*. 2001, Official Gazette, 2002-02-28, : South Africa. p. 1-47.

153. Zhang, W., J. Yang, X. Wu, Y. Hu, W. Yu, J. Wang, J. Dong, M. Li, S. Liang, J. Hu, and R.V. Kumar, *A critical review on secondary lead recycling technology and its prospect.* Renewable and Sustainable Energy Reviews, 2016. **61**: p. 108-122.DOI: https://doi.org/10.1016/j.rser.2016.03.046.

154. Cusano, G., M.R. Gonzalo, F. Farrell, R. Remus, S. Roudier, and L.D. Sancho, *Best Available Techniques (BAT) Reference Document for the Non-Ferrous Metals Industries*, in *Secondary Best Available Techniques (BAT) Reference Document for the Non-Ferrous Metals Industries*, Secondary Cusano, G., M.R. Gonzalo, F. Farrell, R. Remus, S. Roudier, and L.D. Sancho, Editors. 2017: Seville, Spain.[cited 12/05/2019]; Available from: http://eippcb.jrc.ec.europa.eu/reference/BREF/NFM/JRC107041_NFM_bref2017.pdf.

155. Dyosi, S., *Evaluation of Preventive and Control Measures for Lead Exposure in a South African Lead-Acid Battery Recycling Smelter.* Journal of Occupational and Environmental Hygiene, 2007. **4**(10): p. 762-769.DOI: 10.1080/15459620701566324.

156. Thornton, I., R. Rautiu, and S. Brush, *Lead exposure to humans and other organisms*, in *Lead, the facts*. 2001, Ian Allan Printing Ltd: Hersham, Surrey. p. 111-141.ISBN: 0-9542496-0-7.

157. Gupt, Y. and S. Sahay, *Managing Used Lead Acid Batteries in India: Evaluation of EPR-DRS Approaches.* Journal of Health and Pollution, 2015. **5**(8): p. 52-63.DOI: 10.5696/i2156-9614-5-8.52.

158. Ferracin, L.C., A.E. Chácon-Sanhueza, R.A. Davoglio, L.O. Rocha, D.J. Caffeu, A.R. Fontanetti, R.C. Rocha-Filho, S.R. Biaggio, and N. Bocchi, *Lead recovery from a typical*

Brazilian sludge of exhausted lead-acid batteries using an electrohydrometallurgical process. Hydrometallurgy, 2002. **65**(2–3): p. 137-144.DOI: http://dx.doi.org/10.1016/S0304-386X(02)00087-7.

159. Fingland, J.J., *The Betts Electrolytic Lead Refining Process in Practice.* Transactions of the American Electrochemical Society, 1930. **57**(1): p. 177-204.DOI: 10.1149/1.3492149.

160. González-Domínguez, J.A., E. Peters, and D.B. Dreisinger, *The refining of lead by the Betts process.* Journal of Applied Electrochemistry, 1991. **21**(3): p. 189-202.DOI: 10.1007/BF01052570.

161. Habashi, F., *Extractive metallurgy and national policy.* International Journal of Nonferrous Metallurgy, 2013. **2**: p. 31-34.DOI: 10.4236/ijnm.2013.22004.

162. Ballantyne, A.D., J.P. Hallett, D.J. Riley, N. Shah, and D.J. Payne, *Lead acid battery recycling for the twenty-first century.* Royal Society open science, 2018. **5**(5): p. 171368-171368.DOI: 10.1098/rsos.171368.

163. Volpe, M., D. Oliveri, G. Ferrara, M. Salvaggio, S. Piazza, S. Italiano, and C. Sunseri, *Metallic lead recovery from lead-acid battery paste by urea acetate dissolution and cementation on iron.* Hydrometallurgy, 2009. **96**(1–2): p. 123-131.DOI: http://dx.doi.org/10.1016/j.hydromet.2008.09.001.

164. Gaumann, A.F. and V. Dancilovic-Matulas, *Process for the recovery of lead from scrapped lead batteries*. 1978, Google Patents.

165. Sonmez, M.S. and R.V. Kumar, *Leaching of waste battery paste components. Part 1: Lead citrate synthesis from PbO and PbO2.* Hydrometallurgy, 2009. **95**(1–2): p. 53-60.DOI: http://dx.doi.org/10.1016/j.hydromet.2008.04.012.

166. Sonmez, M.S. and R.V. Kumar, *Leaching of waste battery paste components. Part 2: Leaching and desulphurisation of PbSO4 by citric acid and sodium citrate solution.* Hydrometallurgy, 2009. **95**(1–2): p. 82-86.DOI: http://dx.doi.org/10.1016/j.hydromet.2008.04.019.

167. Zhu, X., X. He, J. Yang, L. Gao, J. Liu, D. Yang, X. Sun, W. Zhang, Q. Wang, and R.V. Kumar, *Leaching of spent lead acid battery paste components by sodium citrate and acetic acid.* Journal of Hazardous Materials, 2013. **250–251**: p. 387-396.DOI: http://dx.doi.org/10.1016/j.jhazmat.2013.02.018.

168. Sun, X., J. Yang, W. Zhang, X. Zhu, Y. Hu, D. Yang, X. Yuan, W. Yu, J. Dong, H. Wang, L. Li, R. Vasant Kumar, and S. Liang, *Lead acetate trihydrate precursor route to synthesize novel ultrafine lead oxide from spent lead acid battery pastes.* Journal of Power Sources, 2014. **269**(0): p. 565-576.DOI: http://dx.doi.org/10.1016/j.jpowsour.2014.07.007.

169. Caravanos, J., *Environmental Contamination in Nigeria.* Journal of health & pollution, 2017. **7**(13): p. 1-1.DOI: 10.5696/2156-9614-7-13.1.

170. Wheeler, W. and M.J. Brown, *Blood Lead Levels in Children Aged 1–5 Years — United States, 1999–2010.* Morbidity and Mortality Weekly Report, 2013. **62**(13): p. 245-248.

171. Errington, B., P. Arthur, J. Wang, and Y. Dong, *The ISA-YMG Lead Smelting Process*, in *PbZn 2005 Conference*. 2005, ISASMELT: Kyoto, Japan.

172. Pavlov, D., P. Nikolov, and T. Rogachev, *Influence of expander components on the processes at the negative plates of lead-acid cells on high-rate partial-state-of-charge cycling. Part I: Effect of lignosulfonates and BaSO4 on the processes of charge and*

discharge of negative plates. Journal of Power Sources, 2010. **195**(14): p. 4435-4443.DOI: http://dx.doi.org/10.1016/j.jpowsour.2009.11.060.

173. Pavlov, D., *Additives to the Pastes for Positive and Negative Battery Plate*, in *Lead-Acid Batteries - Science and Technology - A Handbook of Lead-Acid Battery Technology and its Influence on the Product*. 2011, Elsevier: Amsterdam. p. 311-361.

174. Prengaman, R.D., *Improvements to active material for VRLA batteries.* Journal of Power Sources, 2005. **144**(2): p. 426-437.DOI: https://doi.org/10.1016/j.jpowsour.2004.11.004.

175. MacFarlane, D.R., J.M. Pringle, P.C. Howlett, and M. Forsyth, *Ionic liquids and reactions at the electrochemical interface.* Physical chemistry chemical physics, 2010. **12**(8): p. 1659-1669.DOI: 10.1039/b923053j.

176. Schrodt, J.P., W.J. Otting, J.O. Schoegler, and D.N. Craig, *A Lead Dioxide Cell Containing Various Electrolytes.* Transactions of The Electrochemical Society, 1946. **90**(1): p. 405-417.DOI: 10.1149/1.3071755.

177. McDonald, G.D., E.Y. Weissman, and T.S. Roemer, *Lead-fluoroboric acid battery.* J. Electrochem. Soc.; (United States), 1972: p. Medium: X; Size: Pages: 660-663.

178. Goodwin, H.M. and R. Haskell, *The Electrical Conductivity of very Dilute Hydrochloric and Nitric Acid Solutions.* Physical Review (Series I), 1904. **19**(6): p. 369-386.DOI: 10.1103/PhysRevSeriesI.19.369.

179. Krishna, M., L.P.J. Wallis, R.G.A. Wills, D. Hall, and A.A. Shah, *Measurement of key electrolyte properties for improved performance of the soluble lead flow battery.* International Journal of Hydrogen Energy, 2017.DOI: https://doi.org/10.1016/j.ijhydene.2017.05.004.

180. Ropp, R.C., *Chapter 5 - Group 14 (C, Si, Ge, Sn, and Pb) Alkaline Earth Compounds*, in *Encyclopedia of the Alkaline Earth Compounds*. 2013, Elsevier: Amsterdam. p. 351-480.ISBN: 978-0-444-59550-8.

181. Pavlov, D., *Methods to Restore the Water Decomposed During Charge and Overcharge of Lead–Acid Batteries. VRLA Batteries*, in *Lead-Acid Batteries: Science and Technology*. 2011, Elsevier: Amsterdam. p. 567-603.ISBN: 978-0-444-52882-7.

182. Schick, K.G., V.G. Magearu, N.L. Field, and C.O. Huber, *Lead dioxide-catalyst electrode sensitive to hydrogen peroxide.* Analytical Chemistry, 1976. **48**(14): p. 2186-2188.DOI: 10.1021/ac50008a033.

183. Bancroft, W.D. and N.F. Murphy, *Oxidation and Reduction with Hydrogen Peroxide.* The Journal of Physical Chemistry, 1934. **39**(3): p. 377-398.DOI: 10.1021/j150363a006.

184. Yuasa, *NP Series: NP7-12*, Y.B. Inc., Editor. 2008: Laureldale.

185. Orapeleng, K., R. Wills, and A. Cruden, *Developing Electrolyte for a Soluble Lead Redox Flow Battery by Reprocessing Spent Lead Acid Battery Electrodes.* Batteries, 2017. **3**(2): p. 15.DOI: https://doi.org/10.3390/batteries3020015.

186. Fitch, A., *Lead Analysis: Past and Present.* Critical Reviews in Analytical Chemistry, 1998. **28**(3): p. 267-345.DOI: 10.1080/10408349891194207.

187. Vogel, A.I. and G.H. Jeffery, *Vogel's Textbook of Quantitative Chemical Analysis*. 1989: Longman Scientific & Technical.ISBN: 9780582446939.

188. Yuasa. *Yuasa Technical Manual*. [Technical manual] 2003 04 December 2015 [cited FORM NO.YUA-069 (Rev. 4/03); Available from: http://ktm950.info/library/assets/pdfs/Yuasa%20Batteries.pdf.

189. IEEE-SA, *IEEE Recommended Practice for Maintenance, Testing, and Replacement of Valve-Regulated Lead-Acid (VRLA) Batteries for Stationary Applications*, in *IEEE Std 1188-2005 (Revision of IEEE Std 1188-1996)*. 2006, American National Standards Institute: New York. p. 1-44.

190. Orapeleng, K., R.G.A. Wills, and A. Cruden, *Performance of recovered and reagent grade electrolyte in a soluble lead redox cell.* Journal of Energy Storage, 2018. **20**: p. 49-56.DOI: https://doi.org/10.1016/j.est.2018.08.017.

191. Prengaman, R.D., *Lead Alloys for Valve-regulated Lead-Acid Batteries*, in *Valve-Regulated Lead-Acid Batteries*, D.A.J. Rand, et al., Editors. 2004, Elsevier: Amsterdam. p. 15-35.ISBN: 978-0-444-50746-4.

192. BSI, *Lead and Lead Alloys: Lead*, in *BS EN 12659:1999* 1999, British Standard Institution: United Kingdom.

193. Paces, J.B., D. Weis, and T.R. Ireland, *Mass Spectrometry*, in *Encyclopedia of Scientific Dating Methods*, W. Jack Rink and J.W. Thompson, Editors. 2015, Springer Netherlands: Dordrecht. p. 533-542.ISBN: 978-94-007-6304-3.

194. Fisher, A.C., *Electrode Dynamics*. 1st ed. Oxford Chemistry Primers, ed. G.R. Compton. Vol. 34. 1996, New York: Oxford University Press. 83.

195. Evans, D.H., K.M. O'Connell, R.A. Petersen, and M.J. Kelly, *Cyclic voltammetry.* Journal of Chemical Education, 1983. **60**(4): p. 290.DOI: 10.1021/ed060p290.

196. A. Pletcher, D., *A First Course in Electrode Processes*. 1991.

197. Elgrishi, N., K.J. Rountree, B.D. McCarthy, E.S. Rountree, T.T. Eisenhart, and J.L. Dempsey, *A Practical Beginner's Guide to Cyclic Voltammetry.* Journal of Chemical Education, 2018. **95**(2): p. 197-206.DOI: 10.1021/acs.jchemed.7b00361.

198. Pletcher, D. and R. Wills, *A novel flow battery - A lead acid battery based on an electrolyte with soluble lead(II) - III. The influence of conditions on battery performance.* Journal of Power Sources, 2005. **149**: p. 96-102.DOI: https://doi.org/10.1016/j.jpowsour.2005.01.048.

199. Oury, A., A. Kirchev, and Y. Bultel, *Oxygen evolution on alpha-lead dioxide electrodes in methanesulfonic acid.* Electrochimica Acta, 2012. **63**(0): p. 28-36.DOI: http://dx.doi.org/10.1016/j.electacta.2011.12.028.

200. Lu, L., X. Han, J. Li, J. Hua, and M. Ouyang, *A review on the key issues for lithium-ion battery management in electric vehicles.* Journal of Power Sources, 2013. **226**: p. 272-288.DOI: https://doi.org/10.1016/j.jpowsour.2012.10.060.

201. Fan, J. and S. Tan, *Studies on Charging Lithium-Ion Cells at Low Temperatures.* Journal of The Electrochemical Society, 2006. **153**(6): p. A1081-A1092.DOI: 10.1149/1.2190029.

202. Wang, Q., J. Sun, X. Yao, and C. Chen, *Thermal Behavior of Lithiated Graphite with Electrolyte in Lithium-Ion Batteries.* Journal of The Electrochemical Society, 2006. **153**(2): p. A329-A333.DOI: 10.1149/1.2139955.

203. Arora, P., R.E. White, and M. Doyle, *Capacity Fade Mechanisms and Side Reactions in Lithium ‐ Ion Batteries.* Journal of The Electrochemical Society, 1998. **145**(10): p. 3647-3667.DOI: 10.1149/1.1838857.

204. Lujano-Rojas, J.M., G.J. Osório, and J.P.S. Catalão. *Cycle charging strategy for optimal management of vanadium redox flow batteries connected to isolated systems*. in *2017 IEEE Manchester PowerTech*. 2017.

205. Rashid, M. and A. Gupta, *Effect of Relaxation Periods over Cycling Performance of a Li-Ion Battery.* Journal of The Electrochemical Society, 2015. **162**(2): p. A3145-A3153.DOI: 10.1149/2.0201502jes.